uOttawa

L'Université canadienne
Canada's university

FACULTÉ DES ÉTUDES SUPÉRIEURES ET POSTOCTORALES

uOttawa

L'Université canadienne
Canada's university

FACULTY OF GRADUATE AND POSDOCTORAL STUDIES

Taline Boghossian
AUTEUR DE LA THÈSE / AUTHOR OF THESIS

M.Sc. (Chemistry)
GRADE / DEGREE

Department of Chemistry
FACULTÉ, ÉCOLE, DÉPARTEMENT / FACULTY, SCHOOL, DEPARTMENT

Synthesis of Trifluorinated Threonine and its Incorporation into AFP and AFGP Mimetics

TITRE DE LA THÈSE / TITLE OF THESIS

R. Ben
DIRECTEUR (DIRECTRICE) DE LA THÈSE / THESIS SUPERVISOR

CO-DIRECTEUR (CO-DIRECTRICE) DE LA THÈSE / THESIS CO-SUPERVISOR

A. Beauchemin

J. Manthorpe

Gary W. Slater
Le Doyen de la Faculté des études supérieures et postdoctorales / Dean of the Faculty of Graduate and Postdoctoral Studies

Synthesis of Trifluorinated Threonine and its Incorporation into AFP and AFGP Mimetics

Taline Boghossian

Thesis submitted to the Faculty of Graduate & Postdoctoral Studies

University of Ottawa

In partial fulfillment of the requirements for the M.Sc. degree in the Ottawa-Carleton Chemistry Institute

Candidate	Supervisor
Taline Boghossian	Prof. Robert N. Ben

© Taline Boghossian, Ottawa, Canada, 2009

Library and Archives Canada

Published Heritage Branch

395 Wellington Street
Ottawa ON K1A 0N4
Canada

Bibliothèque et Archives Canada

Direction du Patrimoine de l'édition

395, rue Wellington
Ottawa ON K1A 0N4
Canada

Your file Votre référence
ISBN: 978-0-494-74196-2
Our file Notre référence
ISBN: 978-0-494-74196-2

NOTICE:

The author has granted a non-exclusive license allowing Library and Archives Canada to reproduce, publish, archive, preserve, conserve, communicate to the public by telecommunication or on the Internet, loan, distribute and sell theses worldwide, for commercial or non-commercial purposes, in microform, paper, electronic and/or any other formats.

The author retains copyright ownership and moral rights in this thesis. Neither the thesis nor substantial extracts from it may be printed or otherwise reproduced without the author's permission.

AVIS:

L'auteur a accordé une licence non exclusive permettant à la Bibliothèque et Archives Canada de reproduire, publier, archiver, sauvegarder, conserver, transmettre au public par télécommunication ou par l'Internet, prêter, distribuer et vendre des thèses partout dans le monde, à des fins commerciales ou autres, sur support microforme, papier, électronique et/ou autres formats.

L'auteur conserve la propriété du droit d'auteur et des droits moraux qui protège cette thèse. Ni la thèse ni des extraits substantiels de celle-ci ne doivent être imprimés ou autrement reproduits sans son autorisation.

In compliance with the Canadian Privacy Act some supporting forms may have been removed from this thesis.

While these forms may be included in the document page count, their removal does not represent any loss of content from the thesis.

Conformément à la loi canadienne sur la protection de la vie privée, quelques formulaires secondaires ont été enlevés de cette thèse.

Bien que ces formulaires aient inclus dans la pagination, il n'y aura aucun contenu manquant.

Canada

Acknowledgements

I would like to first extend my gratitude and appreciation to my research supervisor, Prof. Robert Ben. I would like to thank you for taking a chance on me, and giving me the opportunity of joining your research group. This has truly been a fulfilling experience and especially a pleasant one. Being a part of your group has opened many doors for me, and I will always remember that you had a large part in my future endeavors.

Mathieu Leclere, thank you for all of the discussions and suggestions, you have been an integral part in my research. It has been rewarding working with you and I consider myself lucky and privileged to have been able to learn from you, as you are truly one of a kind. Thank you.

Roger Tam, I cannot thank you enough. I have learned a lot from you and am very grateful for it. Your motivation, patience, modesty and willingness to help is inspiring. Thank you for being a friend and a pleasant colleague to work with.

I would also like to thank all of my past and present colleagues who have made everyday enjoyable: Pawel Czechura, Liz von Moos, John Trant, Ruoying Gong, Wendy Campbell, Sandra Santos Ferreira, and Michael Souweha. A very special thanks to Jennifer Chaytor, Jacqueline Tokarew, Taz Cheema and Chantelle Capicotti for their help during my last few weeks – your assistance and guidance was very valuable. Thank you!

I would like to acknowledge the members of my Thesis Comittee, Prof. Jeff Manthorpe and Prof. André Beauchemin for their guidance, suggestions and time.

Lastly, I would like to thank my friends and family for their constant love, support, and encouragement.

Abstract

The discovery of antifreeze proteins (AFPs) and antifreeze glycoproteins (AFGPs) has sparked the interest of researchers due to its potential commercial, industrial and medicinal applications. AF(G)Ps are unique as they have the ability to suppress the growth of ice. Two physical properties associated with these antifreeze compounds are thermal hysteresis (TH) and ice crystallization inhibition (IRI). It was previously believed that TH and IRI worked hand-in-hand, however, the discovery of an AFP from rye grass possessing only IRI suggested otherwise. It was thus believed that the presence of AFPs possessing only IRI played a vital role in cryoprotection as they allow organisms to survive in the presence of small ice crystals. As such, the synthesis of novel AF(G)Ps possessing only IRI are sought after. Herein, we describe the synthesis of a fluorinated threonine, **T(F)**, and its incorporation in peptides for the synthesis of AFP mimetics ($[T(F)AA]_4$ and $[T(F)GG]_4$). As the putative binding site of AFP type I is debated, as well as its mode of action, the introduction of a fluorinated threonine may provide insight as it may be used as a tool to investigate the factors influencing antifreeze activity. Furthermore, fluorine amino acids have proven to be beneficial in the production of biologically active agents, thus highlighting the importance of the use of fluorines. The synthetic route to $[T(F)AA]_4$ and $[T(F)GG]_4$ is described within this thesis, and the results obtained from the TH and IRI assays performed.

The synthetic route to the building block **T(F)** was performed over 13 steps in 15 % yield. The incorporation of **T(F)** in peptides to build AFP mimetics was done via SPPS. MALDI-TOF spectroscopy revealed a mass peak for the polyalanine AFP analog but was not apparent for $[T(F)GG]_4$. Nuclear magnetic resoncance experiments (^{19}F) revealed a single fluorine resonance for both $[T(F)AA]_4$ and $[T(F)GG]_4$ suggesting the presence of a fluorinated compound. The repeating nature of these polymers may account for the single resonance observed. The TH assay did not reveal dynamic ice shaping (DIS) or a thermal hysteric gap. The IRI results were

unfortunately contradictory but did reveal that the introduction of fluorine into AFPs do not alter the recrystallization inhibition activity as in the case of $[T(F)AA]_4$ and $[TAA]_4$. The outcome of these results may be due to the solubility issues encountered, which affected the concentration and purity of the sample solutions tested. Despite the solubility issues and misrepresentative results, additional experiments ought to be performed to determine the effects of fluorine on antifreeze activity.

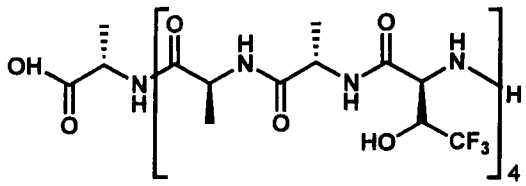

$[T(F)AA]_4$

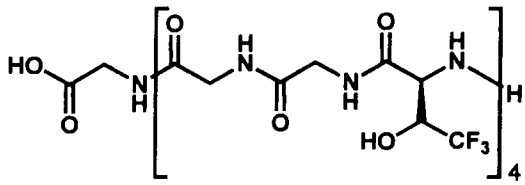

$[T(F)GG]_4$

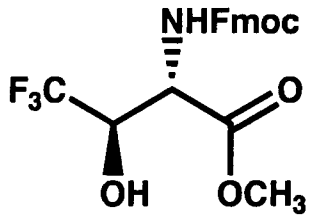

T(F)

TABLE OF CONTENTS

CHAPTER 2

CHAPTER 3:

SUPPORTING INFORMATION

Page

LIST OF FIGURES

CHAPTER 1

CHAPTER 2

CHAPTER 3

LIST OF SCHEMES

CHAPTER 2

CHAPTER 3

LIST OF TABLES

CHAPTER 1

CHAPTER 2

CHAPTER 3

LIST OF ABBREVIATIONS

2D	two-dimensional
3D	three-dimensional
Ac	acety
AFGP(s)	antifreeze glycoprotein
AFGP8	antifreeze glycoprotein fraction
AFP(s)	antifreeze protein(s)
AFP I	antifreeze protein type I
Ala	alanine
All	Allyl
$BF_3 \bullet OEt_2$	boron trifluoride diethyl etherate
Bn	benzyl
Boc	*tert*-butyloxycarbonyl
Boc_2O	Di-*tert*-butyl dicarbonate
br	broad
Bz	benzoyl
BzCl	benzoyl chloride
Cat.	Catalyst
CD	circular dichroism
CH_3CN	acetonitrile
cm^{-1}	wavenumber
d	doublet
dd	doublet of doublets
DIPEA	diisopropylethyl amine
DIS	dynamic ice shaping
DMF	dimethyl formamide
DMSO	dimethyl sulfoxide
dt	doublet of triplets
ESI	electrospray ionization
Et	ethyl
Et_2O	diethyl ether
EtOAc	ethyl acetate
EtOH	ethanol
Fmoc	9-fluorenylmethyloxycarbonyl
FmocOsucs	N-(9-Fluorenylmethoxycarbonyloxy) succinimide
Gal	galactose
GalNAc	*N*-acetyl-galactosamine
Glc	glucose
GlcNHAc	*N*-acetyl glucosamine
Gly	glycine
HBTU	2-(1H-benzotriazole-1-yl)-1,1,3,3-tetramethylaminium hexafluorophosphate
HCTU	2-(6-Chloro-1H-benzotriazole-1-yl)-1,1,3,3-tetramethylaminium hexafluorophosphate
HI	Hydration Index
HOBT	*N*-hydroxyl benzotriazole

HPLC	high performance liquid chromatography
IRI	ice-recrystallization inhibition
IR resin	Amberlite ion exchange resin
kDa	kiloDaltons
m	multiplet
M	molar
M^+	parent molecular ion
Man	mannose
MD	molecular dynamics
Me	methyl
MeOH	methanol
MGS	mean grain size
MHz	mega Hertz
mM	millimolar
MS	mass spectrometry
MS	molecular sieves
NHAc	*N*-acetyl
NaH	sodium hydride
Na_2SO_4	Sodium sulfate
$NaHCO_3$	sodium bicarbonate
NaOH	sodium hydroxide
NaOMe	sodium methoxide
NIS	N-iodosuccinimide
OGG	ornithine-glycine-glycine
OMe	*O*-methoxy
P	protecting group
PBS	phosphate-buffered saline
Pd/C	palladium on carbon
PMC	partial molar compressibility
PMV	partial molar volume
ppm	parts per million
q	quartet
s	singlet
Ser	serine
SM	starting material
SPPS	solid-phase peptide synthesis
t	triplet
Tal	talose
TBAF	*tert*-butylammonium fluoride
TFA	trifluoroacetic acid
T(F)	trifluorinated threonine building block
TH	thermal hysteresis
THF	tetrahydrofuran
Thr	threonine
TIPS	triisopropyl silane
TMS	trimethylsilyl
TMSOTf	trimethylsilyl trifluoromethanelsulfonate

Chapter 1: Introduction to Biological Antifreezes

Among all the macromolecules (carbohydrates, nucleic acids and lipids), proteins are the most structurally diverse with refined functionality. Their shape, structure and varied amino acid content often dictate their route and role in which they partake. Although there are many factors required for a living system to survive, peptides and proteins have proven to be a crucial element for many processes as they have diverse roles in organisms. Listed in Table 1 are various proteins, the organism by which the protein is isolated from, their structure and role.

Table 1. Various proteins found in nature, their structure and role.

Protein	Organism	Role
Hemoglobin[1]	Mammals	**Transport Metalloprotein** Transports oxygen from lungs to tissues and cells
Keratin[2]	Mammals	**Structural protein** Essential for normal tissue structure and function
Kinesin[3]	Eukaryotes	**Motor protein** Organelle transport and chromosome segregation
Insulin[4]	Mammals	**Hormonal Protein** Regulate glucose homeostasis
Isomerase i.e. Peptidyl-prolyl *cis-trans*, PPIase)[5]	Mammals	**Enzyme** Catalyze chemical reactions. PPIase catalyzes *cis-trans* isomerization of proline peptide bonds of oligopeptides

As tabulated above, a protein is capable of many things such as transporting molecules from one location to another or serving as a structural protein for cell maintenance and tissue integrity. It may also participate in the movement of organelles and catalyze reactions essential for cell survival, proliferation and differentiation. All of these functions together allow for an organism to live and survive and are essential for biological processes. [1-5]

Glycoproteins also have diverse roles and functions but differ greatly in structure. A Glycoprotein is typically composed of a sugar residue (mono-, di, or oligosaccharide) covalently bonded to a peptide moiety. For example, transferrin, a blood plasma transport glycoprotein found in humans, is responsible for transporting iron ions to cell tissue,[6] while collagen (types 1-5), the most abundant protein in humans, is a structural glycoprotein found in bones, tendons, ligaments and connective tissue mostly involved for protection.[7] It is obvious that the diverse roles of both proteins and glycoproteins play a crucial role for organisms to maintain biological processes and survive.

The focus of this chapter is to introduce the concept of biological antifreezes (protein and glycoprotein), their function, mechanism of action and studies that have been done to elucidate their role on a microscopic level.

1.1 Biological Antifreezes: Structure, Properties and Mode of Action

As early as 1953, there were reports[8] by Scholander and co-workers of Arctic fish blood serum having an unusually low freezing point due to non-colligative solutes. It has been long known that fish residing in the deep waters of the Arctic and Antarctic oceans are able to survive due to the warmer temperatures. However, when these fish are placed in a colder environment surrounded by ice seeds, they die due to freezing. This observation then lead to the question of how some fish residing in shallow waters among ice are able to endure the colder temperatures.[9] In 1970, DeVries, Feeney and co-workers published a series of papers[10-12] addressing this question. These authors report that this survival mechanism is due to a glycoprotein in the blood sera of Antarctic fish (*Trematomus borchgrevinki* and *Dissostichus mawsoni*). These fish had blood with a freezing point of -2.0 to -2.1°C allowing them to sustain subzero temperatures where the freezing point of seawater could be as low as -1.9°C. It is known that colligative salts (NaCl) are able to depress the freezing point of a solution, but for the Antarctic fish these solutes only reduce the freezing point by approximately 50%. Therefore, the presence of these glycoproteins further enhances the freezing point depression of blood sera. In fact, thirty percent of this depression is due to non-dialyzable solutes (i.e. glycoproteins) while the remaining 70% is due to colligative salts.[10]

Since the discovery of these biological antifreezes, many others have been found among various species like plants,[13] insects,[14] moths,[15] snow fleas,[16] and

bacteria.[17] Even though these compounds are known to be present in various organisms, they all share the ability to suppress the growth of ice crystals at subzero temperatures and can be categorized in two groups: antifreeze proteins (AFP) and antifreeze glycoproteins (AFGP). Although these compounds differ structurally (section 1.1.1), they do share the same physical properties (discussed in section 1.2)

1.1.1 Structure of Antifreeze Proteins and Glycoproteins

There are many types of AFPs found in nature and they are classified in five categories (I to V) based on their respective structure. These AFPs are unique as they are all isolated from various organisms (fish, insect, plants) and vary in primary, secondary and tertiary structure. With respect to AFGPs, eight isoforms have been isolated (AFGP1-8) and vary slightly from one another in terms of molecular weight.[10] Below is a detailed explanation of each.

1.1.1.i. Type I AFP (AFP I)

DeVries and Duman were the first to report the existence of type I AFPs as they successfully isolated and characterized these proteins in 1975.[18] Type I AFPs were extracted from the Winter Flounder (*Pseudopleuronectes Americanus)* residing in the Atlantic ocean and are the most extensively studied due to their simple structure and known peptide sequence. Their primary structure consists of 37 amino acids in which there are 11 repeating amino acid residues with the general sequence TxxNxxxxxxxx, where T, N and X are threonine, asparagine or threonine,

and alanine, respectively.[19] As seen from the primary structure, AFP I is mostly made of alanine residues (more than 60 mol%) resulting in a highly helical secondary structure (~85%) having a "rod-like" shape (Table 2).[20] X-ray diffraction data collected by Yang and co-workers revealed two facets to type 1 AFPs; a binding site containing four polar residues (threonine) among alanine residues and a non-binding site containing alanine residues. [21] The effect of these surfaces will be further discussed in sections 1.3.1.

1.1.1.ii. Type II AFP (AFP II)

Type II AFPs are unique in that they are found in a wide array of organisms. Not only are they present in fish (sea raven, smelt and herring)[22] they have also been isolated from insects (larvae of beetle)[23] and the spruce budworm.[24] These proteins are characteristic for their high cysteine content and their ability to form disulfide bridges. The secondary structure has not been studied in great detail compared to AFP I but it has been reported that the structure of this protein isolated from the sea raven is 18% helices, 38% β-sheets and 44% random coil. Although there has not been a substantial amount of research done regarding this AFP, some experiments indicate that the removal of these bridges is detrimental to antifreeze activity.[23] Sönnichsen et al. have further reiterated the importance of cysteine. They suggest that the disulfide bridges determine the structure of AFP II and results in a primary chain bearing hydrophilic residues to be exposed to the aqueous media

allowing for protein-ice interactions and hence antifreeze activity to take place.[22] Their structure and properties are listed in Table 2.

1.1.1.iii. Type III AFP (AFP III)

Type III AFPs are isolated from the ocean pout, wolfish and eelpout[25] and are not as extensively studied as AFP I. They comprise of 62-66 amino acids and are not particularly abundant in any amino acid.[22] Unlike AFP I, there are no sequence repeats and the protein has a globular tertiary structure.[26] NMR studies conducted by Sönnichsen et al. further revealed an extensive network of β-sheets that are packed orthogonally into a β-sandwich.[27] Refer to Table 2 for a summary of these details.

1.1.1.iv. Type IV AFP (AFP IV)

Type IV AFPs were identified from the longhorn sculpin. As it is a relative to the sculpin (comprising of type I AFPs in its sera) it was assumed that it too would contain AFP I.[28] However, further analysis by circular dichroism revealed an AFP completely unrelated. The isolated type IV protein revealed a primary sequence of 108 amino acid residues highly abundant in glutamine (17%). Furthermore, this antifreeze protein is highly helical and has four α-helices bundled together. [28]

1.1.1.v. Hyperactive AFPs from Insects (AFP V)

As early as 1968 there were reports in which *Tenebrio* larvae (of beetles) had antifreeze activity but it was not until 1997 when the antifreeze protein was successfully isolated and purified without loss of activity.[14] These proteins are termed as "hyperactive" due to their enhanced activity (100x) compared to fish and have 12 amino acid repeats highly concentrated in cysteine and threonine. Hyperactive AFPs have a relative molecular mass of 8,400 Da. Their physical properties will be further discussed and compared to fish AFPs in section 1.1.2.)

Table 2. Summary of antifreeze proteins found in nature. The organism from which they are isolated, their size, structure and key features are also tabulated.

	AFP I	**AFP II**	**AFP III**	**AFP IV**	**AFP V**
Species	Right-eye flounder, Sculpin	Sea raven, smelt, herring	Ocean pout, wolfish, eel pout	Longhorn sculpin	Beetle larvae
Mass (kDa)	3.3-4.5	11-24	6.5	12	8.3-12.5
Key Properties	Alanine rich	Disulfide bridges, Cysteine Rich	β-sandwich; flat globular	Alanine rich; α-helical bundle	Cysteine rich
Structure					

1.1.1.vi. Antifreeze Glycoproteins (AFGPs)

In 1971, DeVries and co-workers extracted the serum of Antarctic fish from which they isolated antifreeze glycoproteins with differing molecular weights. Gel electrophoresis revealed eight different glycopeptides later identified to contain alanine, threonine, galactose and *N*-acetylgalactoseamine.[10] Each antifreeze glycopeptides (1 through 8) have the same sugar moiety, but differ in the length of their peptide backbone. As seen in Figure 1, the carbohydrate component is a disaccharide (3-*O*-(*β*-D-galactosyl)-D-*N*-acetylgalactosamine) with a β-1,3 linkage[29] while the peptide backbone is a repeating tripeptide unit (Ala-Ala-Thr) where threonine's secondary hydroxyl group is glycosylated to the disaccharide. The difference in length is what classifies each AFGP into its own category (Table 3). AFGP 1 is the largest with 55 repeating tripeptide units and a molecular weight of 32 kDa while AFGP 8 is the smallest, with four tripeptide units and a molecular weight of 2.7 kDa. These AFGPs are numbered based on the decreasing molecular weights. [10, 30, 31] The AFGPs with small molecular weights (AFGP 7-8) sometimes have alanine residues replaced by proline and threonine replaced by arginine.[32] Typically, the larger the antifreeze glycoprotein (in terms of molecular weight) the better it is at exhibiting its antifreeze effects.

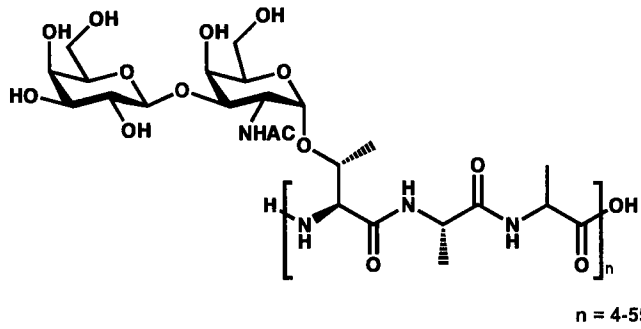

Figure 1. *General structure of antifreeze glycoproteins.* The Thr-Ala-Ala repeating tripeptide unit differs in length for each AFGP. The smallest AFGP 8 has 4 reapeating units while the largest (AFGP I) has 55.[33]

Table 3. AFGP sub-groups and their respective sizes in kDa. The larger the AFGP, the more effective and potent they are for antifreeze activity.[10, 30, 31]

AFGP	Molecular Weight (kDa)
AFGP 1	33.7
AFGP 2	28.8
AFGP 3	21.5
AFGP 4	17.0
AFGP 5	10.5
AFGP 6	5.0
AFGP 7	3.5
AFGP 8	2.6

1.1.2. Properties Associated with Antifreeze Activity

The biological antifreezes described in the previous sections are non-homologous and structurally dissimilar and although they share discrete similarities (i.e. high alanine composition), their diverse structural and amino acid contents are problematic for the determination of the exact mechanism of antifreeze activity Furthermore, the fact the AFPs are strictly composed of peptides and AFGPs contain carbohydrates suggests that they may bind to ice differently. Nevertheless, these

antifreeze molecules share the same properties which define their antifreeze activity; Namely, thermal hysteresis (TH) and ice recrystallization inhibition (IRI).

1.1.2.i. Thermal Hysteresis and Dynamic Ice Shaping (DIS)

As we know, the transition of liquid water to ice is dependant on temperature. At warmer temperatures (T > 0°C) water exists in its liquid state, but as it depresses past its freezing point (0°C), it transforms into a highly ordered crystal lattice forming ice. As the melting point and freezing point of water is the same, the conversion of liquid water to solid is dynamic in that the size of the ice crystal grows as temperature decreases beyond its freezing point, and shrinks as temperature approaches its melting point.

When electrolytes (i.e. NaCl) are present in water they have the ability of decreasing the freezing and melting point of water to the same extent (i.e. m.p. = f.p.) as they disturb water molecules from interacting with one another while trying to form the crystal ice lattice.

Likewise, antifreeze compounds have the ability to alter the freezing point of a solution. In the presence of AF(G)Ps, the freezing point depresses while the melting point remains unchanged and this difference between melting and freezing point temperatures is known as the *thermal hysteric gap*.[9] The three scenarios described above may be illustrated as in Figure 2.

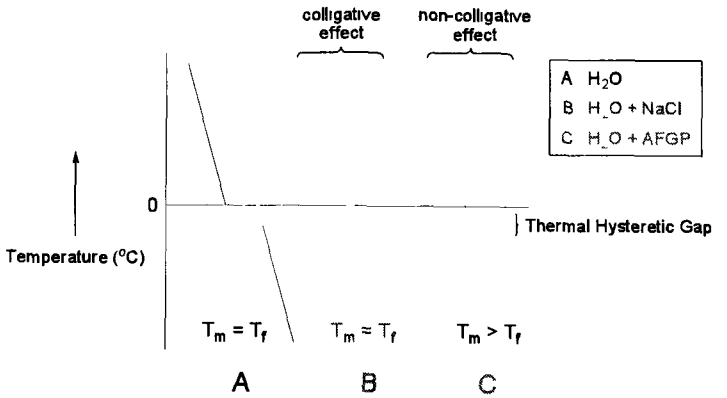

Figure 2. *Diagram depicting thermal hysteresis.* The black line (A) shows the melting and freezing point of water. The blue line demonstrates the colligative effects on water in the presence of NaCl and the red line represents the non-colligative effects of antifreeze compounds. The dashed red lines represent the difference between the melting and freezing point known as the thermal hysteric gap.

Thermal hysteresis (TH) values are a function of AF(G)P concentration.[34] At low concentrations the relationship is linear and as the concentration increases and becomes saturated, a plateau is reached. For fish AFPs, the TH value is typically above 1°C (Figure 3). As expected, these values vary from one organism to another.[34] Note that the hyperactive AFPs discussed in section 1.1.1. have a very large thermal hysteric gap of approximately 5.5°C which is four times greater than fish AFP.[14]

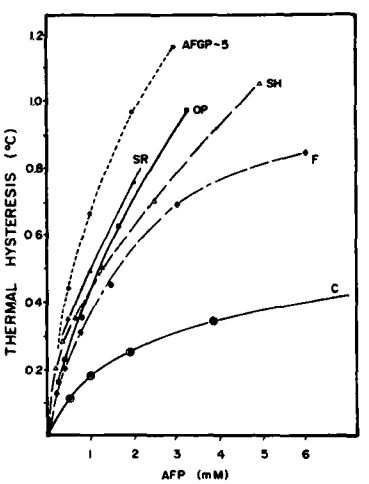

Figure 3. *AF(G)P thermal hysteresis (°C) as a function of concentration (mM).* At saturated concentrations, TH valued for most fish AF(G)Ps reach a plateau which is just over 1°C .[34]

Within this TH gap, the ice crystal with bound AF(G)Ps remains static in size and acquire a hexagonal bipyramidal morphology.[35] However, as the temperature decreases beyond the freezing point, the size of the crystal grows rapidly and expands into sharp needle-like crystals[34, 36] This shape is a result of AF(G)Ps preferential binding to the prism face, hindering the addition of water molecules and inhibiting its growth along the a-axis. As a result, water molecules are forced to add on to the basal plane, expanding in the direction of the c-axis (Figure 4).[34, 37]

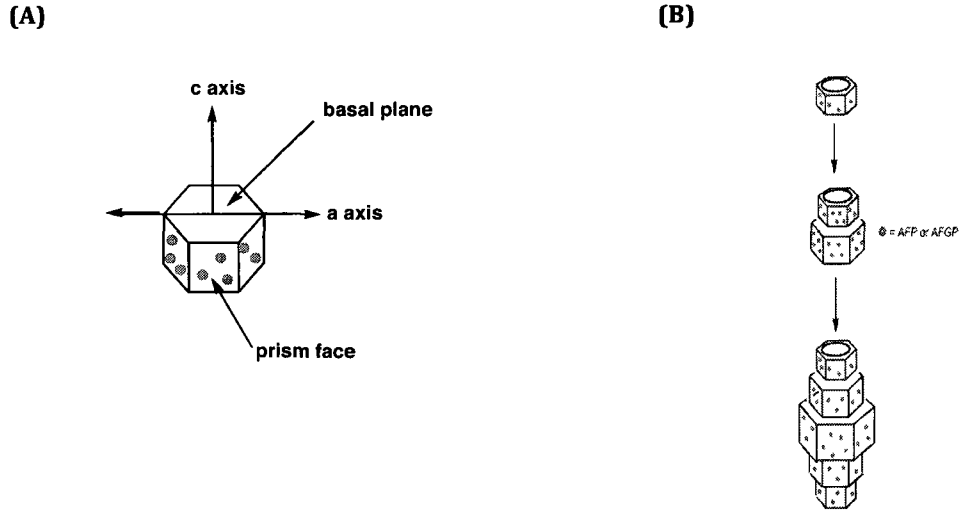

Figure 4. (A) *Representation of a hexagonal ice crystal.* The vertical arrow represents the direction in which ice grows. The AF(G)Ps preferentially bind to the prism face thus blocking its growth in the direction of the a-axis (horizontal lines). Additional water molecules add on the basal plane resulting in a hexagonal bipyramidal ice growth.[34] (B) *Ice growth along the c-axis.* AF(G)Ps (blue circles) bound to the prism face force water molecules to add on the basal plane and grow into sharp needle-like crystals.

This unique growth is associated with thermal hysteresis and is referred as *dynamic ice shaping*. Figure 5 illustrates the different morphologies taken by ice in the absence (A) and presence (B) of AFPs. As for the hyperactive AFPs produced by

insects, their shape is slightly different. Fish AFPs have a distinct hexagonal bipyramidal structure with flat well-defined facets, while insect AFPs have curved ends (Figure 5D). The difference in shape was attributed to hyperactive AFPs binding and recognizing various ice surfaces thereby increasing the frequency of binding and resulting in a distinguished crystal. Furthermore, the remarkable TH gap could also be due to closer spacing of the AFP onto the ice surface.[14]

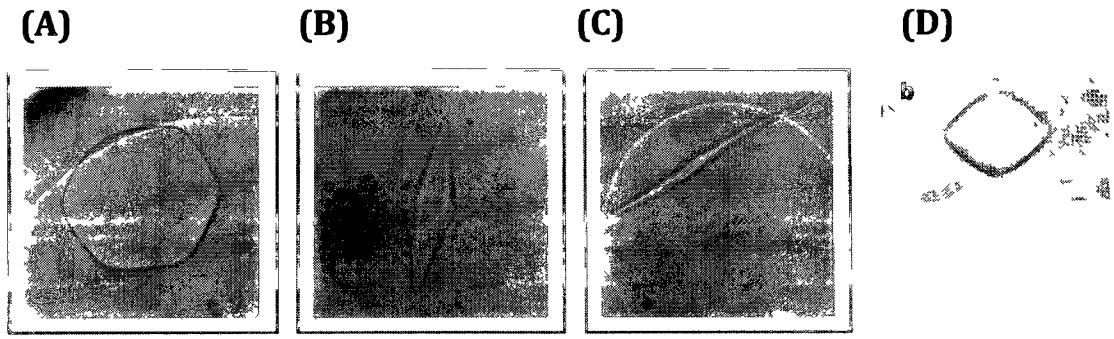

Figure 5. *Ice morphology in the presence and absence of antifreeze proteins.* (A) In the absence of AFP, ice crystal grown has a round/hexagonal shape as it grows along the a-axis. (B) In the presence of AFP, the crystal grown has a hexagonal bipyramidal shape due to the growth along the c-axis. (C) At elevated AFP concentrations, a sharp needle-like crystal is grown[34]. (D) Unusual morphology of ice in the presence of hyperactive AFPs.[14]

1.1.2.ii. Ice Recrystallization Inhibition (IRI)

In addition to its TH properties, AF(G)Ps are also capable of inhibiting ice recrystallization. In the absence of these antifreeze compounds, ice is capable of recrystallizing and growing into large crystals by combination of smaller ones. However, when AF(G)Ps are present, this process of recrystallization is inhibited. Figure 6 shows ice crystals at the same magnification.[31] Image A illustrates crystals grown in the presence of an AFGP8 solution (10 mg/ml) and image B shows crystals of a phosphate-buffered saline solution.

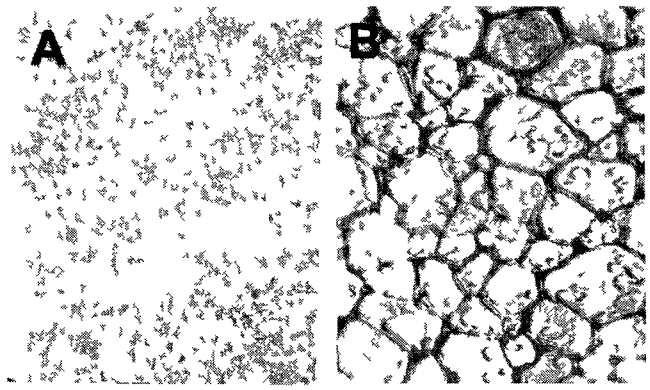

Figure 6. *Ice crystal images of an AFGP (A) and phosphate buffer saline (B) solution* The magnification of each image is the same. The small size of AFGP8 crystals in comparison to PBS indicates its ice recrystallization ability.

It is obvious from these images that the relative size of these crystals are quite dramatic and that the presence of antifreeze compounds greatly influences the size of the crystals. It had been previously believed that all antifreeze compounds in nature must possess both TH and IRI.[38] However, it is now evident that some biological antifreezes are capable of suppressing ice growth while exhibiting no TH activity.[13] Sidebottom et al. were the first to report such an AFP extracted from grass (*Lolium perenne*). They noted that their grass AFP had a significantly higher IRI activity than usual, as it was able to inhibit ice crystal growth at low concentrations (10μg/ml), which is 200 times less than type III AFP from the ocean pout. While this AFP had enhanced IRI, it showed no significant TH. The thermal hysteric gap that was measured was approximately 0.1°C which is considerably less than fish (1.0-1.5°C) and insect (5-6°C). What this may suggest, as others have as well,[39] is that ice recrystallization inhibition is likely to be the key property for cryoprotection. Since TH is associated with DIS, the hexagonal bipyramidal crystals formed could cause cell damage and be detrimental for cryoprotection.[40] Therefore, it is believed that

these AFPs are present to protect some insects from intracellular ice formation at extreme cold temperatures by allowing them to tolerate the formation of small ice crystals. [39]

1.2 Antifreeze Mechanism of Action

The way in which AF(G)Ps exhibit their TH activity is generally regarded as a *absorption-inhibition* mechanism.[30, 31, 37, 41, 42] It is believed that these biological antifreezes bind irreversibly to ice and prevent its growth and recrystallization. As mentioned earlier, AF(G)Ps differ greatly from one another structurally and the differences between these two classes of antifreeze compounds make it difficult to propose a joint mode of action. As AFGPs differ slightly in structure from one another and AFP I is easily synthesized, the structure of these two have been greatly studied and characterized. To this end, the exact mechanism of action is unknown but as AFP I and AFGPs share some similarities in terms of their mode of action, the explanation of how AF(G)Ps function is generally from the point of view of AFGP.

From a macroscopic point of view, these biological antifreezes are believed to attach irreversibly on the prism face of an ice crystal preventing the addition of water molecules.[33, 42] Once the AF(G)P is bound, additional water molecules may only be added between each antifreeze compound (Figure 7) which would eventually form a curved ice front to which more water molecules may be added. However, the accumulation of water molecules on the convex surface requires a lot of energy, making the addition of extra water molecules unfavourable.

Consequently, the freezing point depresses while the melting point remains unchanged giving rise to thermal hysteresis. This entire process is referred to as the *Kelvin Effect,* which can be illustrated (Figure 7) in one of two ways; the mattress model or the step pinning model.[31, 43]

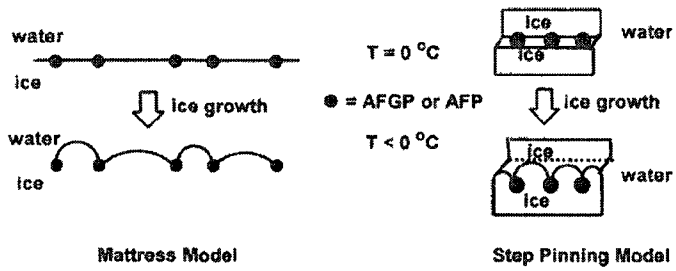

Figure 7. *The matress (2D) and step pinning model (3D) depicting the Kelvin Effect.* Both models illustrate the high degree of curvature formed between AF(G)P molecules. The curved ice front causes a freezing point depression while keeping the melting point unchanged thus giving rise to thermal hysteresis.[31]

Recent studies in fact indicate that these proteins bind irreversibly and that the binding site for AF(G)Ps is usually hydrophobic and topologically flat.[44]

The exact manner in which these antifreeze molecules bind is still unknown and since the ice-water interface is not well defined[31] researchers are delayed from determining the exact mode of action. In addition, the fact that each AFP is of a different structure suggests that they may each bind in a different manner.[30] For example, structurally related AFP type I proteins from the winter flounder and the sculpin both bind to the prism face but are more specifically located on different facets.[37] Nevertheless, structure-activity studies have been performed to elucidate certain aspects pertaining to the mechanism of action on a microscopic level.

1.3 Structure Activity Relationship Studies of AFPs & AFGPs

Most of the SAR studies performed has been to elucidate antifreeze activity in terms of TH. Since it was previously believed that TH and IRI are properties that work hand-in-hand, most of the focus had been on TH while IRI remained unexplored. Having said this, the next couple of sections cover SAR studies done to shed light on antifreeze activity based on TH and IRI.

1.3.1. SAR of Antifreeze Protein Type I

The research concerning AFPs has been based on AFP I due to its small size and simple construction via solid-phase peptide synthesis (SPPS). Many argue that the protein-ice adhesion is due to a hydrophilic effect (via hydrogen bonds) while others debate that it is related to a hydrophobic effect.[45]

Since AFP I of the Winter Flounder contains four threonine residues protruding from the same face of the α-helix, researchers believe that the secondary hydroxyl groups of these threonine residues are important for hydrogen bonding with the ice surface allowing for protein-ice adhesion (Figure 8).[44] This was also thought to be true since the calculated distance between each hydroxyl group participating in hydrogen bonding was 16.5 ± 0.5 Å matching well with the spacing of the oxygen atoms of water molecules on the surface of ice.[46, 47] Therefore, the surface containing these four threonine residues is referred to the "binding site".

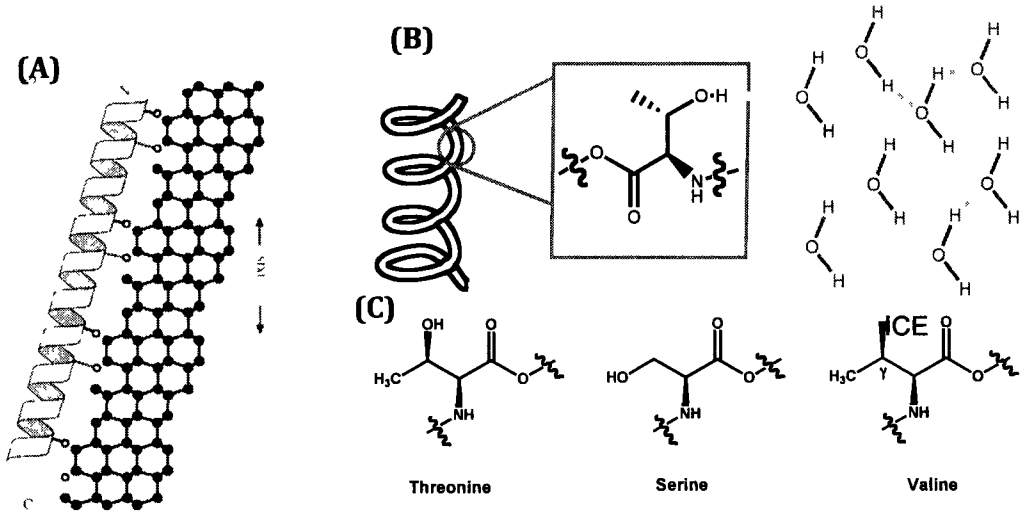

Figure 8. *AFP binding to ice via hydrogen bonding.* (A) Solid lines indicate hydrogen bonding from threonine and dashed lines are possible hydrogen bonds from aspartic acid or asparagine residues to oxygen atoms of water molecules.[44] (B) Closer view of threonine's hydrogen bonding capabilities to ice. (C) Site directed mutagenesis at positions 12 and 23 for AFP type I where threonine (native system), serine and valine were the amino acids of choice. These point mutations were performed to elucidate antifreeze activity.

To test this hydrophilic effect, the two middle threonine residues (T12 and T23) were replaced by serine which resulted in a mutant AFPI that had nearly lost all of its activity.[45] This was an unexpected result due the assumption that serine's primary alcohol could hydrogen bond in a similar fashion to threonine. Although the replacement of two threonine residues with serine abolished TH, the presence of two threonine amino acids (T2, T35) on the hydrophilic face along with Asx (aspartic acid or asparagine) does not rule out the effects of hydrogen bonding on antifreeze activity. Instead, what is generally accepted is that hydrogen bonding may work hand in hand with non-polar interactions to prevent ice growth.[47] Interestingly, when threonine was replaced by valine (to conserve the β-methyl group), comparable activity was observed to the native winter flounder AFPI. What

this suggests is that the methyl groups of threonine may be contributing to ice binding. [44]

These results then gave rise to a whole new argument on how AFP type I binds to ice, being the hydrophobic effect. Since the hydrophilic surface of AFP type I isoforms has variable residues and the hydrophobic surface is highly conserved of alanine, it was believed that the conserved residues are of greater importance with respect to ice binding.[44] To test this hypothesis, the first experiment conducted had certain alanine residues replaced by leucine. It was believed that some of these substitutions (on the hydrophobic face) would hinder AFPI from contacting the ice surface due to leucine's longer side chain. When these analogues were tested for TH, it was found that the alanines residing on the *hydrophilic* surface, which were replaced with leucine (A19L and A20L), had little loss in activity and produced a wild-type crystal, while those replaced on the *hydrophobic* surface (A17 and A21) were completely inactive. Therefore, this suggests that antifreeze activity is reflective of a hydrophobic effect. Some speculate that the secondary hydroxyl groups are not enough and that they merely work with the hydrophobic residues to promote ice adhesion.[45, 47] The conclusions that were drawn from the above experiment were that the conserved alanine residues on the hydrophobic surface are essential for ice binding and although the alanine residues are among threonines, they are not extended to neighbouring hydrophilic asparagines, thus suggesting that the β-methyl group of threonine is of greater importance than its adjacent hydroxyl. [44]

Table 4. Series 1 and 2 AFP I Winter Flounder Mutant Peptides. Highlighted in red are the important mutations at positions 2, 13, 24 and 35 where threonines are usually found and highlighted in blue are the incorporated salt bridges.

	Code Name	Sequence
Series 1	TTTT	D TASDAAAAAAL TAANAKAAAEL TAANAAAAAAA TAR-CONH$_2$
	SSSS	D SASDAAAAAAL SAANAKAAAEL SAANAAAAAAA SAR-CONH$_2$
	TSST	D TASDAAAAAAL SAANAKAAAEL SAANAAAAAAA TAR-CONH$_2$
Series 2	TTTT2KE	D TASDAKAAAEL TAANAKAAAEL TAANAKAAAEA TAR-CONH$_2$
	SSSS2KE	D SASDAKAAAEL SAANAKAAAEL SAANAKAAAEA SAR-CONH$_2$
	VVVV2KE	D VASDAKAAAEL VAANAKAAAEL VAANAKAAAEA VAR-CONH$_2$
	AAAA2KE	D AASDAKAAAEL AAANAKAAAEL AAANAKAAAEA AAR-CONH$_2$
	GGGG2KE	D GASDAKAAAEL GAANAKAAAEL GAANAKAAAEA GAR-CONH$_2$

Other researchers like Harding and Haymet have also taken interest in the hydrophobic effect. Their research involved the synthesis of mutant AFP I polypeptides classified in two categories – series 1 and 2 (Table 4, above).

The mutants within these series differ from the above experiment in that most have all four threonines (positions 2, 13, 24 and 35) on the hydrophilic binding site replaced by either glycine, alanine, valine or serine. The goal for these experiments was to reassess the role and importance of the threonine residues.[48] As seen in Table 4, series 1 peptides have all or two threonines replaced with serine

while series 2 peptides have all four threonines replaced by various residues and have two additional salt bridges (K7, E11 and K29 and E33).

The general trend observed was that the mutants with non-polar valine (VVVV2KE) and alanine (AAAA2KE) residues exhibited antifreeze activity (i.e. thermal hysteresis) comparable to the native system (TTTT), while mutants with polar residues such as serine (SSSS2KE) and glycine (GGGG2KE) showed loss of hysteresis.[48] The published data to show this trend is seen in Figure 9. As mentioned, hexagonal bipyrimidal crystals are characteristic of AFPs and AFGPs. Thus, video microscopy was carried out to see how series 2 mutants influence this property. As seen in Figure 10, images a to d represent the ice shaping of TTTT, TTTT2KE, VVVV2KE, and AAAA2KE, respectively. The shape of each crystal (a-d) is similar to the native system (TTTT) indicating that mutant AFPs are bound the ice surface in a similar fashion to the native system and are influencing the direction in which ice grows.

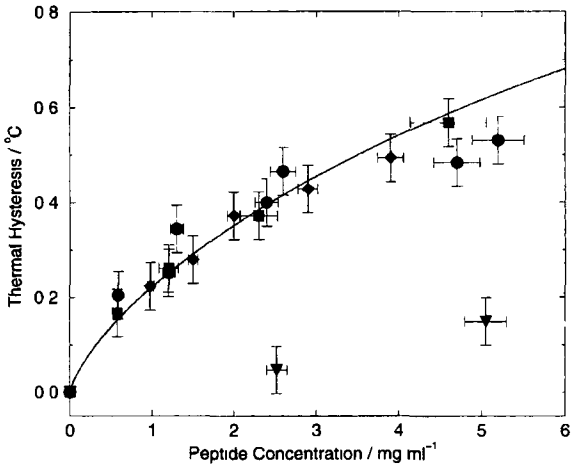

Figure 9. *Measured thermal hysteresis of series 2 mutants at concentrations of 0 to 6 mg/mL.* Solutions of TTTT (sqaures), TTTT2KE (diamonds), VVVV2KE (circles), AAAA2KE (triangles) were tested using a nanoliter osmometer. Note: No thermal hysteresis was observed for any serine or glycine substituted analogs. As the peptide concentration increases, so does the thermal hysteresis gap.[48]

Although the exact mechanism of action to inhibit ice growth is not known, the experiments described on the previous page also suggest the hydrophobic residues (i.e. β-methyl of Thr) are of greater importance than the hydroxyl group (which was believe to hydrogen bond to ice).

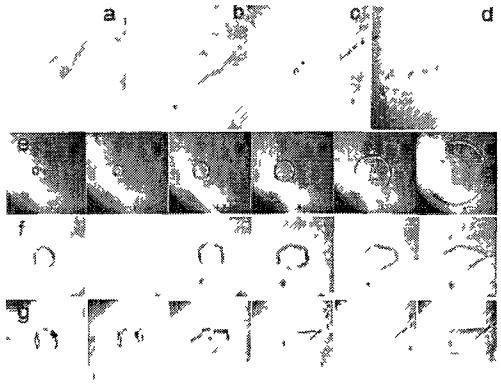

Figure 10. *Ice shaping images of series 1 and 2 mutants.* Hexagonal Bipyrimidal crystal of: (a) TTTT, native AFP I (~5mg/mL), (b) TTTT2KE (4 mg/mL), (c) VVVV2KE (10 mg/mL) and (d) AAAA2KE (5 mg/mL). (e) to (g) are still images taken at intervals over a period of 1 minute of : (e) GGGG2KE (10 mg/mL), (f) TTTT2KE (4 mg/mL) and (g) VVVV2KE (10 mg/mL). Note that GGGG2KE mutant has no TH activity and could not produce a hexagonal bipyramidal shaped crystal.[48]

1.3.2. SAR of AFGPs

Antifreeze glycoproteins have been explored in a variety of ways to determine the importance of their functional groups for TH and IRI. Earlier studies focused on the effects for TH only and not IRI. The revelation that TH and IRI are independent of one another has thus intrigued researchers to probe into its effects for ice recrystallization inhibition.

1.3.2.i. SAR studies of AFGPs for TH Activity

The activity and binding of AFGP to ice has been proposed to be a result of the hydroxyl groups of the saccharide moiety. This hypothesis was thus explored in the early 1970s via SAR experiments performed by DeVries et al. (Figure 11). One of the earliest SAR studies was the enzymatic treatment of AFGP with D-galactose oxidase to oxidize the C6 hydroxyls to aldehydehes. The analogue produced had retained TH activity, implying that the C6 hydroxyl was not crucial for TH.[49] On the other hand, when the C3 and C4 hydroxyls were investigated, the opposite was seen. These hydroxyls appeared to be crucial as the formation of a borate complex resulted in diminished activity.[50] Similarly, the oxidative cleavage of the terminal galactose using sodium periodate afforded two aldehydes at C3 and C4 forming an analogue with abolished TH.[11] Acetylation of all hydroxyl groups further confirmed their importance as it abolished TH while deacetylation reinstated antifreeze activity.[49] Apart from these studies, the disaccharide moiety is also important for TH

as the exposure of AFGP to basic conditions (NaOH) at elevated temperatures cleaves the carbon-oxygen bond at the anomeric position thereby eliminating antifreeze activity.

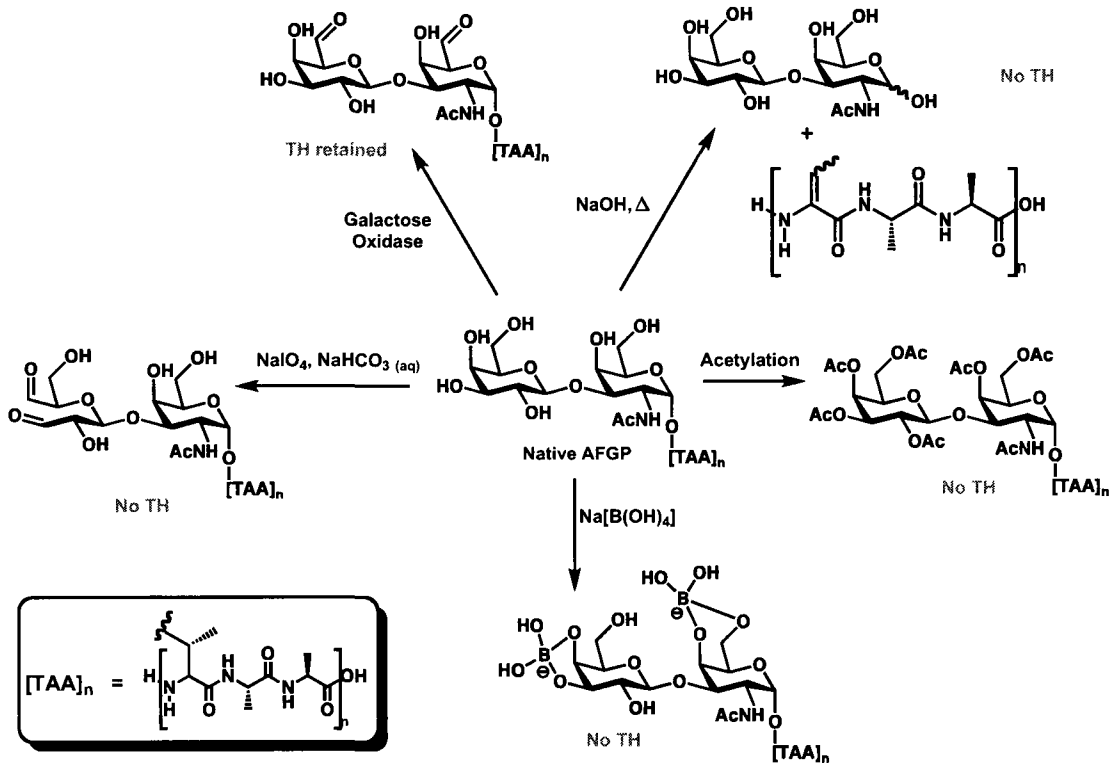

Figure 11. *Early SAR studies to determine the importance of the hydroxyl groups of AFGPs.* Antifreeze activity for these studies was defined by TH activity.

Recent studies performed by Nishimura et al. further elucidates the structural motifs that are important for ice binding, and TH.[51] His research group reported 16 AFGP analogues differing in chain length, conformation and oligosaccharides which were all tested and imaged for TH and DIS. These analogues have led to the following conclusions: antifreeze activity is dependent on the chain length of the polypeptide backbone, where an increase in length results in greater

activity. Nishimura's results also implicate that the presence of a NHAc at C2, an α glycosidic linkage, and a β-methyl group provided by threonine are all essential to antifreeze activity.

1.3.2.ii. SAR studies of AFGPs for IRI Activity

Since TH was better understood than IRI, researchers in the past have been trying to determine the factors affecting it rather than focusing on IRI. Thus, the experiments described above were done based on TH activity alone. Nearly a decade ago, the discovery of an AFP (from ryegrass) possessing only IRI changed the view where TH and IRI are correlated to one another,[13] leading researchers to believe that IRI may be the more important property for cryoprotection.

The factors affecting IRI have been studied and much like TH studies, SAR was done to determine the key features influencing ice recrystallization. AFGP analogues explored had many structural variations in comparison to the native system and are illustrated below in Figure 12.

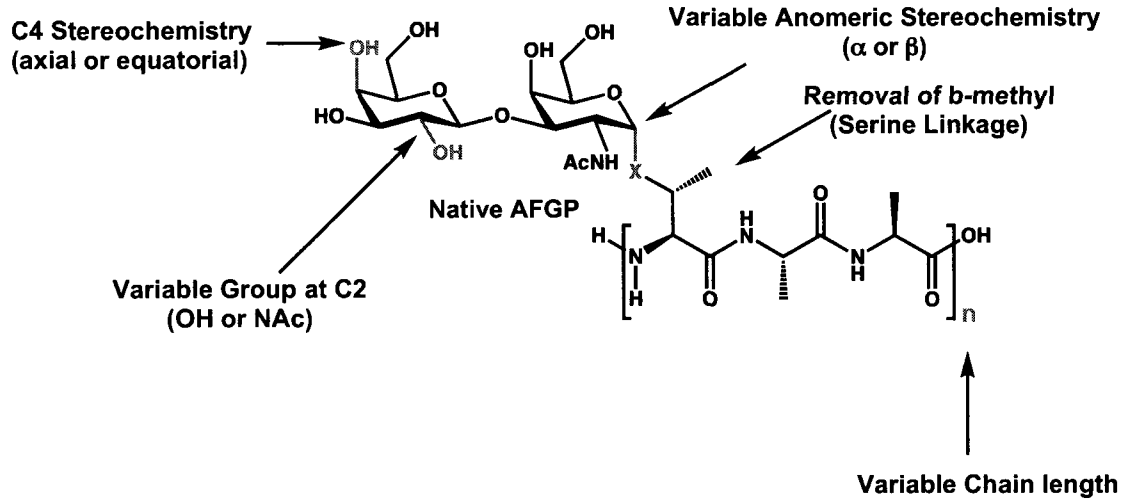

Figure 12. *Structural variations explored relative to the native AFGP and tested for IRI.*

Such variations include the stereochemistry of the hydroxyl at C4, the linker atom at the anomeric position (Figure 12, X = O or C), the removal of the β-methyl group, the length of the polypetide chain, and the use of a monosaccharide rather than a disaccharide.

It was observed that the stereochemistry at C4 was crucial for IRI as an inverted stereochemistry would result in a loss of activity. More specifically, OGG Gal (Figure 13, compound **1**) showed very good IRI activity in comparison to OGG Glc (**2**) indicating a necessity for a C4 hydroxyl in the axial position.[52]

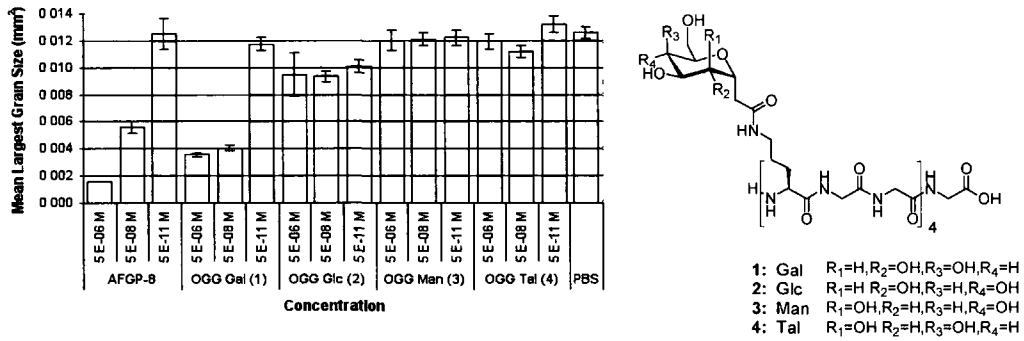

Figure 13. *IRI results of C-linked analogs (**1**-**4**).* These analogs are compared to AFGP8 and PBS, the negative control. The smaller the value for the mean grain size (mm^2) the greater the activity

In addition to the importance of C4 for activity, the length of the chain between the carbohydrate and peptide moiety has also been noted to be an important factor. For the C-linked amide analogs, either an ornithine (Figure 14, compound **5**) or lysine (**6**) linker established the length of the chain. The mean grain size of these analogues revealed that an increase in chain length (lysine linker, compound **6** in figure 14) in fact diminished IRI activity.

Other C-linked analogs have also been synthesized and assayed. *C*-linked alkyl derivatives (also referred to as C-serine) with varying chain length (n = 1,2,3) have given positive results in terms of preventing the growth of ice. When n = 1 (compound **3**, Figure 14) good ice recrystallization inhibition was observed, but as the chain length grew, the mean grain size of the crystal increased thereby resulting in reduced IRI activity (Figure 14).[53]

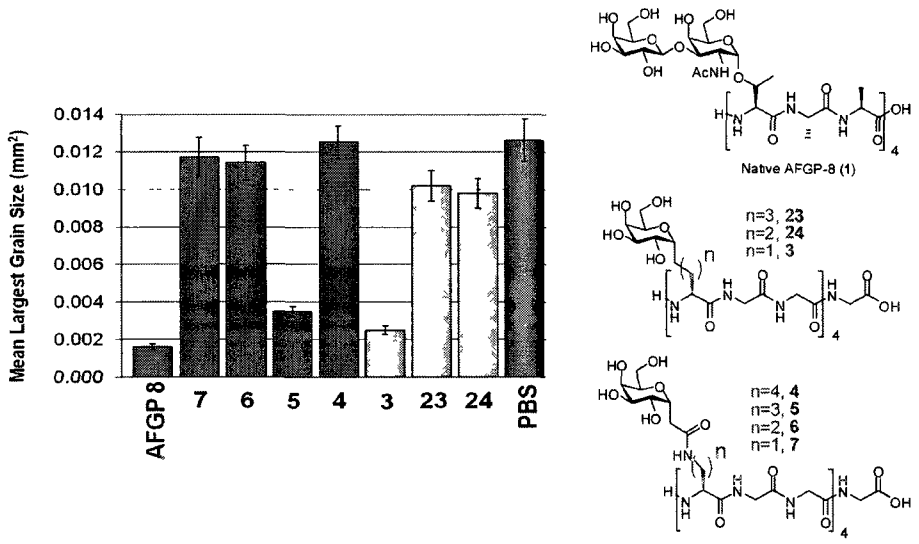

Figure 14. *C-serine analogs synthesized and tested for recrystallization inhibiton.* All analogs are compared to AFGP8 (positive control) and PBS (negative control). Antifreeze activity diminished as the chain length increases. *C*-Serine analog **3** (n = 1) has comparable activity to AFGP8.[53]

1.4 Hydration

Many biological processes involve water and as it is ubiquitous it is not surprising that it may play a key role in antifreeze activity. The "hydration layer" has been defined as water molecules, which tightly surround a macromolecule (protein, carbohydrate, nucleic acid).[40, 54] To understand hydration of AF(G)Ps, it is important to have a general understanding of protein and carbohydrate hydration.

1.4.1. Hydration of Proteins

As early as the 1960's, water was recognized as a key aspect for protein stability.[55] Although protein-water interactions are not well understood, it is known

that the absence of water causes a protein to lose its three-dimensional structure thereby abolishing its specific activity.[54, 56-58] This detrimental outcome arises as water or an aqueous environment provides a protein its conformational flexibility allowing for mobility and movement. Apart from providing structural stability, water occurs in hydrogen bonding networks and screens for electrostatic interactions, which also may account for a protein or enzyme's activity.[56] Furthermore, the hydrogen bond structure around the protein is quite delicate and any disruption in this layer will equally affect the conduct of a protein (discussed in 1.3.3. for antifreeze activity). Although not much is known of protein-water interactions, what is apparent is the dynamic nature of surrounding water molecules and how it plays a vital role for protein function.

1.4.2. Hydration of Carbohydrates

Just as protein hydration is important for mediating biological functions, hydration of carbohydrates has also been recognized as a significant entity for molecular recognition, solution conformation and biological activity.[52] Assessing the hydration of carbohydrates has been proven to be difficult, but over the last few decades various experimental studies have been employed to better understand this property. Galema and co-workers have studied the hydration of commercially available monosaccharides and have determined their partial molar volumes and isentropic partial molar compressibility by use of MD simulations, kinetic

experiments and density and ultrasound measurements.[59] The results of these studies shed light on hydrated carbohydrates and how they occupy space and are compatible with the three-dimensional hydrogen-bonding network of bulk water. The results obtained indicate what has been known before, that hydration is influenced by the stereochemistry of the hydroxyl groups and that the preferred conformation is equatorial rather than axial.[60] D-mannose, D-talose, D-glucose and D-galactose were the sugars studied by Galema, and their partial molar compressibilities are shown in Figure 15. The main difference between each sugar is the stereochemistry at C2 and C4. A low molar compressibility indicates poor hydration as the sugar is not compatible with water and disrupts the hydrogen-bonding network. D-Talose had the highest value, indicating that it is well hydrated and fits well with the 3D structure of water, while D-galactose proved to be the to be the opposite.

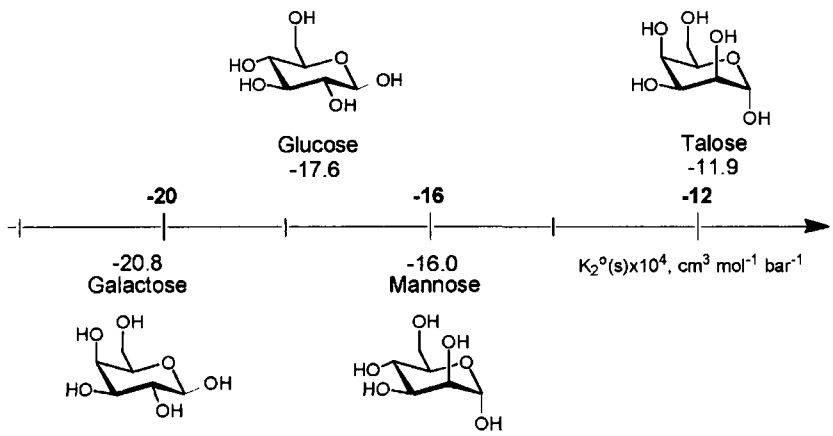

Figure 15. *Partial molar compressibilities of monosaccharides in aqueous solution at 25°C.* These monosaccharides differ in stereochemistry at C2 and C4 giving a wide range of values. The larger values represent monosaccharides which fit well with water.

1.4.3. Hydration and Antifreeze Activity

Hydration has been extensively studied in recent years as it may explain biological processes and how proteins and carbohydrates behave. In terms of antifreeze activity, water molecules surrounding AFGPs analogs have been seen to orientate the carbohydrate moiety differently for α-D-GalNac-Ser and α-D-GalNac-Thr. It was originally believed that hydrogen bonds between the peptide and sugar moieties dictate conformation, however recent studies imply that this is no longer true and that surrounding water molecules are likely the dominating factor. This will further be discussed in section 2.2.

Hydration of carbohydrates is also believed to play a role in IRI. Recall in the previous section, the value of molar compressibility of galactose (-20.8) is small, which implies a poor fit with the three-dimensional hydrogen-bonding network of water. It is believed that this poor compatibility disrupts water molecules to interact and form a stable ice lattice thereby inhibiting ice growth.

Furthermore, a recent publication by Nutt and Smith recognize the influence of the hydration layer around AFPs for ice binding.[42] Atomistic molecular dynamics simulations have shown that when AFP is in aqueous solution, the solvation shell is more structured and less dynamic around the ice-binding face while unorganized around the non-binding sites. The highly ordered region is suggested to overlap

well with the ordered ice surface (between bulk ice and bulk water) thereby incorporating the ordered solvation shell to ice and having the AFP bound. In addition, the hydration of AFPs has been suggested to protect AFPs from engulfment during ice growth. As the first hydration shell is organized, the second and third shells have been observed to have faster dynamics. This suggests that the dynamic and disrupted hydration shells would fail to form hydrogen bonds with surrounding water molecules thereby preventing its addition and ice growth.[42] Figure 16 illustrates this "pre-ordering-binding" mechanism.

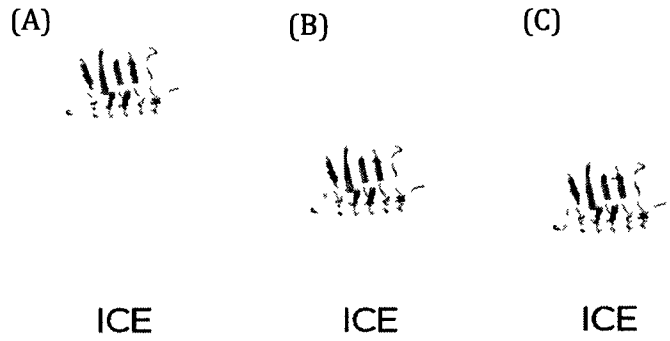

Figure 16. *Hydration and ice-binding.* (A) The turquoise region represents highly ordered ice-water and protein-water interfaces while the light blue region represents unordered and disrupted water. It is believed that the surface of the ordered ice is brought to the protein rather than the protein binding to the ice. (B) The highly ordered regions are incorporated together allowing for protein-ice binding. (C) Once bound, the surrounding water molecules are mobile and have fast dynamic protecting the protein from being overgrown by ice.[42]

Antifreeze compounds are of great interest due to their varied applications. Commercially, such compounds may be used as preservatives for frozen foods in order to improve their quality and texture during freezing and thawing.[61] As for

medical purposes, it had been confirmed that certain antifreeze compounds and concentrations may either protect or injure cells and tissue. As such, these compounds have been use as cryoprotectants and preservatives for cells or for non-invasive cryosurgical techniques to treat cancer. [62-64] For these diverse reasons, the synthesis of an antifreeze compounds possessing only IRI has gained a large degree of interest. This thesis will therefore enclose the synthesis of a potentially active fluorinated antifreeze protein and the results obtained from assaying each AFP for TH and IRI.

1.5 References

1. Perutz, M. F.; Rossmann, M.G.; Cullis, A.F.; Muirhead, H.; Will, G. *Nature* **1960,** *185*, 416-422.

2. Schweizer, J. *J. Cell. Biol.* **2006,** *174*, 169-174.

3. Kull, J. F.; Sablin, E.P.; Lau, R.; Fletterick, R.J.; Vale, R.D. *Nature* **1996,** *380*, 550-555.

4. Melloul, D.; Marshak, S.; Cerasi, E. *Diabetologia* **2002,** *45*, 309-326.

5. Fischer, G.; Wittmann-Liebold, B; Lang, K.; Kiefhaber, T.; Schmid, F.X. *Nature* **1989,** *337*, 476-478.

6. Yang, F.; Lum, J.B.; McGill, J.R.; Moore, M.C.; Naylor, S.L.; van Bragt, P.H.; Baldwin, W.D.; Bowman, B.H. *Proc. Natl. Acad. Sci. USA* **1984,** *81*, 2752-2756.

7. Di Lullo, G. A.; Sweeney, S.M.; Korkko, J.; Ala-Kokko, L.; San Antonio, J.D. *J. Biol. Chem.* **2002,** *277*, 4223-4231.

8. Scholander, P. F.; Flagg, W.; Walters, V.; Irving, L. *Physiol. Zool.* **1953,** *26*.

9. Scholander, P. F.; Maggert, J.E. *Cryobiology* **1971,** *8*, 371-374.

10. DeVries, A. L.; Komatsu, S.K.; Feeney, R.E. *J. Biol. Chem* **1970,** *245*, 2901-2908.

11. Komatsu, S. K.; DeVries, A.L.; Feeney, R.E. *J. Biol. Chem.* **1970,** *245*, 2909.

12. DeVries, A.L., Vandenheede, J.; Feeney, R.E. *J. Biol. Chem.* **1971,** *246*, 305-308.

13. Sidebottom, C.; Buckley, S.; Pudey, P.; Twigg, S.; Jarman, C.; Holt, C.; Telford, J.; McArthur, A.; Worrall, D.; Hubbard, R.; Lillford, P. *Nature* **2000,** *406*, 256.

14. Graham, L.A.; Liou, Y-C.; Walker, V.K.; Davies, P.L. *Nature* **1997,** *388*, 727-728.

15. Grather, S.; Kuiper, M.J.; Gagné, S.; Walker, V.K.; Jia, Z.; Sykes, B.D.; Davies, P.L. *Nature* **2000,** *406*, 325-328.

16. Graham, L. A.; Davies, P.L. *Science* **2005,** *310*, 461.

17. Gilbert, J. A.; Hill, P.J.; Dodd, C.E.R.; Laybourn-Parry, J. *Microbiology* **2004,** *150*, 171-180.

18. Duman, J. G.; DeVries, A.L. *Comp. Biochem. Physiol.* **1976,** *54B*, 375-380.

19. Davies, P. L.; Sykes, B.D. *Curr. Opin. Struct. Biol.* **1997,** *7*, 828-834.

20. Ananthanarayanan, V. S.; Hew, C.L. *Biochem. Biophys. Res. Commun.* **1977,** *74*, 685-689.

21. Yang, D. S. C.; Sax, M.; Chakrabartty, A.; Hew, C.L. *Nature* **1988,** *333*, 232-237.

22. Yeh, Y.; Feeney, R.E. *Chemical Reviews* **1996,** *96*, 601-618.

23. Patterson, J. l.; Duman, J.G. *J. Exp. Zool.* **1982,** *219*, 381.

24. Hew, C. L.; Kao, M.H.; So, Y.S.; Lim, K.P. *Can. J. Zool.* **1983,** *61*, 2324.

25. Harding, M. M.; Anderberg, P.; Haymet, A.D.J. *Eur. J. Biochem.* **2003,** *270*, 1381-1392.

26. Jia, Z. C.; Deluca, C.I.; Davies, P.L. *Protein Sci.* **1995,** *4*, 1236-1238.

27. Sönnichsen, F. D.; Sykes, B. D.; Chao, H. *Science* **1993,** *259*, 1154-1157.

28. Deng, G.; Andrews, D.W.; Lauresen, R.A. *FEBS lett.* **1997,** *402*, 17-20.

29. Vandenheede, J. R.; Ahmed, A.I.; Feeney, R.E. *J. Biol. Chem.* **1972,** *247*, 7885-7889.

30. Knight, C. A.; Driggers, E.; DeVries, A.L. *Biophys J.* **1993,** *64*, 252-259.

31. Bouvet, V.; Ben, R.N. *Cell Biochem. Biophys.* **2003,** *39*, 133-144.

32. Morris, H. R.; Thompson, R.; Osuga, D.T.; Ahmed, A.I. *J. Biol. Chem.* **1978,** 5155-5162.

33. Ben, R. N. *Chembiochem* **2001,** *2*, 161-166.

34. Davies, P. L.; Hew, C.L. *The FASEB Journal* **1990,** *4*, 2460-2468.

35. Wilson, P. W.; Beaglehole, D.; DeVries, A.L. *Biophys J.* **1993,** *64*, 1878-1884.

36. Raymond, J. A.; DeVries, A.L. *Crybiology* **1972,** *9*, 541-547.

37. Knight, C. A.; Cheng, C.C.; DeVries, A.L. *Biophys J.* **1991,** *59*, 409-418.

38. Hall, D. G.; Lips, A. *Langmuir* **1999,** *15*, 1905-1912.

39. Knight, C. A.; Duman, J.G. *Cryobiology* **1986,** *23*, 256-262.

40. Tam, R. Y.; Fereirra, S.S.; Czechura, P.; Chaytor, J.L.; Ben, R.N. *J. Am. Chem. Soc.* **2008,** *130*, 17494-17501.

41. Raymond, J. A.; DeVries, A.L. *Proc. Natl. Acad. Sci. USA* **1977,** *74*, 2589-2593.

42. Nutt, D. R.; Smith, J.C. *J. Am. Chem. Soc.* **2008,** *130*, 13066-13073.

43. Knight, C. L. *Nature* **2000,** *406*, 249-251.

44. Davies, P.L.; Baardsnes, J. K.; M.J.; Walker V.K. *Phil. Trans. R. Soc. Lond. B.* **2002,** *357*, 927-935.

45. Chao, H.; Houston M.E. Jr.; Hodges, R. S.; Kay, M.K.; Sykes, B.D.; Loewen, M.C.; Davies, P.L.; Sönnichsen, F.S. *Biochem.* **1997,** *36*, 14652-14660.

46. Ewart, K. V.; Lin, Q.; Hew, C.L. *Cell. Mol. Life Sci.* **1999,** *55*, 271-283.

47. DeVries, A. L.; Lin, Y. *Biochim. Biophys. Acta* **1977,** *495*, 388-392.

48. Haymet, A. D. J.; Ward, L.G.; Harding, M.M. *J. Am. Chem. Soc.* **1999,** *121*, 941-948.

49. Ahmed, I. A.; Osuga, D.T.; Feeney, R.E. *J. Biol. Chem.* **1973,** *248*, 8524-8527.

50. Ahmed, I. A.; Yin, Y.; Osuga, D.T.; Feeney, R.E. *J. Biol. Chem.* **1977,** *251*, 3033-3036.

51. Tachibana, Y.; Fletcher, G.L.; Fujitani, N.; Tsuda, S.; Monde, K.; Nishimura, S.I., *Angew. Chem. Int. Ed.* **2004,** *43*, 856-862.

52. Czechura, P.; Tam, R.Y.; Dimitrijevic, E.; Murphy, A.V.; Ben, R.N. *J. Am. Chem. Soc.* **2008,** *130*, 2928-2929.

53. Tam, R.Y.; Rowley, C.N.; Petrov, I.; Zhang, T.; Afagh, N.A.; Woo, T.K.; Ben, R.N. *J. Am. Chem. Soc.* **2009,** *131*, 15745-15753.

54. Frauenfelder, H.; Fenimore, P.W.; McMahon, B.H. *Biophys. Chem.* **2002,** *98*, 35-48.

55. Franks, F. *Biophys. Chem.* **2002,** *96*, 118-127.

56. Levy, Y.; Onuchic, J.N. *Proc. Natl. Acad. Sci. U.S.A.* **2004,** *101*, 3325-3326.

57. Pal, S. K.; Zewail, A.H. *Chem. Rev.* **2004,** *104*, 2099-2123.

58. Zhang, L.; Wang, L.; Kao, Y.T.; Qiu, W.; Yang, Y.; Okobiah, O.; Zhong, D. *Proc. Natl. Acad. Sci. U.S.A.* **2007,** *104*, 18461-18466.

59. Galema, S.; Howard, E.; Engberts, J.B.F.N.; Grigera, J.R. *Carbohydr. Res.* **1994,** *265*, 215-225.

60. Uedaira, H.; Ikura, M.; Uedaira, H. *Bull. Chem. Soc. Jpn.* **1989,** *62*, 1-4.

61. Griffith, M; Ewart, K.V. *Biotechnol. Adv.* **1995,** *13*, 375-402.

62. Hammerstedt, R. H.; Graham, J. K.; Nolan, J. P. *J. Androl.* **1990,** *11*, 73-88.

63. Koushafar, H.; Pham, L.; Lee, C.; Rubinsky, B. *J. Surg. Oncol.* **1997,** *66*, 114-121.

64. Pham, L.; Dahiya, R.; Rubinsky, B. *J. Surg. Oncol.* **1999,** *38*, 1-7.

Chapter 2: Research Goals and Objectives

There are several non-homologous biological antifreezes that exist in nature which share the same unique property of binding to ice and inhibiting its growth and recrystallization. This distinct property has sparked the interest of many in the medical, biotechnological, commercial and industrial fields as these types of compounds can be used for cryopreservation, cryosurgery and food storage.[1, 2] As previously mentioned, biological antifreezes can be isolated from plants[3] and insects,[4] but the most extensively studied AFGP and AFP are of the teleost fish and the winter flounder, respectively. Unfortunately, the cost and time associated with the isolation and purification of these biological antifreezes is a constraint and a new method such as chemical synthesis is required for producing these antifreeze compounds.

While AFPs differ greatly in their primary sequences and three-dimensional structures, the chemical synthesis of various analogues allows one to determine which factors contribute to the prevention of ice growth and how these properties can be optimized. With respect to AFGPs, various analogues have also been studied which shed light on their mode of action. These analogues and their properties will be discussed in the next section (2.1).

The scope of my research, as will be discussed in greater detail, involves the synthesis of fluorinated AFPs and AFGPs, and determining their respective antifreeze activities with respect to thermal hysteresis (TH) and ice recrystallization inhibition (IRI) in an effort to understand the mechanism of action

of these processes. In order to do this, the synthesis of a trifluorinated threonine building block (denoted as **T(F)**) was necessary to allow for solid-phase peptide synthesis (Scheme 1). The importance of the methyl group of threonine in AF(G)Ps (section 1.2.1 and 2.1) and the chemical properties of fluorine have greatly influenced the direction of this research which will be discussed within this chapter.

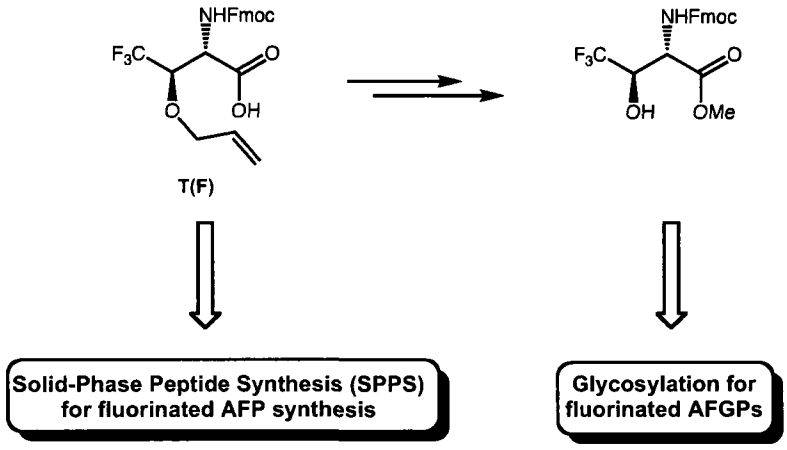

Scheme 1. *Synthesis of **T(F)** building blocks for the construction of fluorinated AF(G)Ps.*

2.1 The Importance of the Threonine Methyl Group in the AFGP Mechanism of Action

As mentioned in section 1.2.1, threonine's methyl group plays an important role in type I AFPs for the prevention of ice growth in biological systems (i.e. due to hydrophobic interactions). Recent molecular dynamic simulation studies of *N*-acetyl galactose-peptide model systems **10** and **11** (Scheme 2) by Corzana and co-workers[5] show that the methyl group of the threonine has a large influence on the conformation of the glycosidic linkage of the glycopeptide. It is well precedented

that the three-dimensional orientation of the carbohydrate moiety differs among glycopeptides that have different linkers (i.e. threonine or serine).[6-8] Also, it has been understood that when threonine is the linker, the presence of the methyl group restricts rotation around the glycosidic bond and alters the torsion angle in comparison to the serine analogue; the torsion angle for α-D-GalNHAc-Thr is 120° and for α-D-GalNHAc-Ser it is 180°.[5] It was previously believed that glycopeptides had their respective conformations due to intramolecular hydrogen bonds between the carbohydrate and peptide moiety.[9] Mimura and co-workers were the first to propose this and suggest that a hydrogen bond between the amide hydrogen of the C2-NHAc group with the carbonyl of the *O*-linked threonine occurs (Scheme 3). Although hydrogen bonding was observed for analogue **11**, it was never detected for the serine analogue **10**.[10] In addition to these results, Corzana and co-workers were not able to detect NOEs between the *N*-acetyl group of GalNHAc and the methyl group of threonine **11**. Thus, they concluded that although there may be hydrogen bonding, it is too weak to promote conformational changes and that other factors must be responsible.[10]

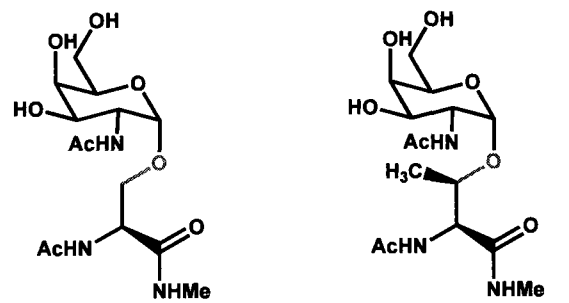

Scheme 2. *Glycopeptides used for conformational studies by Corzana et al.*[5]

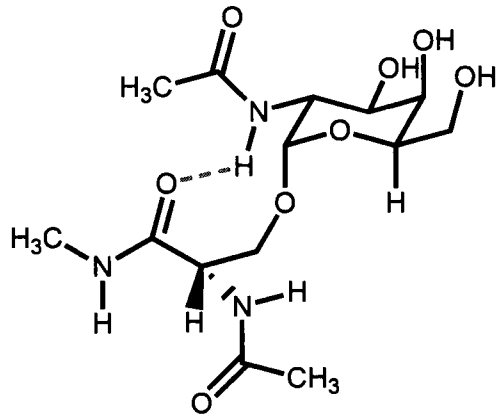

Scheme 3. *The suggested hydrogen bonding between the carbohydrate and peptide moiety of α-O-D-GalNHAc-Ser.*[9]

An interesting difference between α-D-GalNHAc-Ser and α-D-GalNHAc-Thr, is the presence of water pockets in the surrounding environment; while the serine analogue (**10**) can accommodate water pockets around the GalNHAc and carbonyl region of the serine, the threonine (**11**) derivative could not, suggesting a more efficient hydrogen-bonding network around **10**.[5] This difference in water pocket patterns can also infer the ability of α-D-GalNHAc-Thr to irreversibly bind to the ice lattice via hydrogen bond networks, which could explain the loss of antifreeze activity of α-D-GalNHAc-Ser (**10**).[5] To further determine the factors involved in the difference of orientations of the carbohydrate moiety, DFT studies were conducted. It was determined that the difference in conformation for **11** is predominantly due to the steric interactions between the carbohydrate moiety (endocyclic oxygen) and the β-methyl group which results in an eclipsed conformation for α-D-GalNHAc-Thr and a torsion angle of 120° (Scheme 4).[5]

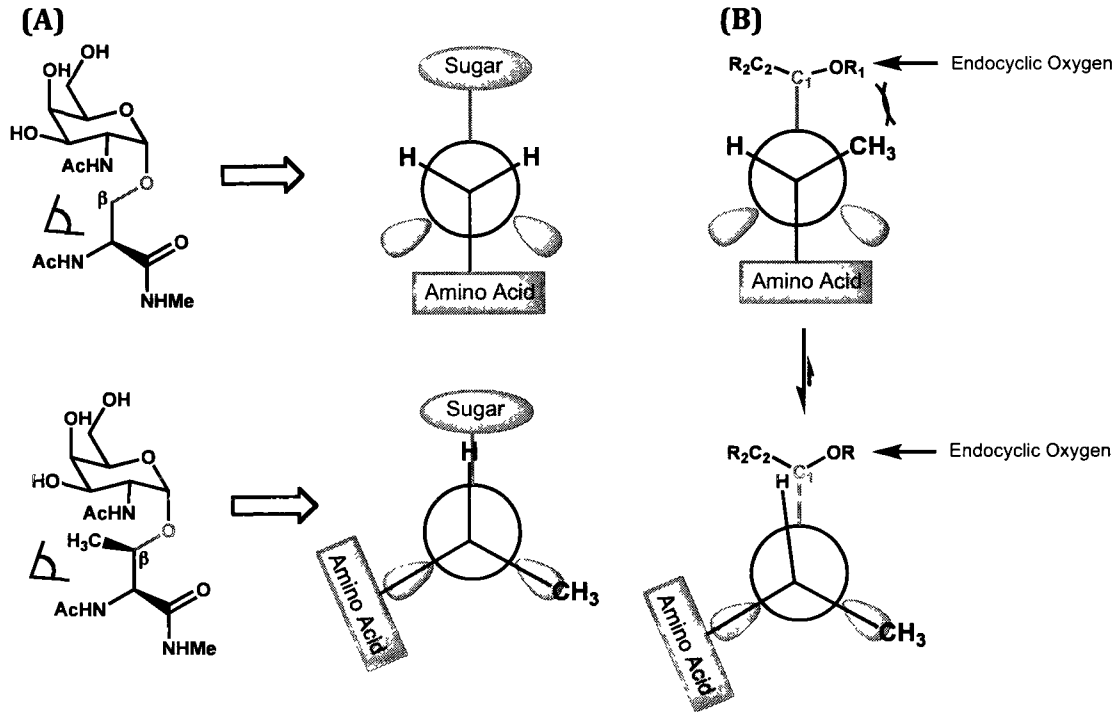

Scheme 4. *Newman Projections of model glycopeptides.* Looking at the βC-O bond, the serine (top) model has an anti arrangement while the threonine (bottom) model has an eclipsed arrangement. The difference in carbohydrate conformation is believed to be a result of water pockets between the peptide and sugar and steric repulsions between the methyl (at β carbon) and the sugar endocyclic oxygen. (B) The steric interactions between the carbohydrate moiety (endocyclic oxygen) and the β-methyl group. The eclipsed conformation is preferred for α-D-GalNHAc-Thr resulting in a torsion angle of 120°.

2.2 Properties and Reactivity of Fluorine

Fluorinated compounds have been known to have interesting properties and reactivities due to many distinguished characteristics of the fluorine atom. Firstly, fluorine has the largest electronegativity (3.98) of all elements from the periodic table and as such has a considerable influence inductively on a molecule. Secondly, it is capable of forming very strong bonds with carbon, and lastly, fluorine has a large Van der Waals radius (1.47 Å), contributing to the steric effects of a molecule.

Although they are the least abundant natural organohalides, fluorinated compounds have proven to be very influential in chemistry (i.e. synthesis, drug design, peptide therapeutics, etc.)[11-13]

2.2.1 Electronic Effects with Fluorine

(i) Acidity and Basicity of Fluorinated Compounds

Many factors affect the acidity and basicity of a compound including resonance, the size of an atom and electronegativity. Therefore, the presence of one or more fluorine atoms will undoubtedly affect the pK_a of a compound due to its powerful electron withdrawing effects. In fact, increasing the fluorine content lowers the pKa depending on where the fluorine is located, and this trend is observed with acidic compounds such as acetic acid and alcohol derivatives (Table 1).

In general, the introduction of a trifluoromethyl (CF_3) group adjacent to a carboxylic acid or alcohol increases the acidity by 3.5-4.0 pK_a units, and the farther away the fluorine atom (or fluorine substituent group) is, then the less it is expected to affect the acidity. As seen in table 1, an increase in fluorine atoms at the alpha position of acetic acid (entries 1-4) results in a stronger inductive effect (CH_2F < CHF_2 < CF_3) due to an increase in electronegative atoms. As a result, the oxygen-hydrogen bond of the acid is weakened causing the proton to be more susceptible to dissociation. This same trend is observed for alcohols (entries 5-8) bearing halogen

Table 1. pK_a of saturated (acetic acid and alcohol derivatives) and unsaturated systems.[14-16]

Entry	Acid	X	pK_a	
			H_2O	DMSO
1	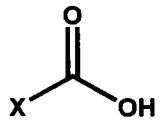	CH_3	4.76	12.3
2		CH_2F	2.59	-
3		CHF_2	1.34	-
4		CF_3	0.5	-
5	CX_3CH_2OH	CH_3	15.9	-
6		CF_3	12.5	23.5
7	$(CX)_3COH$	H	19.20	-
8		F	5.10	-
9	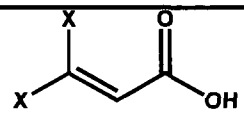	H	4.25	-
10		Cl	1.21	-
11		F	1.80	-

atoms; As electronegativity of a halogen increases (F > Cl > Br > I), so does the inductive effect resulting in a substantial decrease in pK_a compared to its non-halogenated form (Table 1).

While fluorine has a very pronounced effect on saturated compounds, they have different effects in unsaturated systems. As mentioned, the electronegativity of atoms greatly enhances acidity. Comparing fluorine with chlorine, it is expected that the pK_a of an acid bearing a fluorine will be lower than one having chlorine (i.e. CCl_3CH_2OH vs. CF_3CH_2OH) due to its larger electronegativity. However, in the presence of an unsaturation, the opposite is actually observed. It appears (Table 1, entries 9-11) that the vinyl fluorides slightly increases the pK_a. This is due to the unique nature of fluorine in that not only does it withdraw electrons away, but it

can also donate a pair of electrons. This phenomena is thought to occur as one of the lone pairs of electrons (from the p-orbital) of fluorine may donate into the p orbital of an adjacent unsaturated carbon due to the similarity in size of these two orbitals, thereby forming a conjugated system. As a result, electrons are donated into this π system, increasing electron density and thus decreasing acidity for unsaturated/fluorinated compounds.[13] An illustration of this electron donating effect of fluorine is seen in Scheme 5B.

(ii) Electronic Effects of "F" vs. "CF_3" Substituent

As mentioned in the previous section, fluorines are strongly electron withdrawing but at the same time, can be electron donating through their lone pair of p-electrons. Whether fluorine withdraws or donates electrons is highly dependent on the type of fluorinated substituent and if it is next to a σ or π system.

If the substituent group is simply a fluorine atom then it can either inductively withdraw electrons away from the reaction centre of a σ system or donate them through a π system by conjugation. For example, the nitration of fluorobenzene (Scheme 5A) is deactivated due to the presence of fluorine, yet it is ortho and para directing for the addition of the nitro group. The ability of fluorine to donate electrons through conjugation explains the latter result of the reaction. As fluorine has three lone pairs of electrons and its 2p orbitals (Scheme 5B) are at the proper size for π-orbital overlap, electron donation into the aromatic ring is

possible causing an increase in electron density at the ortho and para positions (Scheme 5C) promoting electrophilic additions at these sites.

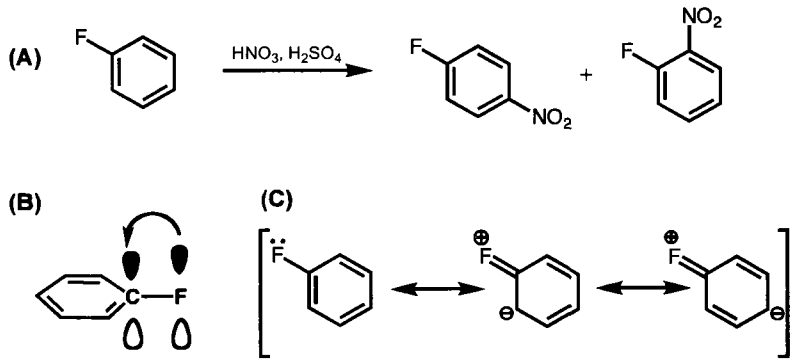

Scheme 5. *The effects of fluorine in unsaturated systems.* (A) The nitration of fluorobenzene results in ortho- and para- products. (B) This is due to electron donation from the fluorine atom into the π system.

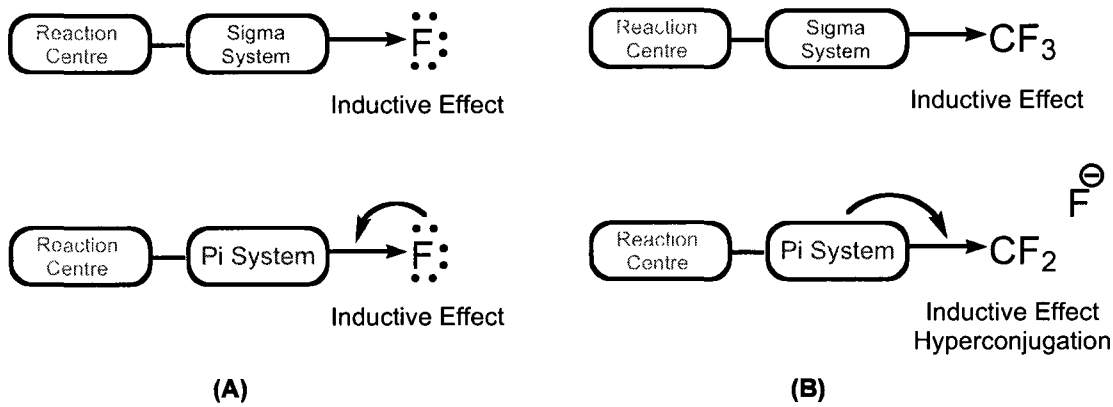

Figure 1. The effects of fluorines on both π and σ systems. (A) Fluorine substituents are electron withdrawing in pi and sigma systems but are only electron donating in pi systems. (B) CF_3 groups, similarly to fluorine alone, are electron withdrawing by inductive effect but cannot donate electrons in pi and sigma systems but can promote negative hyperconjugation in pi systems.

On the other hand, if the substituent is a CF_3 group then it behaves completely differently than a single fluorine atom (Figure 1B). Having a trifluoromethyl group adjacent to a π-system affects the entire compound by

inductively withdrawing electrons but will not promote electron donation. Furthermore, if the CF_3 group is adjacent to a π-system, then a phenomenon known as negative hyperconjugation may take place through an electron withdrawing resonance effect and this will promote nucleophilic additions (Scheme 6). This phenomenon occurs as the C-F bond is elongated by the electron donating effects of the π-system thus allowing for nuclophilic attack.

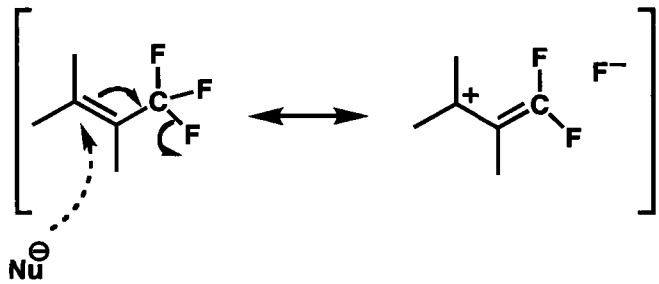

Scheme 6. *Negative Hyperconjugation.*

(iii) Steric Effects of Fluorine

Fluorine is often used as a substitution for hydrogen in structure activity relationship (SAR) studies for many reasons with the intention of improving the reactivity or stability of its hydrogen counterpart. Firstly, fluorine substitutions are an alternative to hydrogen since it forms stronger bonds with carbon, making this an attractive feature for metabolic stability in drug design. This was in fact observed with the synthesis of ezetimibe, a lipid-adsorption inhibitor drug with low bioavailability (Scheme 7A-B). Secondly, while fluorine is larger than hydrogen, its size does not disturb the overall geometry of certain molecule and therefore acts as a decent mimic for its equivalent hydrogen compound.[16] Thirdly, the presence of fluorine enhances hydrophobicity of organic compounds, which in turn increases

the activity of a variety of fluorinated drugs by ameliorating membrane permeability and stability within a hydrophobic pocket of an enzyme. Such an example is rosuvastatin (an HMGR inhibitors) that inhibit the production of cholesterol (Scheme 7C). It was observed through X-ray structure analysis that the flurophenyl group of this statin was bound to the hydrophobic pocket of HMGR thereby increasing the potency of the drug by inhibiting the substrate HMG-CoA to bind to the hydrophobic pocket and catalyze cholesterol synthesis.[17] While these are all good reasons for substituting hydrogen for fluorine, the fact remains that they are not isosteric. The Van der Waals radii for hydrogen and fluorine are 1.2 Å and 1.47 Å, respectively, and their bond lengths are quite different in that a C-F bond is much longer (1.38 Å) than a C-H bond (1.09 Å). These values all indicate that fluorine is sterically demanding compared to hydrogen, which could potentially be problematic in organic synthesis and drug design. In fact, comparing the Van der Waals volumes of CF_3 (42.6 Å) to a CH_3 (16.8 Å) further reiterates this steric demand. Overall, the use of fluorine has influenced various aspects of chemistry, drug design and synthesis.

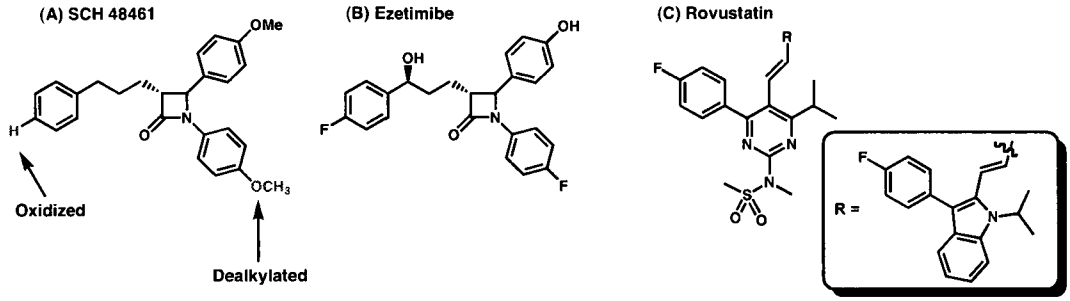

Scheme 7. *The influence of fluorine on drug synthesis.* (A) Structure of a potent lipid-absorption inhibitor drug with low bioavailability (SCH 48461). (B) Via SAR studies, ezetimibe is synthesized by the addition of fluorine atoms to improve bioavailability and enhance metabolic instability of SCH 48461. (C) Rosuvastatin, a mimic of HMG-CoA, which binds to the hydrophobic pocket of HMGR and prevents the biosynthesis of cholesterol.

(iv) Destabilization of Carbonyl Functional Groups

Carbonyl functional groups (ketones and aldehydes) vary in stability depending on the adjacent substituent groups. A carbonyl's carbon atom is quite electron deficient, therefore the addition of neighbouring electron donating groups (alkyl or alkoxy) will stabilize the carbonyl to a greater extent, thus decreasing its electrophilicity. On the other hand, if a carbonyl is surrounded by electron withdrawing groups (i.e. halogens and trifluoromethyl), destabilization occurs rendering them more reactive. A good example of this is shown in Scheme 8, where a Diels-Alder reaction occurs between cyclopentadiene and a 1:1 mixture of α, β-unsaturated ketones **12a** and **12b**.[15]

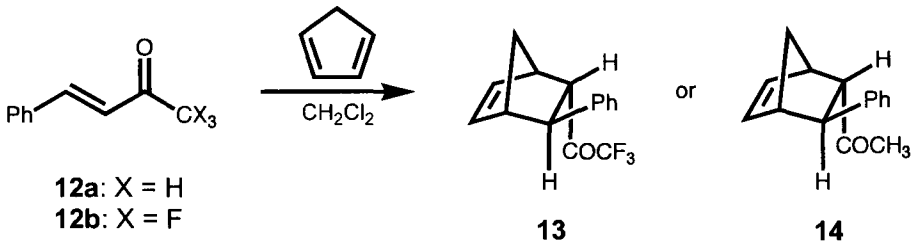

12a: X = H
12b: X = F

13 **14**

Conditions	Product Formed
BF_3OEt, -78°C	14
No Lewis acid	13

Scheme 8. *Diels-Alder [4+2] cycloaddition.* In the presence of BF_3·OEt the non-fluorinated cycloadduct (**14**) is produced while in the absence of BF_3·OEt, the fluorinated cycloadduct (**13**) is the major product.

In the absence of a Lewis acid, the predominant final product is the fluorinated cycloadduct **13** due to the fact that enone **12b** is less electron rich allowing it to undergo a rapid [4+2] with cyclopentadiene. However, if BF_3·OEt is added at -78°C, only compound **14** is formed. These results are not very surprising due to the fact that the trifluoromethyl group inductively withdraws electrons away from the carbonyl making the oxygen less basic thus. As a result, association between the Lewis acid and the carbonyl of **12b** does not occur, and an increase in reaction rate does not occur. However, the carbonyl of compound **12a** is more basic, thus allowing for chelation to the Lewis acid, and hence an increase in its reactivity; it is apparent that Lewis acid catalysis for **12a** strongly out-competes that of **12b**, and therefore, a [4+2] cycloaddition between **12a** and cyclopentadiene is favoured to give compound **14**.

From a medicinal chemistry perspective, drugs with trifluoromethyl groups alpha to a carbonyl have been advantageous as in the case of serine protease

inhibitors (Figure 2), a class of peptide-based drugs used for the treatment of a variety of conditions (blood clotting, inflammation and the immune system). The presence of the trifluoromethyl group enhances the electrophilicity of the adjacent carbonyl group and reaction with the serine alcohol in the active site of the enzyme.

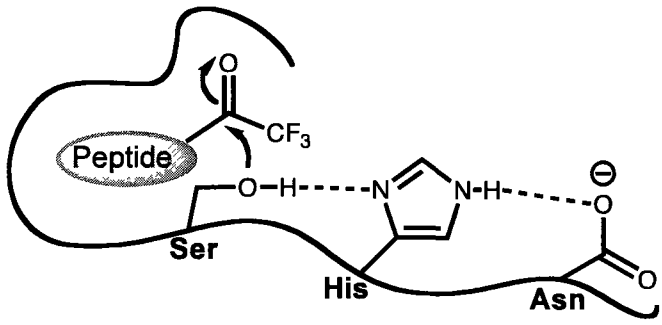

Figure 2. *Serine protease inhibition.* The presence of a peptide-based drug in the active site of the protease can trap serine's hydroxyl group by covalently bonding to the trifluoro acetyl group. The catalytic triad (serine, histidine and asparagine) facilitates this bond formation.

2.2.2. Hydrogen Bonding Capabilities of Fluorine

In 1994 interesting results were published by Eric Kool, which questioned the leading hydrogen bond theory regarding base pair fidelity in DNA replication. Kool's research group synthesized non-polar nuceloside isosteres and revealed that DNA replication is likely influenced by steric effects rather than hydrogen bonds as been thought for so many decades. Naturally, this "change" in paradigm caused a great deal of discussion and debate within the chemistry and biochemistry community questioning fluorine's ability to hydrogen bond.[18]

This new theory arose due to the design and synthesis of the nonpolar nucleoside **dF**, a mimic of the thymidine (dT) (Scheme 9). The purpose of synthesizing this analog was to test for base pair fidelity with nucleosides that mimic steric requirements but cannot form hydrogen bonds. The results obtained were important since it was the first set of experiments that have ever been conducted to test hydrogen bonding and steric effects of nucleosides separately. Bearing this in mind, isostere **dF** was synthesized since it retained structural similarities to the natural nucleoside thymidine but could not hydrogen bond. The design of **dF** was based on two structural differences of thymine. Firstly, the oxygens were switched for its isostere (fluorine) as C-O and C-F bonds are close in length and secondly, the N-H bonds were changed to C-H as they are similar in bond length as well.[18, 19]

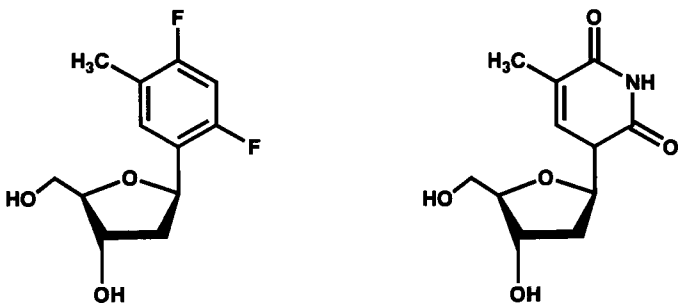

Scheme 9. *Difluorotoluene nucleoside (**dF**) as a mimic of natural thymidine (**dT**).*

Shortly after the synthesis of **dF**, its properties were examined by X-ray crystal structure analysis which revealed its structural similarity to thymidine and

its inability to form hydrogen bonds unlike the carbonyl and N-H bonds of native thymine.[20] These results therefore gave rise to the new hypothesis that base pair fidelity depends on steric effects alone.

If hydrogen bonding rather than steric effects are the predominant factors required for base pairing, then the incorporation of dFTP (nucleoside triphosphate of **dF**) into the elongated primer will not occur. Furthermore, if this hypothesis holds true, then the incorporation of **dA** opposite to **dF** (on the template sequence) will not occur as well (Figure 3). As a matter of fact, when **dF** was included in a DNA template strand in place of dT, the DNA polymerase of *E. coli* accepted this compound and was able to efficiently insert adenine opposite to the difluorotoluene.[21] Again, as **dF** is incapable of hydrogen bonding, DNA polymerase was still able to recognize it and treat it as though it was thymidine suggesting the importance of steric effects over H-Bonds (Scheme 8).[21]

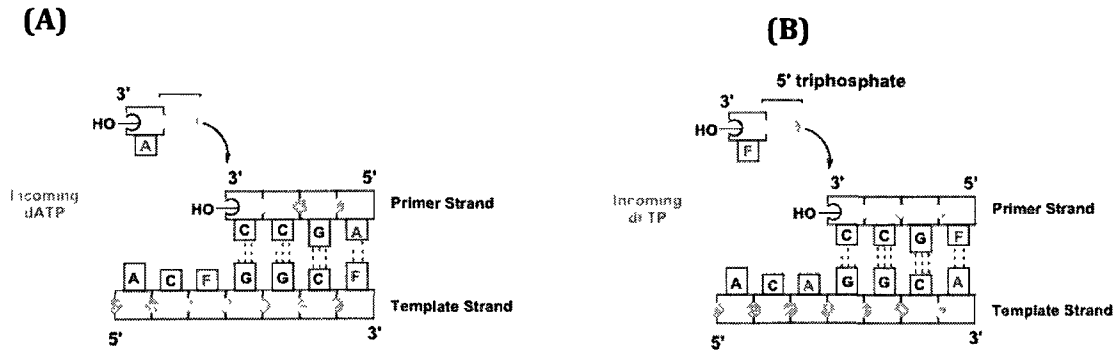

Figure 3. *DNA replication studies by Kool et al.* (A) the inclusion of **dF** (denoted as F) in the DNA template did not affect the base pairing with dATP. DNA polymerase recognized the nonpolar isostere and inserted dATP opposite to it. (B) the presence of dFTP was analogous to dTTP. This triphosphate nucleoside was efficiently attached to the 3' end of the primer similarily to thymidine triphospate.

Unsurprisingly, these published results became of great interest and many other researchers became involved in this topic. While some accepted these results, many refuted and suggested that the experiments were in error and that difluorotoluene was actually polar and could participate in hydrogen bonding which would explain its indistinguishable activity to thymidine. To date, there are no conclusive results to determine whether or not fluorine can hydrogen bond, but the major consensus is that if these interactions do exist then they are so weak that they are immeasurable.[18] The following points are the results that support this conclusion. Firstly, the nucleoside **dF** was tested for hydrophobicity via the partition coefficient (log*P*) and from these calculations it was apparent that it was strongly non polar, diminishing its affinity for water and thereby suggesting its unlikeliness to form hydrogen bonds with water molecules. Also, it is known that fluorocarbons are generally less polar than its hydrocarbon analog and this is effectively seen with the calculated log*P* of difluorotoluene (0.78) compared to regular toluene (0.71). Secondly, the atomic charges of fluorine and hydrogen of difluorotoluene were calculated, and comparing these values to its hydrocarbon analog, they were much smaller. As hydrogen bonding depends on these charges, the results published would suggest that hydrogen bonding must be relatively weak in the fluorinated version. Furthermore, X-ray crystal structure analysis of compounds having C-F bonds shows little or no indication of hydrogen bonding. Lastly, it was observed through various experiments that when **dF** was incorporated into DNA, it was strongly destabilizing when opposite to adenine. The

fact that there is destabilization would suggest that there is steric repulsion between the two bases rather than attractive hydrogen bond forces.[18]

Together, these results do not completely dismiss the hydrogen bonding theory but simply imply that steric effects are of greater importance for base pairing fidelity in DNA replication. To date, some researchers believe fluorine is capable of hydrogen bonding while others have opposing views, and a definitive conclusion is yet to be determined.

2.3 Research Goals

Fluorine's hydrophobic nature and use in peptide synthesis has been very important in the medical field and has been used for diverse applications.[11, 22, 23] The research conducted herein is based on these aspects and involves the synthesis of a non-polar AFP mimic. As mentioned in the previous chapter, type I AFPs have antifreeze activity (TH) which were initially believed to be a consequence of threonine binding to ice via hydrogen bonds.[8] However, recent site directed mutagenesis revealed that the hydroxyl groups of threonine believed to take part in ice binding may not be as important as previously hypothesized.[4] Rather, these latter findings suggested that when hydrophobic amino acids (such as valine) replaced threonine, TH activity is retained, thus implying a greater importance of hydrophobic functional groups (i.e. methyls) in ice binding. Keeping this in mind, we have followed a modified synthetic route[22, 23] to a trifluorinated threonine, **T(F)**,

(scheme 10) and have used this synthetic building block for the preparation of non-polar fluorinated AFPs via for solid-phase peptide synthesis. The targets were two peptides, each 13 amino acids in length with a general structure $[T(F)XX]_4$. The two peptide sequences built were a trifluorinated threonine-alanine-alanine tripeptide repeated four times ($[T(F)AA]_4$) and a trifluorinated threonine-glycine-glycine tripeptide ($[T(F)GG]_4$).

These fluorinated AFPs were thus tested for TH and IRI to determine their antifreeze activities. If non-polar functional groups (such as methyl groups of threonine or alanine) are the putative binding sites to ice, then one would expect for an increase in antifreeze activity in the presence of a very non-polar fluorinated threonine due to the hydrophobic nature of the trifluoromethyl group. Conversely, if the binding sites are in fact the hydroxyls of threonine, as previously hypothesized, then antifreeze activity is expected to be comparable to, or diminished relative to native AFP I. The synthesis and antifreeze assays of AFP derivatives $[T(F)AA]_4$ and $[T(F)GG]_4$ will be discussed in detail in Chapter 3.

The synthesis of **T(F)** was also of interest for glycosylation to further investigate the role of the methyl group with respect to antifreeze activity. In section 2.1, the methyl group of α-D-GalNHAc-Thr was discussed as a possible factor involved in the prevention of ice growth, due to its different conformation compared to the inactive α-D-GalNHAc-Ser.[4] More importantly, it was observed that the water pocket patterns surrounding each glycopeptide differed from one another and hydrated the carbohydrate (and hence the glycoconjugate) differently. As such,

it was proposed that the solvation shell surrounding α-D-GalNHAc-Thr was favourable for disruption of bulk water thus preventing the growth of ice. However, while these recent studies do not provide a conclusive explanation for the mode of action of AFGPs, it does suggest that hydration may be a factor. Since it is precedented that the presence of fluorine atoms alters its surrounding hydration, [24-27] and hydration influences protein function, [24-27] the glycosylation of a fluorinated threonine could be used as a tool to better understand the factors influencing antifreeze activity. The attempted glycosylations will also be of focus in Chapter 3.

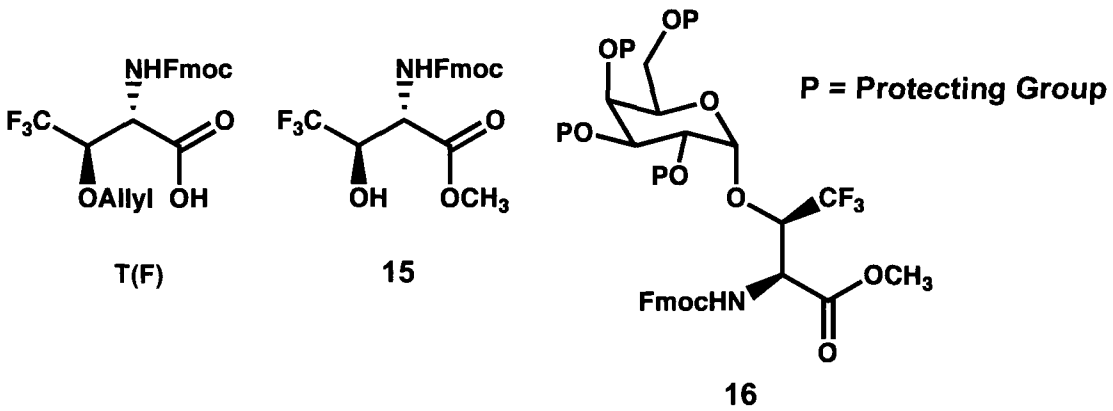

Scheme 10. *Targets for AFP and AFGP synthesis.* **T(F)** is the building block synthesized for automated peptide synthesis and compound **15** was synthesized for various glycosylation reactions. Gycoconjugate **16** is the general structure desired upon glycosylation.

2.4 References

1. Yeh, Y.; Feeney, R.E. *Chemical Reviews* **1996,** *96*, 601-618.

2. Bouvet, V.; Ben, R.N. *Cell Biochem. Biophys.* **2003,** *39*, 133-144.

3. Graham, L. A.; Liou, Y-C.; Walker, V.K.; Davies, P.L. *Nature* **1997,** *388*, 727-728.

4. Corzana, F.; Busto, J.H.; Jimenez-Oses, G.; Garcia de Luis, M.; Asensio, J.L.; Jimenez-Barbero, J.; Peregrina, J.M.; Avenoza, A. *J. Am. Chem. Soc.* **2007,** *129*, 9458-9467.

5. Tachibana, Y.; Fletcher, G.L.; Fujitani, N.; Tsuda, S.; Monde, K.; Nishimura, S.I. *Angew. Chem. Int. Ed.* **2004,** *43*, 856-862.

6. Ben, R.N. *Chembiochem* **2001,** *2*, 161-166.

7. Tam, R.Y.; Rowley, C.N.; Petrov, I.; Zhang, T.; Afagh, N.A.; Woo, T.K.; Ben, R.N. *J. Am. Chem. Soc.* **2009,** *131*, 15745-15753.

8. Mimura, Y.; Inoue, Y.; Maeji, N.J.; Chujo, R. *Int. Pept. Protein Res.* **1989,** *34*, 363-368.

9. Corzana, F.; Busto, J.; Jimenez-Oses, G.; Asensio, J.L.; Jimenez-Barbero, J.; Peregrina, J.M.; Avenoza, A. *J. Am. Chem. Soc.* **2006,** *128*, 14640-14648.

10. Meng, H.; Subrahmanian, T.K.; Beinborn, M.; Kumar, K. *J. Med. Chem.* **2008,** *51*, 7303-7307.

11. Jiang, Z.-X.; Yu, B. *J. Org. Chem.* **2007,** *72*, 1464-1467.

12. Clader, J. W. *J. Med. Chem.* **2004,** *47*, 1-9.

13. Chambers, R. D. *Fluorine in Organic Chemistry.*; Blackwell Publishing: Boca Raton, **2004**; p. 93-99.

14. Abraham, M.H.; Grellier, P.L.; Prior, D.V.; Duce, P.P. *J. Chem. Soc. PERKIN TRANS. II* **1989**, 699-711.

15. Uneyama, K. *Organoflorine Chemistry.*; Blackwell Publishing: Oxford, UK, **2006**; p. 33-34.

16. Chambers, R. D. *Fluorine in Organic Chemistry*; CRC Press: Boca Raton, NY, **2004**; p.1-8.

17. Istvan, E.S.; Deisenhoger, J. *Science* **2001,** *292*, 1160-1164.

18. Kool, E. T., Sintim, H.O. *Chem. Commun.* **2006**, 3665-3675.

19. Schweitzer, B. A., Kool, E.T. *J. Am. Chem. Soc.* **1995,** *117*, 1863-1872.

20. Guckian, K. M., Kool, E.T. *Angew. Chem, Int. Ed. Engl.* **1997,** *36*, 2825-2828.

21. Moran, S., Ren R. X.-F., Rumney, S., Kool, E.T. *J. Am. Chem. Soc.* **1997,** *119*, 2056-2057.

22. Jiang, Z-X.; Qin, Y-Y.; Qing, F-L. *J. Org. Chem.* **2003,** *68*, 7544-7547.

23. Xiao, N.; Jiang, Z-X.; Yu, B. *Biopol. Pept. Sci.* **2007,** *88*, 781-796.

24. Czechura, P.; Tam, R.Y.; Dimitrijevic, E.; Murphy, A.V.; Ben, R.N. *J. Am. Chem. Soc.* **2008,** *130*, 2928-2929.

25. Frauenfelder, H.; Fenimore, P.W.; McMahon, B.H. *Biophys. Chem.* **2002,** *98*, 35-48.

26. Zhang, L.; Wang, L.; Kao, Y.T.; Qiu, W.; Yang, Y.; Okobiah, O.; Zhong, D. *Proc. Natl. Acad. Sci. U.S.A.* **2007,** *104*, 18461-18466.

27. Franks, F. *Biophys. Chem.* **2002,** *96*, 118-127.

28. Samsonov, S.A.; Salwiczek, M.; Anders, G.; Koksch, B.; Pisabarro,T. *J. Phys. Chem. B* **2009,** *113*, 16400-16408.

Chapter 3: Discussion and Results

Within the last few decades, fluorinated amino acids have been of great interest. As mentioned in chapter 2, the introduction of fluorine atoms greatly enhances physical properties, metabolic stability and has influenced the world of pharmaceuticals.

Fluorinated amino acids have been of great interest as they have been used to probe biochemical reactions, inhibit certain enzymes and act as antitumour and antibacterial agents.[1] The synthesis of trifluoroleucine and trifluorovaline have demonstrated the importance of fluorinated amino acids as they have both thermal and chemical stability. The synthesis of a trifluorothreonine has been of interest as it could play an important role in pharmaceuticals but may also be a suitable chiral building block for other synthetic pathways as it has three functionalities (hydroxyl, amino and carboxylic acid groups).

Over 50 years ago, Walborsky and Baum published the first synthetic route[2] to a fluorinated threonine and since then various others have been reported.[3-5] The predominant drawback, however, was the difficulty in obtaining enantiopure products. Devising a stereselective route was therefore of great importance and had been the main synthetic challenge until a recent publication by Qing et al. described the synthesis of an enantiopure fluorinated threonine.[1] A few years later, Xiao and Jiang published a modified route, which was also stated to be efficient.[4]

Within the last two years, we have attempted to follow a synthetic route originally devised by Xiao and Jiang, and while it was a successful approach, many changes were required to afford the final fluorinated threonine in good yield (approximately 15 % for 13 steps). This newly revised route combines some of the synthetic steps used by Qing but various protecting groups were interchanged. Schemes 1 to 3 on the following pages illustrates all steps taken to produce **T(F)**.

3.1 Synthesis of T(F)—The building block for Solid-Phase Peptide Synthesis (SPPS)

Similarly to the Jiang route, commercially available 4,4,4-trifluorocrotonate (**17**) was the substrate of choice to initiate the synthesis (Scheme 1). To begin, ethyl ester **17** was reduced with lithium aluminium hydride in the presence of $AlCl_3$. Upon formation of the primary alcohol, the crude product was treated with triethylamine and benzoyl chloride to give **18**, a benzoyl protected intermediate in 70 % yield over two steps. The next step performed was the key transformation for installing the stereocentres at the α and β positions. To do so, the Jiang group performed an asymmetric Sharpless dihydroxylation across the olefin of **18** using AD-mix α. This transformation was done in quantitative yield. AD-mix α was used to ensure the proper stereochemistry at the α position. Although the stereochemistry at the β position is opposite to the native structure, the stereocentre at the α carbon is of greater importance. The stereochemistry at the β

position is of less importance as precedented by Laursen et al. who revealed that the stereochemistry of threonine does not affect the antifreeze activity of AFP I and that the D-enantiomer possesses similar activity to the natural L-enantiomer.[6]

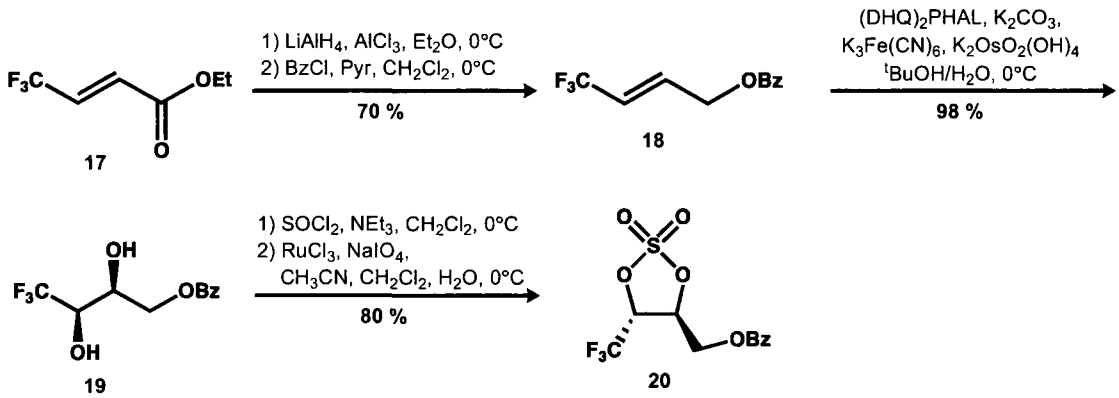

Scheme 1. *Initial synthesis to a trifluorinated threonine, **T(F)**.* The first few steps establish the stereocentre at the β carbon.

The next key step (Scheme 2) is to introduce a nitrogen atom at the α position to establish the amino functionality of the amino acid. To do this, diol **19** was treated with $SOCl_2$ and triethylamine to afford an unstable cyclic sulfite intermediate, which was readily oxidized to its cyclic sulfate (**20**) by ruthenium chloride and sodium periodate. The overall yield for these two transformations was 80 %. To introduce the nitrogen atom, the cyclic sulfate **20** was reacted with sodium azide. In situ, the azide nucleophile attacks the α carbon in an S_N2 fashion and inverts the stereochemistry to mimic that of native threonine. Once the azide intermediate (**21**) was obtained (85 % yield), the subsequent step was to convert it to an amino group. A one-pot synthesis was carried out, similar to Qing's method,

by reacting intermediate **21** with Pd/C and di-*tert*-butyl dicarbonate under hydrogen gas. By doing so, the azide was reduced to a secondary amine and immediately protected with a *tert*-butyloxycarbonyl (Boc) group to give compound **22** in 92 % yield.

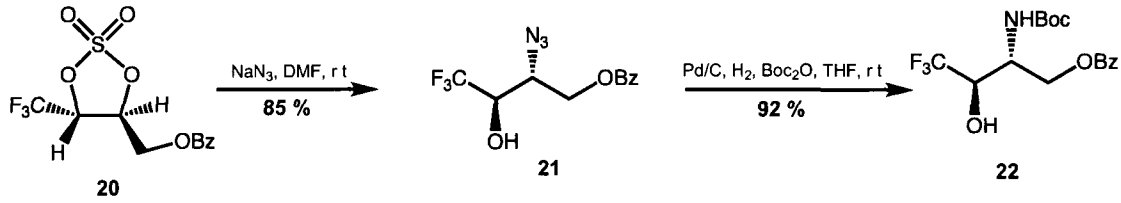

Scheme 2. *The Synthetic steps towards intermediate **22**.* These steps incorporate a nitrogen atom at the α position in order to convert it to an amine and create the amino functional group of T(F).

The subsequent steps performed involved modification of the protecting groups necessary to install the carboxylic acid at the α position (Scheme 3). The goal was to install protecting groups at the amine and secondary hydroxyl that are inert to the conditions of a Jones Oxidation to form the building block required for solid-phase peptide synthesis.

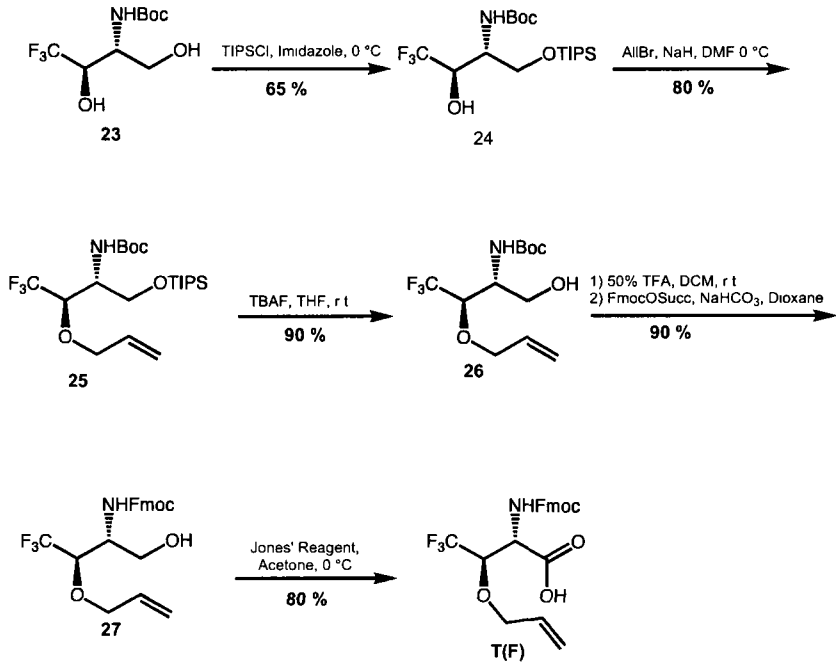

Scheme 3. *Protecting group manipulations done to produce **T(F)**.* These protecting groups were used to convert **23** into a stable substrate for a Jones oxidation.

Firstly, the benzoyl group of **22** was removed by treatment with sodium methoxide to afford the primary alcohol **23** in 92 % yield. Upon removal of the benzoyl group, the primary alcohol was re-protected with TIPSCl and imidizole (65 %). This protecting group was chosen to selectively protect the primary alcohol in order for the secondary alcohol to be protected with a neutral group such as an allyl group. Once compound **24** was formed, it was carefully reacted with allyl bromide and NaH to exclusively protect the secondary hydroxyl, as allylation of the nitrogen was also possible in the presence of excess NaH. This gave intermediate **25** (80 % yield), which was treated with TBAF to selectively remove the TIPS group on the

primary alcohol, to afford substrate **26** (90 %). While **26** could have been oxidized via Jones oxidation to provide the necessary building block for automated SPPS for fluorinated peptides $[T(F)AA]_4$ and $[T(F)GG]_4$, two important limitations prevented this step. Firstly, the acid labile nature of the Boc protecting group to the Jones oxidation conditions (H_2SO4/CrO_3) severely lowered the yield. Secondly, Boc protecting groups for automated peptide syntheses have become less popular while 9H-fluoren-9-ylmethoxycarbonyl (Fmoc) chemistry has become widely accepted and a better alternative as the latter uses milder and safer conditions.[7] Thus, converting the Boc protecting group to an Fmoc appeared as a viable option. This was easily achieved by reacting compound **26** with TFA followed by *N*-(9-fluorenylmethoxycarbonyloxy)-succinimide and sodium bicarbonate in dioxane. This gave adduct **27** in 90 % yield which was readily converted to carboxylic acid **28** via Jones oxidation. This was easily achieved in 80 % yield to give the resulting building block which was submitted on the automated peptide synthesizer (APEX) which simultaneously built $[T(F)AA]_4$ and $[T(F)GG]_4$ (Scheme 4).

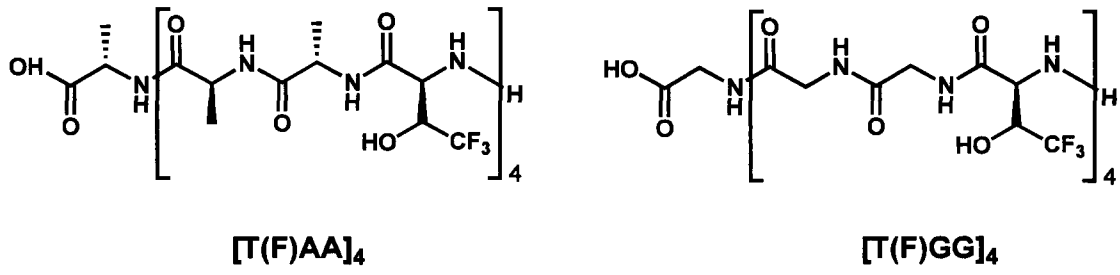

Scheme 4. *Target antifreeze peptides synthesized via SPPS.*

Compound **21** was also subjected to a one-pot reaction using Pd/C, H_2 and Fmoc-succinimide instead of *tert*-butyl dicarbonate as previously described in an attempt to directly synthesize compound **28** (Scheme 5). Unfortunately, low yields (10 %) were obtained, as it was likely that competing hydrogenolysis was occurring for compound **28**.

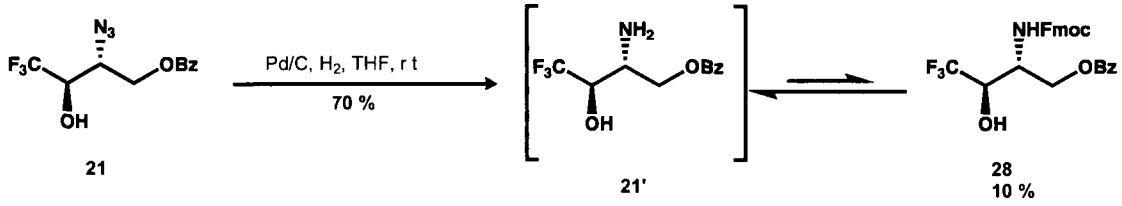

Scheme 5. *The one-pot reaction of compound **21** to form an Fmoc protected analog.*

3.2 Synthesis of AFP analogues $[T(F)AA]_4$ and $[T(F)GG]_4$ via SPPS

The target AFPs synthesized were prepared via solid-phase peptide synthesis (SPPS) by means of pre-loaded Fmoc-Wang resins. Depending on the AFP to build, either Fmoc-Ala-Wang or Fmoc-Gly-Wang resins were used. To remain consistent, Wang resins preloaded with alanine were used for $[T(F)AA]_4$ while those pre-loaded with glycine were employed for $[T(F)GG]_4$. The loading capacity for the Fmoc-Ala-Wang and Fmoc-Gly-Wang are 0.60 mmole/g and 0.61 mmole/g, respectively. The synthesis of standards $[TAA]_4$ and $[TGG]_4$ were also carried out at the same time.

During peptide synthesis, chain elongation proceeded from the C to N-terminus. To enhance coupling yields and reaction times HCTU (an activating reagent) was used and double couplings were done for commercially available amino acids. Once the first coupling reaction was complete, treating the resins with 20% piperidine (in DMF) afforded a deprotected amine of the newly attached amino acid thus allowing for a second coupling reaction to occur with another amino acid. This cycle was continued until a desired length (12 amino acids) was reached.

Once the peptide synthesis was complete, the allyl protecting groups of the trifluorinated threonine's secondary hydroxyl remained to be cleaved. The most efficient manner to proceed was to deprotect the allyl groups while the peptide was still supported on the bead. Although there has not been any precedence for this type of allyl deprotection, a similar protocol was published by Arya in which allyloxycarbonyl (alloc) groups were cleaved from amino acid residues while still bound to resins. [8] Thus, test reactions were carried out to determine the proper conditions for allyl removal, which led to the use of an iridium catalyst (1 eq. to peptide). These deprotections required 24 hours to ensure a complete isomerization of the allyl to which the resulting beads were treated with a cleavage cocktail (TFA:triisopropylsilane:DCM, 95:2.5:2.5) to cleave the enol ether at the secondary hydroxyl and release the peptide from the resin.

The resulting peptides were then submitted for mass spectral analysis using MALDI-TOF and LC-MS. While no mass peak was observed for $[T(F)GG]_4$, MALDI analysis of $[T(F)AA]_4$ furnished a molecular ion using the DHB (2,5-

dihydroxybenzoic acid) matrix. However, the insoluble nature of $[T(F)AA]_4$ was problematic as it prevented subsequent purification. As a result, structural characterization by NMR spectroscopy proved to be difficult. The proton NMR revealed the presence of alanine methyl groups however, impurities complicated analysis of the spectrum. In addition, the low solubility (Table 1) also affected the quality of the carbon-13 NMR. As the concentration of the sample was low, and relaxation times of highly substituted carbons are slow many carbon signals were not detected. In order to see these carbon resonances HMBC's were taken. Unfortunately, not all of the signals were detected making the characterization of this compound difficult by NMR spectroscopy. Although proton and carbon NMR analysis could not fully characterize the $[T(F)AA]_4$ polymer, fluorine NMR proved to be useful as the occurrence of a single fluorine resonance confirmed the presence of a fluorinated compound. Since MALDI-TOF revealed a mass peak for the polyalanine AFP, and fluorine NMR revealed the presence of fluorine, it was assumed that the repeating nature of the peptide resulted in a single fluorine resonance when measured by the NMR spectrometer. Based upon the MALDI-TOF analysis and ^{19}F NMR, $[T(F)AA]_4$ was successfully synthesized via SPPS.

Similar to $[T(F)AA]_4$, the polyglycine AFP was highly insoluble in organic solvents precluding full spectral analysis of the crude compound. Unfortunately, the MALDI-TOF spectra of $[T(F)GG]_4$ did not produce a molecular ion and the fragmentation pattern observed from the spectra revealed a glycine polymer but could not confirm the presence of the desired fluorinated AFP. In addition, a fluorine NMR was taken which also confirmed the presence of a fluorinated

glycopolymer. Although a mass peak was not observed, the ^{19}F NMR results obtained from $[T(F)GG]_4$ are encouraging as they are similar to the fluorine NMR of $[T(F)AA]_4$, thereby suggesting that the glycopolymer was synthesized.

Table 1. Solvent systems used in attempt to dissolve both $[T(F)GG]_4$ and $[T(F)AA]_4$.

Solvent System	Composition	Result
CH_3CN	100%	Poorly Soluble
$CH_3CN:H_2O$	1:9	Poorly Soluble
	2:8	Poorly Soluble
	1:1	Poorly Soluble
H_2O	100%	Insoluble
CF_3CH_2OH	100%	Poorly Soluble
TFA	100%	Soluble

In order to test for TH and IRI, purification was necessary. Unfortunately, the fluorinated AFPs were insoluble in nearly all solvents, hindering the use of HPLC and recrystallization as purification techniques. Table 1 outlines the solvents used and their respective composition. As the use of organic solvents was not feasible for TH and IRI assays, this posed as a limitation as only water and PBS are used for TH and IRI, respectively. Furthermore all IRI assays are standardized to be performed in aqueous solvents and are very susceptible to solvent additives.[9] Neverthless, various mixtures of acetonitrile and water were attempted in addition to a fluorinated solvent such as trifluoroethanol (Table 1). These AFP peptides were insoluble in nearly all organic solvents and poorly soluble in water and acetonitrile as observed during the transferring of solutions for MALDI samples. The only solvent that completely dissolved the fluorinated peptides was TFA. And even so,

the peptides would precipitate from TFA upon addition of small amounts of water. As time would not permit for further investigation, the crude peptides were dissolved by sonication and tested for TH and IRI. The samples tested for TH were sonicated in doubly distilled water, while those tested for IRI were dissolved in phosphate-buffered saline (PBS) solution.

3.3 Assay for Antifreeze Activity

3.3.1 TH Results

To measure TH, nanolitre osmometry was performed using a Clifton nanoliter osmometer similar to the one employed by Chakrabarrty and Hew.[10] This procedure requires the insertion of a solution (approximately 10 nL of a 10 mg/mL solution) into an oil droplet located within the pores of thin metal plate placed on a cooled Peletier unit, which regulates temperature. The purpose of using mineral oil is for the sample to remain intact and untouched from surrounding wall of the wells and to prevent evaporation. The oil droplet containing the solution to test is then flash frozen (-30°C) and then slowly thawed until one stable ice crystal remained. The temperature at which this single crystal grows and shrinks is referred to as the melting and freezing point, respectively. If an antifreeze additive (possessing TH) is present, then a single hexagonal bipyramidal shaped crystal will form and will remain static in size until the freezing point of the solution is exceeded, resulting in rapid crystal growth.

Figure 1 illustrates the images captured during TH testing of sample solutions (10 mg/mL) of $[T(F)AA]_4$ and $[T(F)GG]_4$. It is obvious from these images that there is no TH activity as the shape of both crystals is completely spherical. As dynamic ice shaping causes crystals to have a hexagonal bipyramial shape, the spherically-shaped ice crystals suggest that these synthetic AFPs do not exhibit DIS implying that they are unable to bind to ice. Furthermore, it was observed experimentally that when the temperature decreased by increments of 0.1°C, the size of the crystal was not uniform and was continuously expanding. Together, these observations clearly indicate the absence of TH.

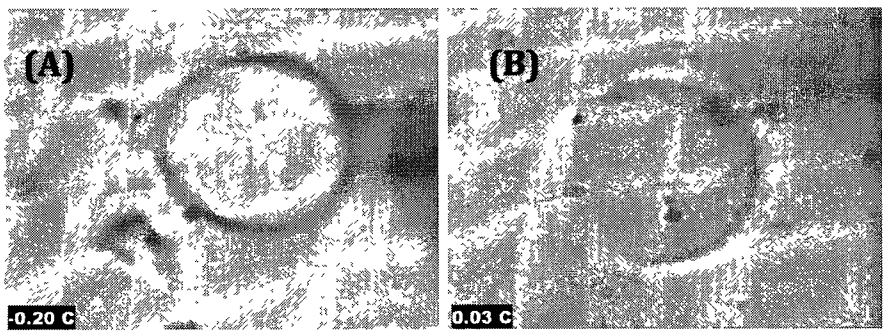

Figure 1. Images of ice crystals grown from solutions of (A) $[T(F)AA]_4$ (10 mg/mL) and (B) $[T(F)GG]_4$ (10 mg/mL). All samples were dissolved in doubly distilled water.

As the hydrophobic effect was investigated for antifreeze activity (in terms of TH), it appears that the presence of fluorine atoms does not influence its adsorption to ice. A possible explanation for these results may be the solubility issues encountered during testing. As TH is reported to be a function of concentration, the low solubility of the fluorinated peptides would give an AFP solution with a sufficiently low concentration.[11] If the concentration of AFP in solution is too low,

then the likelihood of AFPs inhibiting ice growth is diminished, as there may not be enough molecules to bind to ice.

To overcome this solubility issue, a mixture of TFA, acetonitrile and water (9:4:7) was used. This solvent system appeared to be the best combination of solvents containining a minimal amount of non-polar additives. Unfortunately during the assay procedure, the injection of the sample solution into the mineral oil was not successful because the organic additives prevented the proper suspension of the aqueous droplet into the oil.

3.3.2 IRI Results

Nearly ten years ago, a plant AFP was isolated possessing only IRI and lacking TH.[12] This was surprising as it had always been assumed that these two properties worked hand-in-hand. As TH is associated with dynamic ice shaping, the production of needle-shaped crystals is detrimental to biological systems as it may cause damage to cells and tissue.[13] Therefore, it is generally accepted that IRI is of greater importance for cryoprotection, highlighting its importance over TH. Having said this, our research group is interested in the production of antifreeze compounds possessing only IRI due to its applications as a cryoprotectant for the preservation of cells, tissues and organs.[14, 15]

To determine IRI activity for $[T(F)GG]_4$ and $[T(F)AA]_4$, the "splat cooling" method devised by Knight and co-workers was implemented.[16] It has been experimentally observed that IRI activity is greatly dependant on concentration. For example, at exceedingly high concentrations, a false positive may result while at lower concentrations, IRI activity may not be observed. It has been previously shown that the optimal concentration within the dynamic range is 5.5 μM.[14, 17] As such, AFP sample solutions with this concentration were prepared for testing by dissolving each peptide in PBS solution and sonicating for 2-4 hours. To begin the assay, 10 μl of solution was dropped above a pre-cooled aluminum plate (placed on dry ice) thereby freezing instantaneously upon contact. A thin wafer (50 μm) about 5 mm in radius is produced which is carefully scraped off the plate and transferred onto a pre-cooled cover slip and positioned onto a Pelletier unit cooled to -6.4°C. Once placed within the Peletier unit, the wafer was left to anneal for 30 minutes and then photographed under a microscope to determine the mean grain size of the crystals. To ensure consistent results, each sample was dropped three times and photographed multiple times. In addition to the AFP samples, two standards ($[TAA]_4$ and $[TGG]_4$) samples and PBS were assayed.

The IRI results for each AFP solution (5.5 μM) are summarized in Figure 2. A phosphate buffered saline (PBS) solution was used as the negative control to which all samples are compared. Bars shorter than PBS are suggestive of ice recrystallization inhibition activity. Although the bars representing AFPs are slightly shorter than PBS, they indicate very weak activity. The percent mean grain

size (MGS) relative to PBS for $[T(F)AA]_4$, $[T(F)GG]_4$, $[TAA]_4$ and $[TGG]_4$ is 84%, 90%, 84% and 95%, respectively. It appears that the introduction of fluorine for $[TAA]_4$ has no effect on IRI activity and that for $[TGG]_4$ increases activity slightly.

A major concern regarding these results is the purity of the each peptide. As mentioned, the solubility of both fluorinated peptides in various solvents was difficult to achieve, thus preventing their purification via HPLC or recrystallization. Even though misrepresentative results were likely to be attained, testing was carried out to verify for antifreeze activity. While it is difficult to draw definitive conclusions related to activity based on the crude, it appears that peptides primarily made of alanine inhibit ice recrystalliation slightly better than glycine.

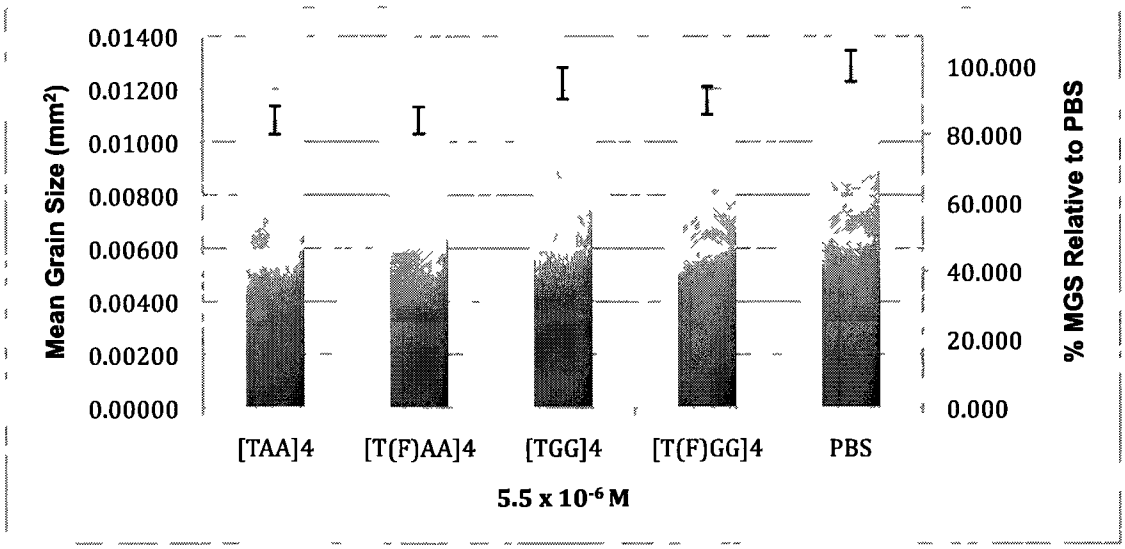

Figure 2. Mean grain size of fluorinated AFPs ($[T(F)AA]_4$ and $[T(F)GG]_4$), standards ($[TAA]_4$ and $[TGG]_4$), and PBS solution annealed for 30 minutes at -6.4°C. The concentration of each AFP solution is 5.5 x 10^{-6} M.

The only viable trend observed in Figure 2 is the fact that peptides containing alanine residues have better IRI activity than glycine. Table 2 summarizes the literature values for partial molar volume (PMV), partial molar compressibility (PMC), hydration number and hydration index (HI) of alanine and glycine.[18] Previous work has shown that these parameters are correlated to IRI activity in carbohydrates.[19] For example, an decrease in PMC or an increase in the hydration index results in an increased IRI activity.

Table 2. The physical properties of alanine and glycine likely to be correlated to IRI activity. Below are the partial molar compressibility (PMC) ($cm^3/mol \cdot bar$), partial molar volumes (PMV) (cm^3/mol), hydration number and hydration index values (mol/cm^3) of Ala and Gly.

Amino Acid	PMC ($cm^3/mol \cdot bar$)	PMV (cm^3/mol)	Hydration Number	Hydration Index
Alanine	-25.56	60.47	6.2	0.102
Glycine	-27.00	43.19	5.5	0.127

The values listed in Table 2 are contradictory to what is observed in Figure 2. Table 2 shows that glycine is expected to be a better amino acid for ice recrystallization inhibition as it has the lowest value for partial molar compressibility, suggesting a poor fit with the hydrogen-bonding network of water thereby resulting in the disruption of bulk water. Furthermore, the calculated HI values are contradictory to the IRI results, in that a larger value (i.e. 0.127 for glycine) would represent better IRI activity, which it does not when compared to $[TAA]_4$ and $[T(F)AA]_4$. This poor correlation between IRI activity and hydration parameters may be due to the fact that peptide hydration is more complicated than simple carbohydrates due to the possibility of various peptide secondary structures

which can affect overall hydration. The ability of polyglycine AFPs to inhibit the growth of ice better than polyalanine AFPs could be to due to the flexible nature of the former (as it lacks a methyl), thus allowing for interaction with multiple ice crystals which subsequently hinders the amalgamation of smaller ice crystals into larger ones.

These results are likely a consequence of impurities present within the AFP samples. It is known that the IRI assay employed is sensitive to impurities as it may prevent some of the water from freezing during annealing temperature.[16]

3.4 Glycosylation of 4,4,4-trifluorothreonine

In addition to AFPs, antifreeze activity has also been observed among glycopeptides. As such, the glycosylation of 4,4,4-trifluorothreonine at its secondary hydroxyl was of interest. Shown in Scheme 7 are three attempts for the formation of an α-*O*-linked fluorinated glycoconjugate.

Before performing glycosylation reactions, building block **T(F)** that was initially synthesized for SPPS required proper protecting group manipulations to produce **31**, the fluorinated threonine to be glycosylated. Scheme 6 illustrates the necessary steps taken. The first transformation involved the protection of the carboxylic acid, in which **T(F)** was methylated by treatment with thionyl chloride and methanol (70 %). Next, the allyl group was cleaved using an iridium catalyst

((1,5-Cyclooctadiene)bis(methyldiphenylphosphine)iridium(I)-hexafluoro-phosphate) to isomerize the terminal double bond into its corresponding enol ether, followed by its cleavage by the addition of excess I_2 and water to afford the secondary hydroxyl. Once the desired fluorinated threonine **30** was attained (60 %), it was exposed to typical glycosylation conditions (Scheme 7).

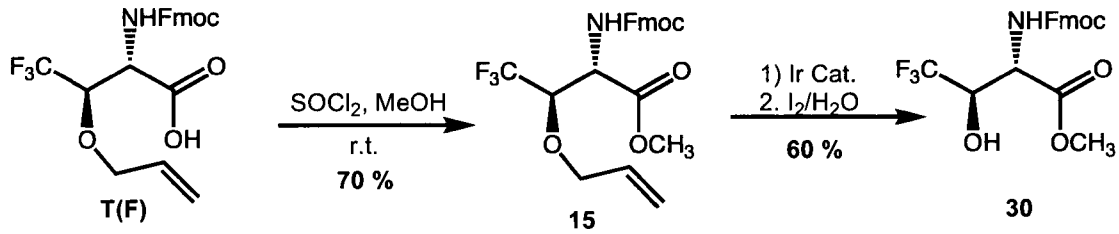

Scheme 6. *Protecting group modifications to produce compound **30**, the fluorinated threonine required for glycosylation.*

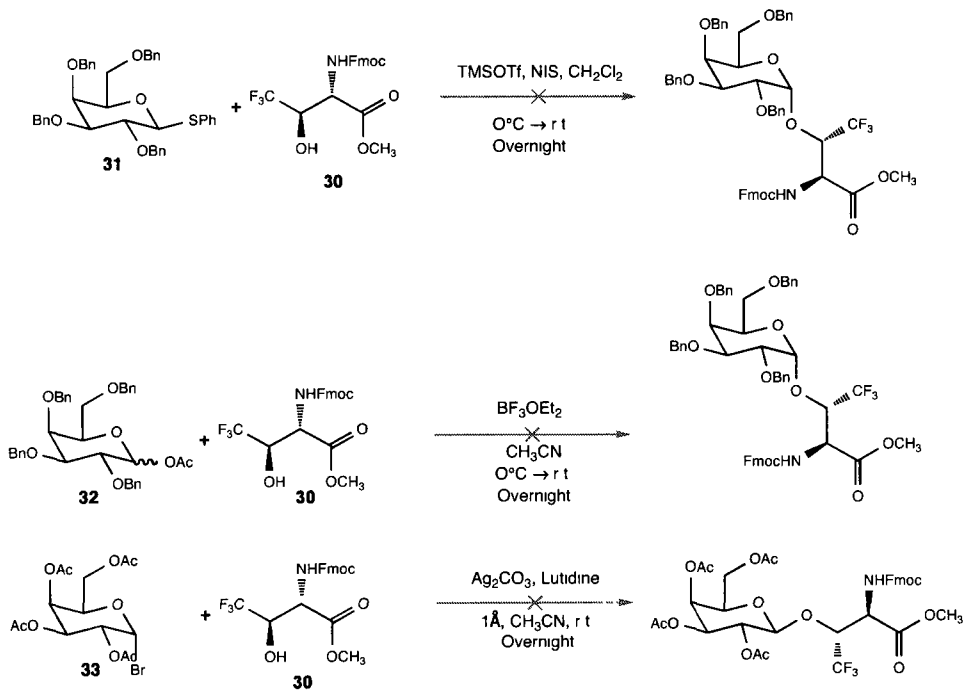

Scheme 7. *Various glycosides and conditions used to glycosylate the secondary hydroxyl of **30**.*

The first glycosylation involved the addition a β-D-thioglycoside (**31**) to threonine **30** followed by the addition of *N*-iodosuccinimide (NIS) and then trimethylsilyl trifluoromethansulfonate (TMSOTf) to activate the carbohydrate donor. The addition order of reagents is important, as this limits unwanted byproducts. Analysis by TLC indicated that the thioglycoside appeared to be consumed while compound **30** still remained present in the reaction mixture. Even though the reaction was left to stir overnight for several days, analysis by electrospray ionization (ESI) and nuclear magnetic resonance (NMR) spectroscopy did not reveal a desired mass peak and formation of a glyconjugate was not apparent. As such, it was concluded that no reaction occurred between **30** and **31**, and that the carbohydrate was likely consumed by iodination of the thiophenol group, which would eventually become hydrolyzed if any moisture were present.

The second glycosylation utilized an anomeric mixture of a perbenzylated galactopyranoside (**32**) treated with a Lewis acid such as $BF_3{\cdot}OEt_2$. During this glycosylation, boron trifluoride was expected to complex to the carbonyl of the anomeric acetate in order to activate the formation of its corresponding oxocarbenium, thereby allowing nucleophilic attack by **30**. Unfortunately, ESI did not reveal a mass peak, and proton NMR did not show a glycoconjugate. Instead, threonine **30** remained unreacted as observed by TLC. After these two failed attempts, it was clear that the fluorinated threonine **30** was inert in these reaction mixtures. Possible explanations for this could be steric hindrance of the trifluoromethyl group and poor nucleophilicity of the secondary alcohol. As fluorines are large atoms, a CF_3 group adjacent to the secondary hydroxyl would

render the reaction site bulky and as fluorines are very electronegative and electron withdrawing, the nucleophilicity of the hydroxyl is expected to decrease. These two factors would cause the fluorinated threonine to become unreactive during glycosylation reactions.

In an attempt to increase the nucleophilicity of **30**, a modified Koenig-Knorr glycosylation was carried out (Scheme 7C) similar to the one reported by Green et al.[20] Green and co-workers modified the procedure by including a base (lutidine) in order to increase the nucleophilicity of *p*-nitrophenol during a reaction with an α-D-glucopyranosyl bromide. The incorporation of a base in the reaction mixture is expected to increase nucleophilicity by deprotonating the hydroxyl and forming a reactive anion. Similarily, lutidine was used for the glyocsylation of **30**, to deprotonate the secondary hydroxyl. For the glycosylation shown in Scheme 7C, the first step taken was to dissolve threonine **30**, lutidine and Ag_2CO_3 (in anhydrous dichloromethane) followed by the addition of the β-D-bromoglycoside **33**. As the previous glycosylations failed to form a glycoconjugate at cold temperatures, the reagents were added at room temperature and stirred overnight. Similarly to the previous two trials, no glycosylation was observed. Rather, NMR spectroscopy revealed a dimer of the carbohydrate **33**. Unfortunately, time did not permit for further investigation into conditions to promote a glycosylation, and formation an *O*-linked glycoconjugate was not attained. Nevertheless, many other glycosylations conditions may be attempted. For example, the glycosylation of threonine may be achieved by using a donor such as a 2-nitroglycal in the presence of potassium *tert*-

butoxide. It is known that these conditions almost exclusively give an α-glycosidic linkage thus making this pathway worth investigating. While there are many glycosyl donors to explore (i.e. glycals, glycosyl fluorides, sulphenyl glycosides or *O*-glycosyl trichloroacetimidates) we may also probe in the use of a base to increase the nucleophilicity of the secondary hydroxyl of threonine by its deprotonation. A variety of bases (i.e. pyridines, trialkylamines) may be used, however, it is important to note that the protecting group chosen for the amine of threonine **30** must not be sensitive to strong bases and must be converted to protecting group that withstands conditions at a high pH (i.e. Boc).[21]

Although the building block **T(F)** was successfully synthesized in decent yield (overall 15 %), the synthesis of fluorinated antifreeze proteins incorporating **T(F)** in the peptide sequence proved to be challenging. The results obtained indicate no thermal hysteresis but very weak IRI activity as the mean grain size of $[T(F)GG]_4$ and $[T(F)AA]_4$ are 90% and 84%, respectively. Although solubility was the primary issue, testing was still carried out. Unfortunately, the results obtained were contradictory to what was expected. The polyglycine AFP was expected to exhibit better IRI activity than $[T(F)AA]_4$ as it is more flexible (due to the absence of methyl groups) thus allowing for better interaction with multiple ice crystals. However, the presence of impurities in these samples could have greatly affected the outcome of these results as they could have interacted with water during annealing. Furthermore, despite not knowing the exact purity of $[TAA]_4$ and $[T(F)AA]_4$, the mean grain size (MGS) of these two AFPs are very close in value suggesting that hydrophobic interactions are not important for IRI. Although these

results are based on crude samples, additional studies are required in order to definitively determine the effects of hydrophobic residues.

To overcome the issues associated of solubility, we may try to incorporate polar residues (i.e. lysine, arginine, serine or threonine) to the beginning and end of the fluorinated peptides to increase solubility in aqueous media without affecting the secondary structure of the peptide or its putative binding sites to ice. Alternatively, a series of fluorinated AFPs which contain an increasing number of fluorinated threonine residues may be synthesized. Since four fluorinated threonine residues ($[T(F)GG]_4$ and $[T(F)AA]_4$) cause solubility issues, then peptide sequences with fewer fluorinated amino acids should be investigated. As such, the synthesis of a peptide sequence with a general structure of $[T(F)XX]_n$ (X = Gly or Ala) should be explored with varying length (n = 1, 2 or 3) in order to accurately determine the effects of fluorinated residues on solubility.

3.5 References

1. Jiang, Z.-X.; Qin, Y-Y.; Qing, F-L. *J. Org. Chem.* **2003,** *68*, 7544-7547.

2. Walborsky, H. M.; Baum, M.E. *J. Am. Chem. Soc.* **1958,** *80*, 187-192.

3. Guanti, G.; Banfi, L.; Narisano, E., *Tetrahedron* **1988,** *44*, 5553-5562.

4. Xiao, N.; Jiang, Z-X.; Yu, B. *Biopol. Pept. Sci.* **2007,** *88*, 781-796.

5. Sting, A. R.; Seebach, D. *Tetrahedron* **1996,** *52*, 279-290.

6. Wen, D.; Laursen, R.A. *FEBS Lett.* **1993,** *317*, 31-34.

7. Chan, W. C.; White, P.D. *Fmoc Solid Phase Peptide Synthesis: A practical approach*; Oxford University Press Inc.: New York; NY, **2000**; p. 12.

8. Nandy, J.P.; Prakesch, M.; Khadem, S.; Reddy, P.T.; Sharma, U.; Arya, P. *Chem. Rev.* **2009,** *109*, 1999-2060.

9. Knight, C. A., DeVries, A.L.; Oolman, L.D. *Nature* **1984,** *308*, 295-296.

10. Chakrabarrty, A.; Hew, C.L. *Eur. J. Biochem.* **1991,** *202*, 1057-1063.

11. Davies, P. L.; Sykes, B.D. *Curr. Opin. Struct. Biol.* **1997,** *7*, 828-834.

12. Sidebottom, C.; Buckley, S.; Pudey, P.; Twigg, S.; Jarman, C.; Holt, C.; Telford, J.; McArthur, A.; Worrall, D.; Hubbard, R.; Lillford, P. *Nature* **2000,** *406*, 256.

13. Bouvet, V.; Ben, R.N. *Cell Biochem. Biophys.* **2003,** *39*, 133-144.

14. Czechura, P.; Tam, R.Y.; Dimitrijevic, E.; Murphy, A.V.; Ben, R.N. *J. Am. Chem. Soc.* **2008,** *130*, 2928-2929.

15. DeVries, A. L. *Cryobiology* **1979,** *16*, 585.

16. Knight, C. A.; Hallett, J.; DeVries, A.L. *Cryobiology* **1988,** *25*, 55-60.

17. Liu, S.; Ben, R.N. *Org. Lett.* **2005,** *7*, 2385-2388.

18. Glinski, J.; Burakowski, A. *Eur. Phys. J.* **2008,** *154*, 275-279.

19. Tam, R. Y.; Ferreira, S.S.; Czechura, P.; Chaytor, J.L.; Ben, R.N. *J. Am. Chem. Soc.* **2008,** *130*, 17494-17501.

20. Green, D. E.; Ferreira, C.L.; Stick, R.V.; Patrick, B.O.; Adam, M.J.; Orvig, C. *Bioconjugate Chem.* **2005,** *16*, 1597-1609.

21. Geiger, J. R., G.; Winterfeld, G.A.; Weber, R.; Przybylski, M.; Schmidt, R.R. *J. Org. Chem.* **2006,** *72*, 4367-4377.

Supporting Information

(a) General Experimental[1]

All anhydrous reactions were performed in flame-dried or oven-dried glassware under a positive pressure of dry argon or nitrogen. Air or moisture-sensitive reagents and anhydrous solvents were transferred with oven-dried syringes or cannulae. All flash chromatography was performed with E. Merck silica gel 60 (230-400 mesh). All solution phase reactions were monitored using analytical thin layer chromatography (TLC) with 0.2 mm pre-coated silica gel aluminum plates 60 F254 (E. Merck). Components were visualized by illumination with a short-wavelength (254 nm) ultra-violet light and/or staining (potassium permanganate, phosphomolybdate or ninhyrin stain solution). All solvents used for anhydrous reactions were distilled. Tetrahydrofuran (THF) and diethyl ether were distilled from sodium/benzophenone under nitrogen. Dichloromethane, acetonitrile, and triethylamine were distilled from calcium hydride. *N,N*-Dimethylformamide (DMF) was stored over activated 4Å molecular sieves under argon.

All spectra (^{1}H, ^{13}C and ^{19}F) were acquired at room temperature. Samples were dissolved in either deuterated chloroform ($CDCl_3$), methanol (MeOD) or water (D_2O). Proton spectra were obtained by either a Bruker Avance 300, 400 or 500 MHz or INOVA 500 MHz. ^{13}C NMR data were recorded from an INOVA 500 MHz spectrometer and fluorine 19 NMRs were all taken on the Bruker Avance 400 MHz. Splitting patterns are designated as follows: s, singlet; d, doublet; t, triplet; q, quartet; m, multiplet and br, broad. Low resolution mass spectrometry (LRMS) was performed on a Micromass Quatro-LC Electrospray spectrometer with a pump rate of 20 μL/min using electrospray ionization (ESI) or a Voyager DE-Pro matrix-assisted desorption ionization-time of flight (MALDI-TOF), (Applied Biosystem, Foster City, CA) mass spectrometer operated in the reflectron/positive-ion mode with DHB in 20% EtOH/H_2O as the MALDI matrix.

(b) General Procedure for Synthesis of T(F)

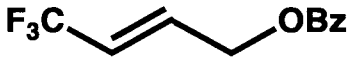

(i) (E)-1-Benzyloxy-4,4,4-trifluoro-2-butene (18)[2]

To a flame-dried flask under argon, $LiAlH_4$ (13.6 g, 0.350 mol) was dissolved in diethyl ether (250 mL) at 0°C to which a solution (40 mL) of $AlCl_3$ (16.7 g, 0.125 mol) was added. The reaction mixture was left to stir at 0°C for 15 minutes to which 4,4,4-trifluorocrotonate (**17**, 25 g, 0.15 mol) was added. The reaction mixture was left to stir for 4 hours until completion. Once the reaction was complete, water (13 mL), 10% NaOH (29 mL) and a second portion of water (43 mL) was added dropwise at 0°C. The resulting reaction mixture was filtered and the solvent was evaporated by distillation. The crude product was then dissolved in anhydrous methylene chloride (50 mL) and pyridine (26 mL, 0.37 mol) and benzoyl chloride (43 mL, 0.37 mol) were added at 0°C and left to stir overnight at room temperature. Once the benzoylation was complete, the reaction mixture was neutralized (10 % HCl) and the organic layer was collected while the aqueous layer was extracted with diethyl ether (3 x 20 mL). The combined organic phases were washed with a saturated solution of Na_2CO_3 (20 mL) followed by brine (20 mL) and then dried over Na_2SO_4 and concentrated *in vacuo*. The crude product was purified multiple times by column chromatography (100 % toluene) to give a clear, colourless oil in 70 % yield. NMR data obtained matched that of literature.[2]

^1H NMR (500 MHz, $CDCl_3$): δ 8.07-7.45 (m, 5H), 6.57-6.51 (m, 1H), 6.00-5.93 (m, 1H), 4.96-4.94 (m, 2H).

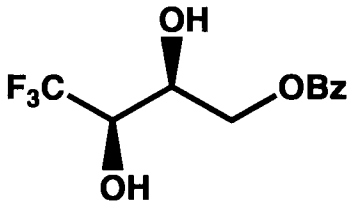

(ii) (2*S*,3*R*)-1-Benzoyl-4,4,4-trifluoro-2,3-butanediol (19)[2]

To a 1:1 mixture of *tert*-butanol (30 mL) and water (30 mL), AD-mix α (8.5 g) was added. Once the AD-mix α was completely dissolved, olefin **18** (1.6 g, 6.9 mmol) was added and the reaction mixture was left to stir overnight at room temperature. Then Na_2SO_3 was added to the orange coloured solution and was stirred for an additional 30 minutes. The resulting clean brown solution was extracted with ethyl acetate (3 x 15 mL). The combined organic layers were washed with brine, dried with Na_2SO_4 and concentrated by rotary evaporation. The crude product was purified by column chromatography (5:1 petroleum ether:ethyl acetate) to give diol **19**, a white solid, in 100 % yield. NMR data obtained matched that of literature.[2]
^{1}H NMR (500 MHz, $CDCl_3$): δ 8.03-7.44 (m, 5H), 4.50-4.43 (m, 2H), 4.36-4.33 (m, 1H), 4.04-3.99 (m, 1H), 3.16 (d, J = 8.7 Hz), 2.73 (d, J = 4.9 Hz).

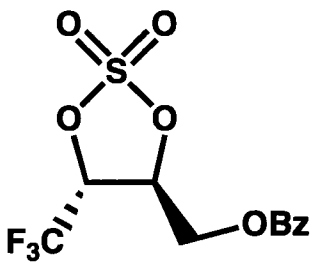

(iii) (3*R*, 4*S*)-3-benzoyl-4,4,4-trifluoromethyl-2,2-dioxo-1,3,2-dioxathiolane (20)[2]

To a flask containing diol **19** (2.14 g, 8.11 mmol), anhydrous methylene chloride (40 mL) and triethylamine (4.5 mL, 33 mmol) were added and cooled to 0°C. Then $SOCl_2$ (1.2 mL, 16 mmol) was added dropwise and the reaction mixture turned into a dark brown solution. The reaction was left to stir at 0°C until completion (1 hour) and then diluted with diethyl ether (20 mL) and water (20 mL). The organic layer was separated and the aqueous layer was extracted with diethyl ether (3 x 15 mL). The combined organic layers were washed with brine, dried over Na_2SO_3, filtered and evaporated. The resulting cyclic sulfite (2.59 g) was dissolved in water (20 mL), DCM (15 mL) and CH_3CN (15 mL) and $NaIO_4$ (2.1 g, 9.9 mmol) was added followed

by $RuCl_3$ (5 mg). The reaction mixture was left to stir for 6 hours until the oxidation was complete and saturdated Na_2CO_3 (20 mL) and diethyl ether (20 mL) were added. The resulting reaction mixture was filtered through a pad of celite and the organic layer was collected while the aqueous layer was extracted with diethyl ether (3 x 15 mL). The combined organic phases were dried over Na_2SO_4, filtered and concentrated *in vacuo*. The brown crude oil was purified by column chromatography (petroleum ether:ethyl acetate 10:1) to give a white solid (80 %). NMR data obtained matched that of literature.[2]
^{1}H NMR (400 MHz, $CDCl_3$): δ 8.06-7.46 (m, 5H), 5.29-5.25 (m, 1H), 5.10 (m, 1H), 4.79 (dd, J_1 = 13.1, J_2 = 3.76 Hz), 4.65 (dd, J_1 = 13.1, 4.32 Hz).

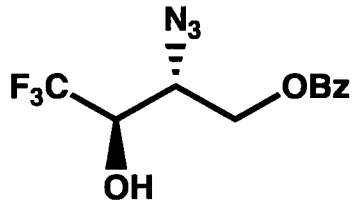

(iv) (2*R*,3*R*)-1-Benzoyl-2-azido-4,4,4-trifluorobutan-3-ol (21)[2]
A solution of cyclic sulfate **20** (1.74 g, 5.61 mmol) and NaN_3 (730 mg, 11.2 mmol) in DMF (23 mL) was stirred for 4 hours at room temperature. Once the reaction was complete, the solvent was removed by distillation under pressure and the resulting crude product was dilutd with THF (20 mL) and water (1 mL) and 75 % sulfuric acid (0.5 mL) and stirred for a half hour. Then $NaHSO_3$ (excess) was added and the reaction was left to stir for an additional hour. The crude product was filtered through a pad of silica and the filtrate was evaporated *in vacuo*. The crude was puridied by column chromatography (petroleum ether:ethyl acetate 8:1) to give a white solid in 85 % yield. NMR data obtained matched that of literature.[2]
^{1}H NMR (500 MHz, $CDCl_3$): δ 8.04-7.44 (m, 5H), 4.72 (dd, J_1 = 11.9, J_2 = 3.1 Hz, 1H), 4.64 (dd, J_1 = 11.9, J_2 = 6.85 Hz, 1H), 4.14 (m, 1H), 3.96 (td, J_1 = 6.8, J_2 = 3.2 Hz, 1H), 3.42 (br d, 1H). IR (film) ν_{max} = 2111.91

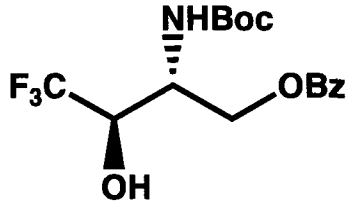

(v) (2*R*,3*R*)-1-Benzoyl-2-(*tert*-butoxycarbonyl)amino-4,4,4-trifluorobutan-3-ol (22)[3]

A one-pot reaction to reduce the azide and protect the primary amine produced was performed by dissolving intermediate **21** (1.07 g, 3.71 mmol) in THF (8 mL) and adding Pd/C and di-*tert*-butyl-dicarbonate (1.2 g, 5.6 mmol). The resulting mixture was degassed and H_2 gas was added. The reaction was left to stir overnight at ambient temperature. Once the reaction was complete, the solution was filtered through a pad of celite and the filtrate was evaporate *in vacuo*. The final product, a white solid, was obtained in 92 % yield. For greater purity, column chromatography was performed (petroleum ether:ethyl acetate 9:1). NMR data obtained matched that of literature.[2]

^{1}H NMR (300 MHz, $CDCl_3$): δ 8.08-7.46 (m, 5H), 5.08 (d, J = 8.1 Hz, 1H), 4.70 (dd, J_1 =11.6, J_2 = 6.9 Hz, 1H), 4.48 (dd, J_1 =11.8, J_2 = 4.1 Hz, 1H), 4.35 (m, 1H), 4.24 (m, 1H), 4.04 (d, J_1 = 6.5 Hz, 1H), 1.45 (s, 9H).

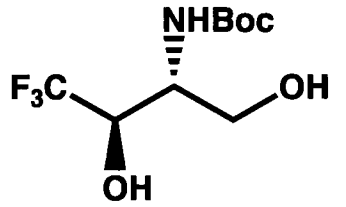

(vi) (2*R*,3*R*)-2-(*tert*-Butoxycarbonyl)amino-4,4,4-trifluoro-1,3-butandiol (23)[3]

To a solution of compound **22** (1.64 g, 4.52 mmol) in methanol (8 mL), NaOMe (1M, 13.5 mL, 13.5 mmol) was added at ambient temperature and stirred for 1 hour. Then acidic resins were added to neutralize the reaction mixture and the filtrate was collected and evaporated *in vacuo*. The crude product was purified from methyl benzoate by column chromatography (7:3 petroleum ether:ethyl acetate), to give a white solid (92 %). NMR data obtained matched that of literature.[3]

^{1}H NMR (300 MHz, MeOD): δ 4.03-3.96 (m, 1H), 3.81-3.65 (m, 3H), 1.41 (s, 9H).

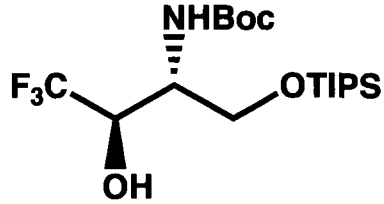

(vii) (2*R*,3*R*)-1-Triisoprpylsilyl-2-(*tert*-Butoxycarbonyl)amino-4,4,4-trifluoro-3-butanol (24)

To a solution of intermediate **23** (700 mg, 2.70 mmol) in anhydrous methylene chloride (14 mL), imidazaole (370 mg, 5.44 mmol) and TIPSCl (700 μL, 3.30 mmol) was added at 0°C. The reaction mixture was left to stir overnight at ambient temperature. Then 10% HCl was used to neutralize the reaction mixture and the organic layer was collected and the aqueous layer was extracted with diethyl ether (3 x 5 mL). The combined organic layer was dried over Na_2SO_4, filtered and evaporated *in vacuo.* The crude product was purified by column chromatography (95:5 petroleum ether:ethyl acetate).

^{1}H NMR (500 MHz, $CDCl_3$): δ 5.34 (d, *J* =8.8 Hz, 1H), 4.63 (d, *J* = 9.2 Hz), 4.17-4.10 (m, 2H), 3.94-3.91 (m, 2H), 1.42 (s, 9H), 1.14-1.07 (m, 21H). ^{13}C NMR (126 MHz, $CDCl_3$): δ 155.25, 124.38 (q, *J* = 283.24), 80.22, 73.33 (q, *J* = 120 Hz), 64.63, 49.41, 28.24, 17.70, 11.55.^{19}F NMR (100 MHz, $CDCl_3$): δ -76.5. LRMS calcd for $(M+H)^+$ 415.236, $(M+Na)^+$ 438.226, found 438.4.

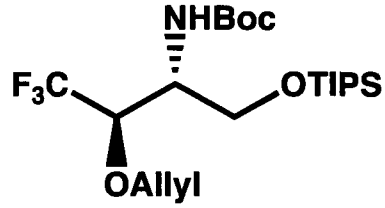

(viii) (2*R*,3*R*)-1-Triisoprpylsilyl-2-(*tert*-Butoxycarbonyl)amino-3-allyl-4,4,4-trifluoro-butane (25)

To a solution of intermediate **24** (1.07 g, 2.58 mmol) in DMF (30 mL), allyl bromide (440 μL, 5.13 mmol) was added. Then in 5 mg portions, NaH was added over period of 1 hour at 0°C, and the reaction mixture was left to stir overnight at room temperature. The DMF was then removed *in vacuo*, and the crude product was purified by column chromatography (98.5:1.5 petroleum ether:ethyl acetate) to give intrmediate **25**, a clear and colourless oil (80 %). ^{1}H NMR (500 MHz, $CDCl_3$): δ 5.90-5.79 (m, 2H), 5.28-5.01 (m, 4H), 4.28-4.19 (m, 2H), 4.02-3.76 (m, 5H), 1.40 (s, 9H),

1.04 (m, 21H). ^{13}C NMR (126 MHz, $CDCl_3$): δ 155.08, 133.39, 125.2 (q, J = 285.33), 79.68, 75.47, 61.68, 51.42, 28.29, 17.95, 11.89. ^{19}F NMR (400 MHz, $CDCl_3$): δ -72.9.

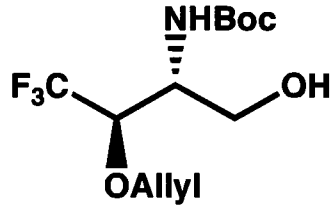

(ix) (2*R*,3*R*)-2-(*tert*-Butoxycarbonyl)amino-3-allyl-4,4,4-trifluoro-1-butanol (26)
For TIPS cleavage, TBAF (235 mg, 0.90 mmol) was added to a solution of **24** (340 mg, 0.747 mmo) in anhydrous THF (5 mL) under argon. The raction was left to stir overnight at room temperature. Then 10 % HCl was added and the organic layer was collected and the aqueous layer was extracted with ethyl acetate (3 x 10 mL). The combined organic layers were washed with saturaded sodium bicarbonate, washed with brine, dried over Na_2SO_4, filtered and concentrated by rotary evaporation under pressure. The crude product was purified by column chromatography (petroleum ether:ethyl acetate 4:1) to give a white solid in 90 % yield. ^{1}H NMR (500 MHz, $CDCl_3$): δ 5.90-5.82 (m, 1H), 5.31-5.25 (m, 3H), 4.33 (dd, J_1 = 12.4, J_2 = 5.7 Hz, 1H), 4.14-4.03 (m, 3H), 3.82 (m, 1H), 3.67 (br d, J = 10.1 Hz, 1H), 1.44 (s, 9H). ^{13}C NMR (126 MHz, $CDCl_3$): δ 155.44, 132.73, 125.74, 123.47, 119.64, 80.17, 74.57, 61.82, 50.40, 28.28. ^{19}F NMR (400 MHz, $CDCl_3$): δ -73.3. LRMS calcd for $(M+H)^+$ 299.134, $(M+Na)^+$ 322.124, found 322.128.

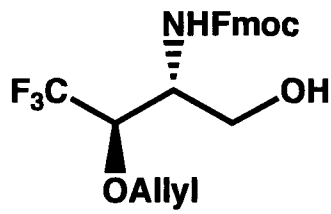

(x) (2*R*,3*R*)-2-(9H-fluoren-9-ylmethoxycarbonyl)amino-3-allyl-4,4,4-trifluoro-1-butanol (27)
To a flask containing **26** (383 mg, 1.28 mmol) a 1:1 mixture of DCM and TFA (g mL), was added and the reaction was stirred for 1 hour at ambient temperature. Then, the solvent was evaporated and a 1:1 mixture of dioxane and 10% sodium bicarbonate was added (8 mL) followed by Fmoc-OSucc (540 mg, 1.99 mmol). The resulting mixture was left to stir overnight at ambient temperature. Ethyl acetate was then added and the organic layer was collected while the aqueous layer was extracted with ethyl acetate (3 x 10 mL). The combined organic layers were was with brine, dried over Na_2SO_4, filtered and evaporated *in vacuo*. The resulting

yellow crude product was purified by column chromatography (petroleum ether:ethyl acetate 4:1) to give a white solid, in 90 % yield. ^{1}H NMR (500 MHz, $CDCl_3$): δ 7.76-7.29 (m, 8H), 5.86-5.80 (m, 1H), 5.55 (br d, *J* = 7.6 Hz, 1H), 5.27 (d, *J* =17.4 Hz, 1H), 5.21 (d, *J* = 10.3 Hz, 1H), 4.45-4.43 (m, 2H), 4.33-4.29 (dd, *J* = 12.5, 1H), 4.22-4.19 (t, *J* = 6.55 Hz, 1H), 4.07-4.00 (m, 3H), 3.92-3.89 (m, 1H), 3.71-3.67 (m, 1H), 2.30 (dd, J_1 = 8.9 Hz, J_2 = 2.8 Hz, 1H). ^{13}C NMR (126 MHz, $CDCl_3$): δ 155.86, 143.74, 143.61, 141.33, 132.62, 127.76, 127.05, 124.92, 120.03, 119.69, 74.70, 66.86, 61.52, 50.75, 47.18. ^{19}F NMR (400 MHz, $CDCl_3$): δ -73.3. LRMS calcd for $(M+H)^+$ 421.150, $(M+Na)^+$ 444.139, found 444.156.

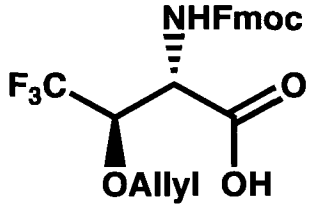

(xi) (2*R*,3*R*)-2-(9H-fluoren-9-ylmethoxycarbonyl)amino-3-allyl-4,4,4-trifluoro-butanoic acid (T(F))

To a solution of **26** (260 mg, 0.62 mmol) in acetone (15 mL), Jones' reagent (0.9 M, 3.7 mL, 3.3 mmol) was added at 0°C and the reaction was left to stir overnight at ambient temperature. Then isopropanol was added until the solution turned blue. The solvent was then evaporated by a rotary evaporator and the crude product was diluted in water (10 mL) and ethyl acetate (10 mL). The organic layer was separated and the aqueous phase was extracted with ethyl acetate (3 x 10 mL). The combined organic layers were washed with brine, dried over Na_2SO_4, filtered and evaporated. The crude product was then purified by column chromatography (petroleum ether:ethyl acetate 2:3). For greater purity, recrystallization was performed (acetone/petroleum ether) to give **T(F)** as a white solid in 80 % yield. ^{1}H NMR (500 MHz, MeOD): δ 7.79-7.28 (m, 8H), 5.93-5.85 (m, 1H), 5.30 (d, *J* = 17.4 Hz, 1H), 5.16 (d *J* = 10.3 Hz, 1H), 4.59 (d, *J* = 6.4 Hz, 1H), 4.38-4.35 (m, 1H), 4.30-4.27 (m, 2H), 4.23 (m, 3H). ^{13}C NMR (126 MHz, MeOD): δ 143.77, 141.11, 133.48, 127.34, 126.74, 124.88, 124.83, 119.45, 116.95, 76.28, 73.06, 66.86 . ^{19}F NMR (400 MHz, MeOD): δ - 74.5. LRMS calcd for $(M+H)^+$ 435.129, $(M+Na)^+$ 458.119, found 458.166. IR (film) ν_{max} = 1697.24

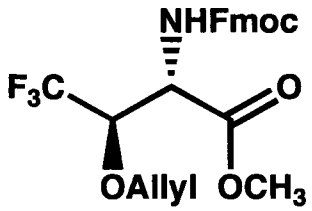

(xii) (2*R*,3*R*)-2-(9H-fluoren-9-ylmethoxycarbonyl)amino-3-allyl-4,4,4-trifluoro-methylbutanoate (15)

To a solution of **T(F)** (95 mg, 0.218 mmol) in methanol (3 mL), $SOCl_2$ (30 µL, 0.412 mmol) was added at ambient temperature and stirred for 2 hours. Then the solvent was removed by rotary evaporation and the crude product was purified by column chromatography (petroleum ether:ethyl acetate 97:3) to give **15** as a white solid in 70 % yield. ^{1}H NMR (500 MHz, $CDCl_3$): δ 7.76-7.29 (m, 8H), 5.89-5.81 (m, 1H), 5.49 (d, *J* = 8.9 Hz), 5.31 (d, *J* = 17.2 Hz, 1H), 5.24 (d, *J* = 10.3 Hz, 1H), 4.85-4.83 (m, 1H), 4.43-4.27 (m, 2H), 4.26-4.13 (m, 4H), 3.78 (s, 3H).^{13}C NMR (500 MHz, $CDCl_3$): δ 168.59, 155.64, 143.6, 141.27, 132.59, 127.76, 127.09, 125.06, 125.04, 120.01, 119.56, 76.11, 73.46, 67.47, 52.93, 46.99. ^{19}F NMR (400 MHz, $CDCl_3$): δ - 72.8. LRMS calcd for $(M+H)^+$ 449.145, $(M+Na)^+$ 472.135, found.

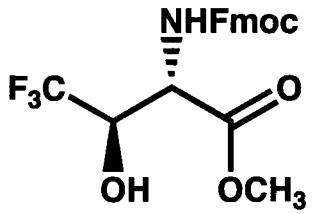

(xiii) (2*R*,3*R*)-2-(9H-fluoren-9-ylmethoxycarbonyl)amino-3-hydroxy-4,4,4-trifluoro-methylbutanoate (15)

To a flame-dried flask, a solution of (1,5-Cyclooctadiene)bis-(methyldiphenylphosphine)iridium(I)-hexafluorophosphate (10 mg, 0.012 mmol) in anhydrous THF (2 mL) was stirred under H_2 gas. Once the red solution turned into a clear yellow colour, argon was passed through the flask to remove any remaining H_2 gas. The iridium catalyst solution was then transferred to a flask containing a solution of **15** in THF (2 mL) under argon and the resulting solution was stirred for one hour. Then excess I_2 and a few drops of H_2O were added and stirred for an addition 15 minutes. The resulting mixture was then transferred to a separatory funnel and a saturated solution of sodium thiosulphate (10 mL) was added. The organic phase was collected and the aqueous layer was extracted with ethyl acetate

(3 x 10 mL), dried over Na_2SO_4, filtered and concentrated *in vacuo*. The crude product was then purified by column chromatography (petroleum ether:ethyl acetate 4:1) to give **15**, a white solid in 60 % yield. ^1H NMR (500 MHz, $CDCl_3$): δ 7.77-7.29 (m, 8H), 5.86 (d, J = 5.45 Hz, 1H), 4.97 (d, J = 9.05 Hz, 1H), 4.73 (br d, J = 3.75 Hz, 1H), 4.54-4.49 (m, 2H), 4.39-4.36 (m, 1H), 4.22 (t, J = 6.85 Hz, 1H), 3.83 (s, 3H). ^{13}C NMR (126 MHz, $CDCl_3$): δ 168.02, 157.55, 143.24, 141.22, 127.79, 127.07, 124.87, 120.00, 71.84, 67.99, 55.16, 53.51, 46.85. ^{19}F NMR (400 MHz, $CDCl_3$): δ -75.3. LRMS calcd for $(M+H)^+$ 409.113, $(M+Na)^+$ 432.103, found 432.071.

(c) General Procedure for Solid-Phase Synthesis of [T(F)AA]$_4$ and [T(F)GG]$_4$

All peptides were synthesized using conventional Fmoc solid-phase synthesis on an APEX 396 using acid labile Wang resin. A typical procedure started from Fmoc-glycine Wang resin (or Fmoc-alanine) with loading capacities of ~0.066 mmol/g. The resin was swollen in DMF for 30 minutes in the reaction vessel. The solvent was then drained and 20% piperidine solution in DMF was added. The solution was allowed to stir for 1 hour, drained, and the resin was then washed with three aliquots of DMF. Kaiser and TNBS tests for free amine were then performed. The next successive building block (5 equivalents) to be coupled (commercially available amino acid) was premixed with 5 equivalents of HBTU and 10 equivalents of DIPEA in DMF for 20 minutes. The reaction solution was then transferred to the resin, and the reaction mixture was allowed to stir for 4 hours. Kaiser and TNBS tests were performed to verify the coupling had reached completion (negative test outcome). The reaction vessel was drained and the resin was rinsed three times with DMF. The resin was treated with 20% piperdine in DMF solution for 1 hour, the flask was drained and the resin was washed thoroughly with DMF. Kaiser and TNBS tests were performed to ensure the presence of free amine. The fluorinated threonine (**T(F)**) building block (1.5 equivalents) was premixed with 1.6 equivalents of HBTU in DMF, followed by the addition of 3.0 equivalents of DIPEA in DMF. The reaction was stirred for 30 minutes, transferred to the reaction vessel and stirred for 36 hours. The Fmoc deprotection and coupling steps were repeated until twelve amino acid residues were coupled to the resin. To cleave the allyl groups, anhydrous THF was added to the beads followed by a solution of iridium catalyst ((1,5-Cyclooctadiene)bis-(methyldiphenylphosphine)iridum(I)-hexafluorophosphate, 1.0 equiv.) that was gassed with H_2 then argon. The beads were gently stirred with the use of a stir bar overnight at ambient temperature. The enol ether formed by the isomerization of the allyl group was cleaved when the peptide was cleaved from the resin. This was done by successively rinsing the beads

with DMF, MeOH, and CH_2Cl_2, and stirred for 2 hours in 1:1 (v:v) trifluoroacetic acid and CH_2Cl_2. The solution was then filtered and concentrated.

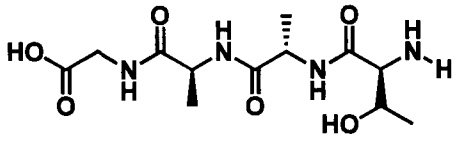

(xiv) Spectral data for crude $[TAA]_4$
^1H NMR (500 MHz, $CDCl_3$): δ 4.20-3.97 (m, 4H), 1.24-1.03 (m, 9H). LRMS calcd for $(M+H)^+$ 1047.519, $(M+Na)^+$ 1071.5094, found 1048.471, 1071.476.

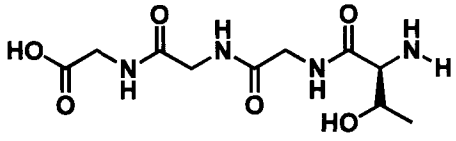

(xv) Spectral data for crude $[TGG]_4$
^1H NMR (500 MHz, $CDCl_3$): δ 4.22-4.12 (m, 2H), 3.99-3.69 (m, 6H), 1.04-1.02 (m, 3H). LRMS calcd for $(M+H)^+$ 935.395, $(M+Na)^+$ 958.284, found 958.306, 935.396.

(d) General Procedure for IRI Assay[1]

Samples were assayed for recrystallization-inhibition (RI) activity using the "splat cooling" method as described previously.[4] A total of three images of the resulting ice wafer were photographed through a Leitz compound microscope equipped with an Olympus 20X (infinity corrected) objective with a Nikon CoolPix digital camera. Sample analysis for ice crystal sizes were analyzed using the mean elliptical method. In this method, the twelve largest ice crystals were chosen from the field of view (FOV) in each image. Selection of these crystals was arbitrary in that they were chosen after a visual inspection of the image. The two dimensional surface area of each of these ten crystals was then calculated via approximation of

the crystal as an elliptical area. The major and minor elliptical axes were defined by the two largest orthogonal dimensions across the ice grain surface. The surface area of each ice grain was then calculated based on the formula: $A = \pi ab$, in which A represented area; a and b represented the length of the major and minor elliptical axes. Totalling all individual measurements for each FOV produces a value for the average grain surface area referred to as the mean largest grain size (MLGS). Error was calculated using standard error of the mean (SEM).

(e) General Procedure for TH Assay[1]

Nanoliter osmometry was performed using a Clifton nanoliter osmometer (Clifton Technical Physics, Hartford, NY) as described by Chakrabartty and Hew.[5] All measurements were made in double distilled water. Ice crystal morphology was observed through a Leitz compound microscope equipped with an Olympus 20X (infinity corrected) objective, Leitz Periplan 32X photo eyepiece and a Hitachi KP-M2U CCD camera connected to a Toshiba MV13K1 TV/VCR system. Still images were captured directly using a Nikon CoolPix digital camera.

(f) Spectra of all Intermediates (18-27, T(F), and 30) and of Peptides $[TAA]_4$,$[T(F)AA]_4$,$[TGG]_4$ and $T(F)GG]_4$.

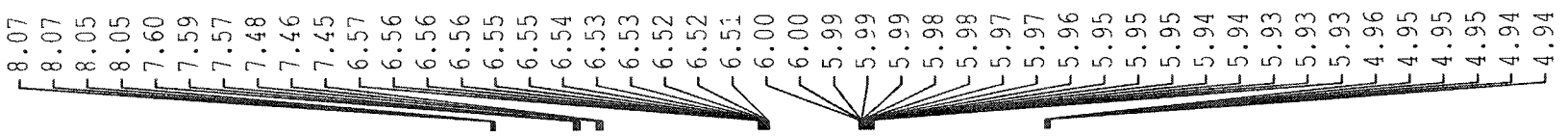

^{1}H NMR

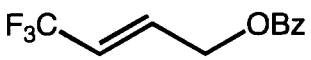

18

^{1}H NMR

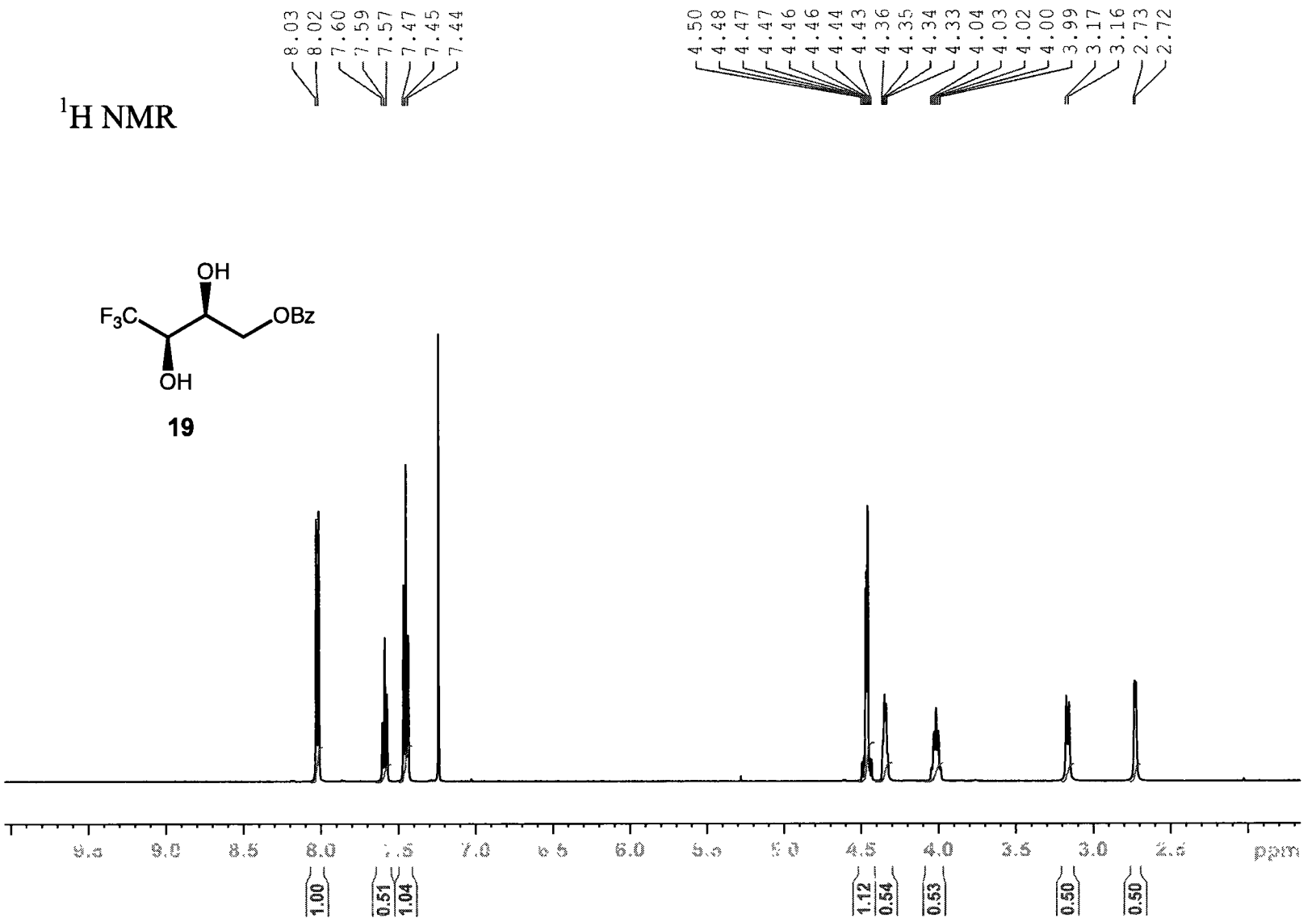
8.03
8.02
7.60
7.59
7.57
7.47
7.45
7.44
4.50
4.48
4.47
4.47
4.46
4.46
4.44
4.43
4.36
4.35
4.34
4.33
4.04
4.03
4.02
4.00
3.99
3.17
3.16
2.73
2.72
OH
F3C
OBz
OH
19
ppm
1.00
0.51
1.04
1.12
0.54
0.53
0.50
0.50

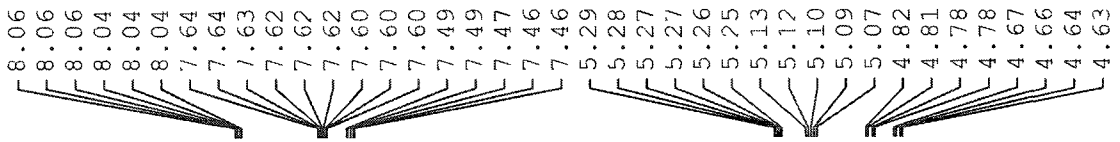
8.06
8.06
8.06
8.04
8.04
8.04
7.64
7.64
7.63
7.62
7.62
7.62
7.60
7.60
7.60
7.49
7.49
7.47
7.46
7.46
5.29
5.28
5.27
5.27
5.26
5.25
5.13
5.12
5.10
5.09
5.07
4.82
4.81
4.78
4.78
4.67
4.66
4.64
4.63

^{1}H NMR

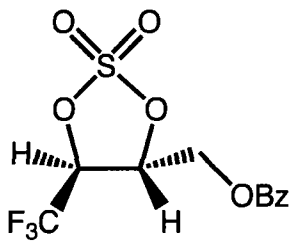
O
O
S
O
O
H
OBz
F3C
H

20

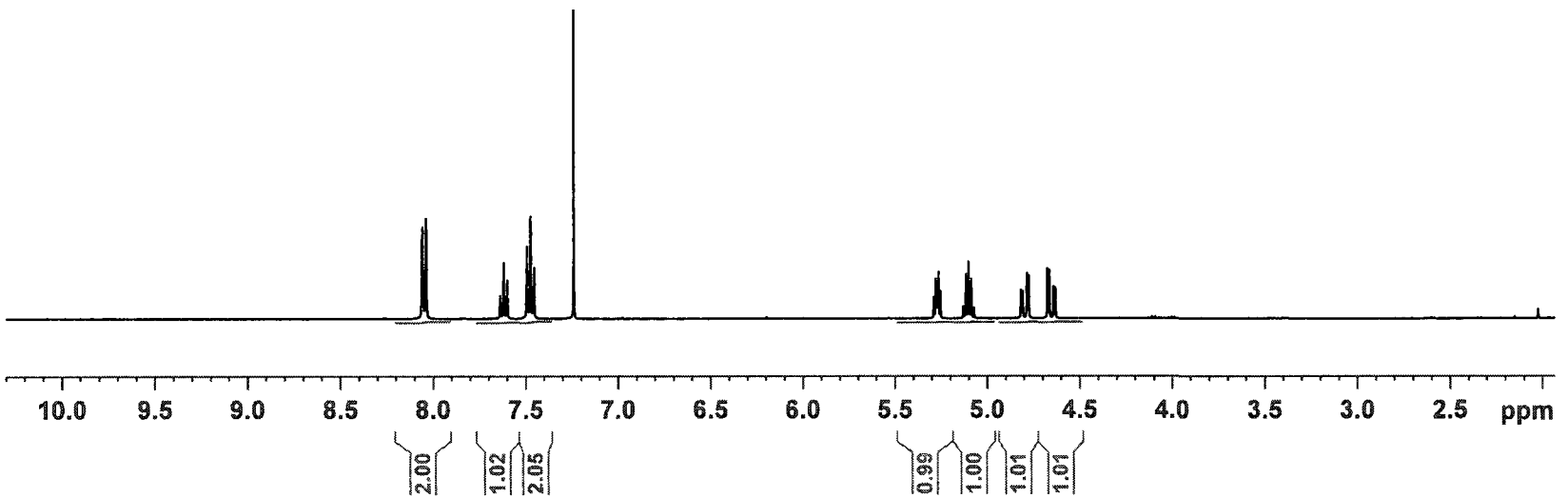
10.0
9.5
9.0
8.5
8.0
7.5
7.0
6.5
6.0
5.5
5.0
4.5
4.0
3.5
3.0
2.5
ppm
2.00
1.02
2.05
0.99
1.00
1.01
1.01

^{1}H NMR

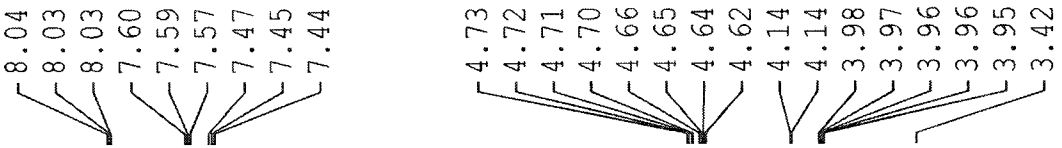
8.04
8.03
8.03
7.60
7.59
7.57
7.47
7.45
7.44
4.73
4.72
4.71
4.70
4.66
4.65
4.64
4.62
4.14
4.14
3.98
3.97
3.96
3.96
3.95
3.42

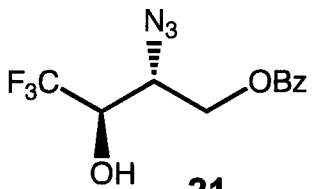
N3
F3C
OBz
OH

21

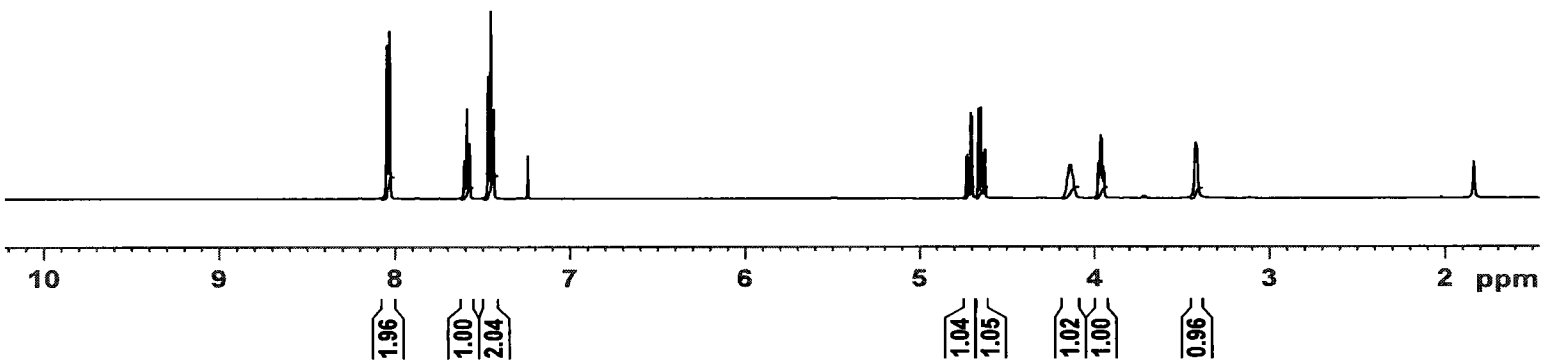
10
9
8
7
6
5
4
3
2
ppm
1.96
1.00
2.04
1.04
1.05
1.02
1.00
0.96

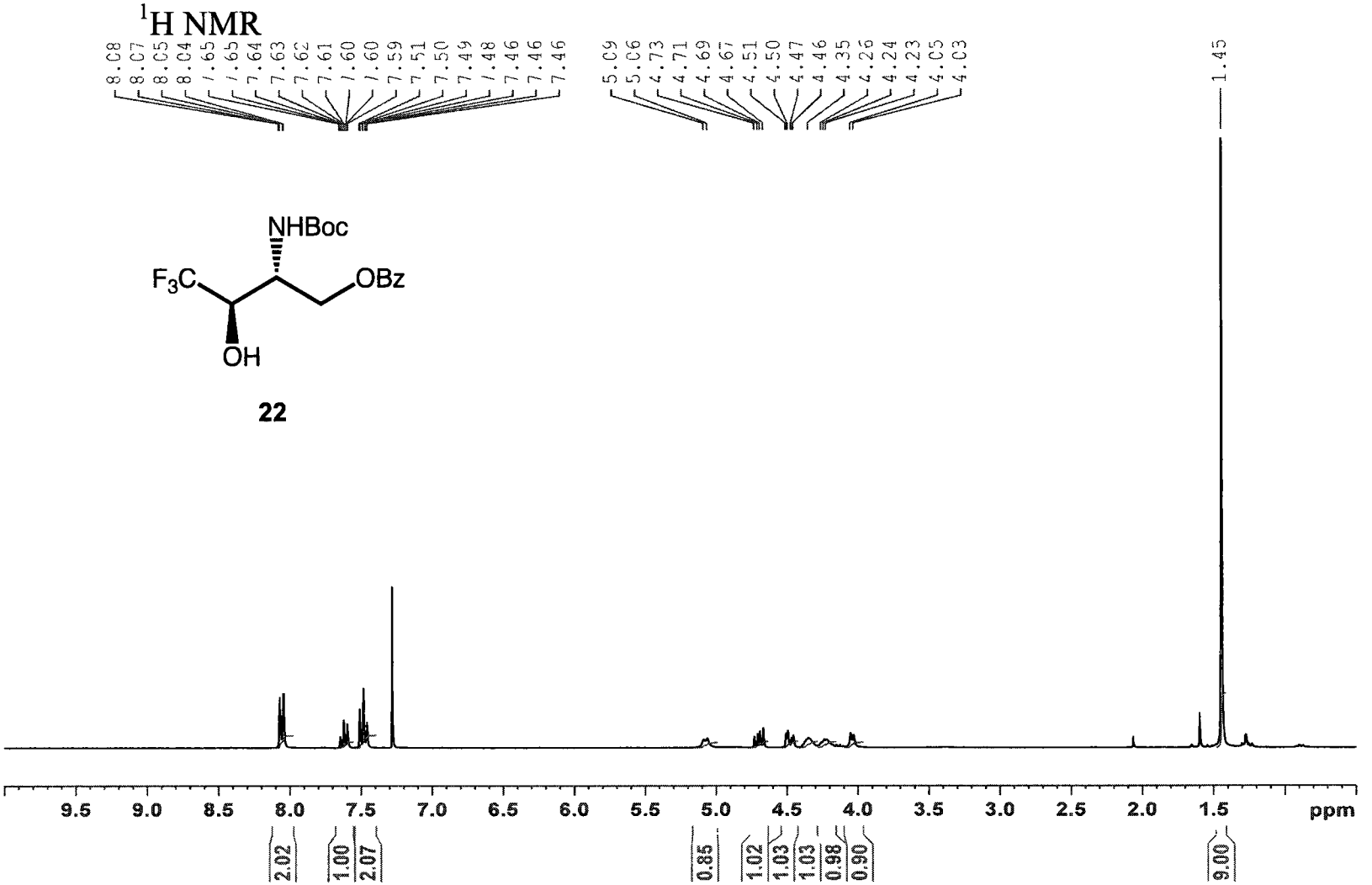
1H NMR
8.08
8.07
8.05
8.04
7.65
7.65
7.64
7.63
7.62
7.61
7.60
7.60
7.59
7.51
7.50
7.49
7.48
7.46
7.46
7.46
5.09
5.06
4.73
4.71
4.69
4.67
4.51
4.50
4.47
4.46
4.35
4.26
4.24
4.23
4.05
4.03
1.45
NHBoc
F3C
OBz
OH
22
9.5
9.0
8.5
8.0
7.5
7.0
6.5
6.0
5.5
5.0
4.5
4.0
3.5
3.0
2.5
2.0
1.5
ppm
2.02
1.00
2.07
0.85
1.02
1.03
1.03
0.98
0.90
9.00

^{1}H NMR

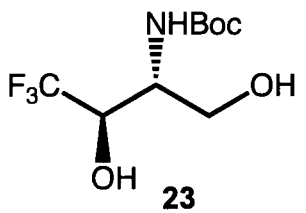
NHBoc
F3C
OH
OH

23

4.03
4.01
4.00
3.98
3.96
3.81
3.79
3.78
3.78
3.77
3.75
3.74
3.72
3.71
3.68
3.67
3.65
3.65
1.41
9.5
9.0
8.5
8.0
7.5
7.0
6.5
6.0
5.5
5.0
4.5
4.0
3.5
3.0
2.5
2.0
1.5
1.0
ppm
0.98
2.97
9.00

^{19}F NMR

^{1}H NMR

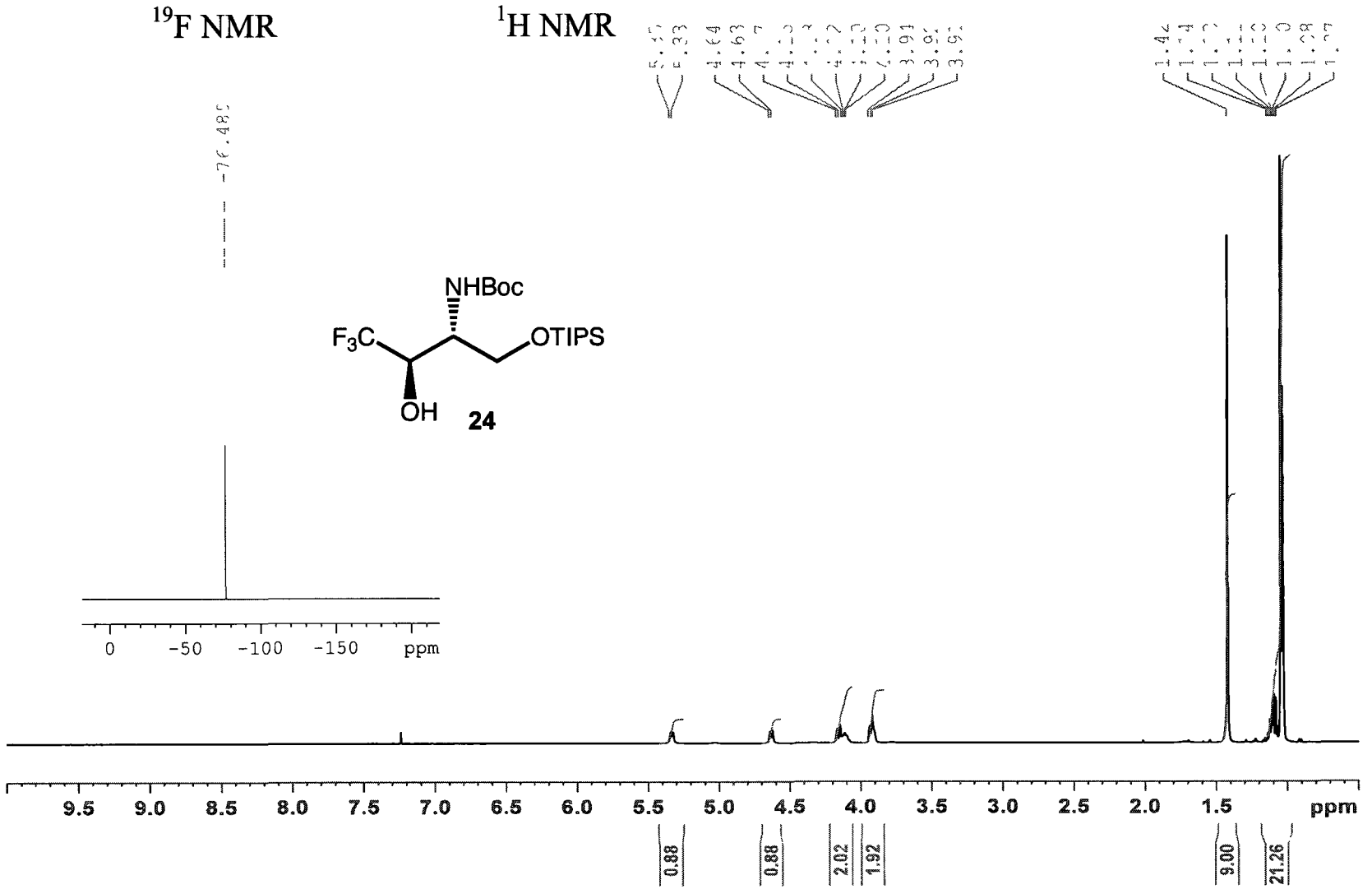

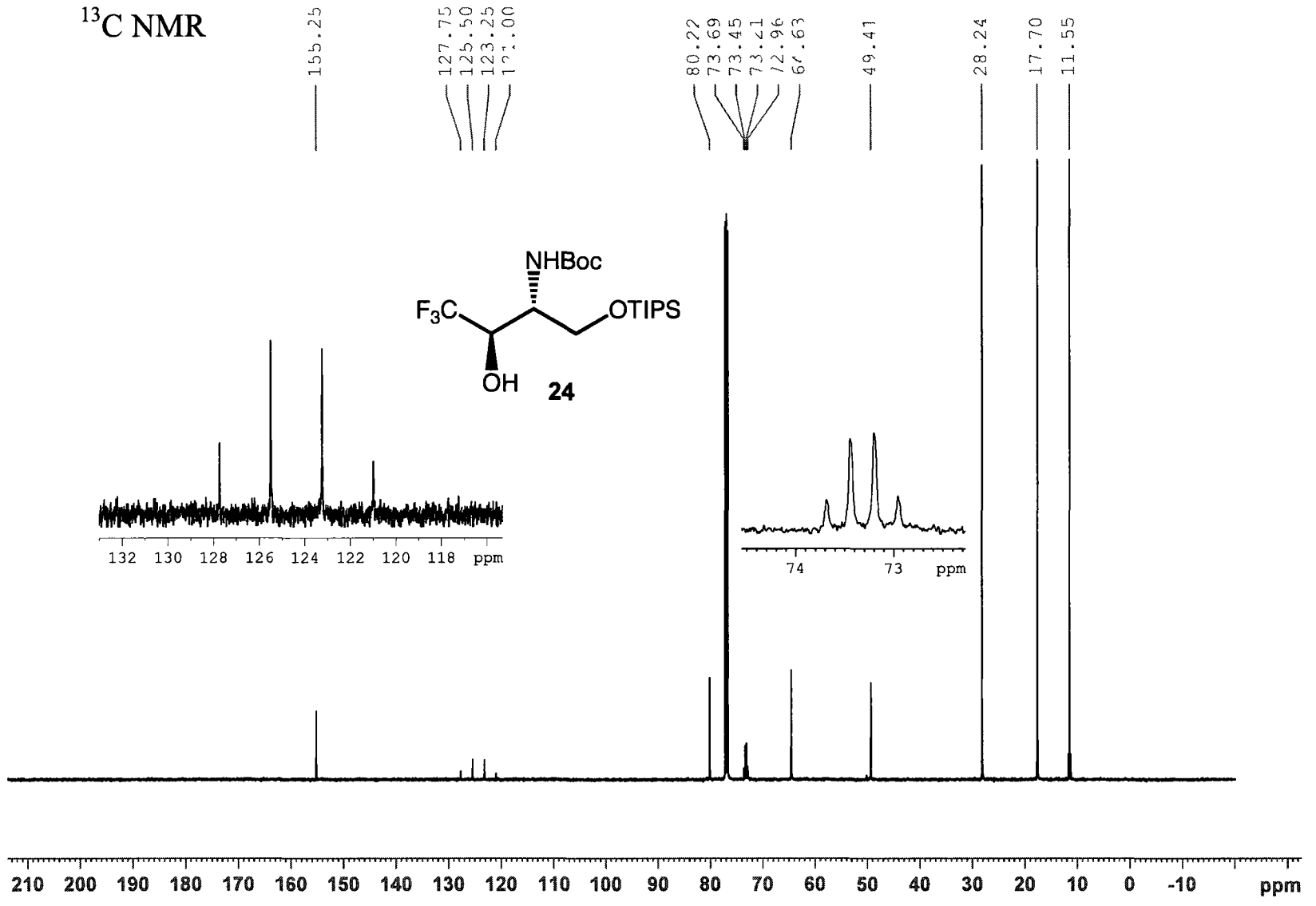
13C NMR
155.25
127.75
125.50
123.25
122.00
80.22
73.69
73.45
73.21
72.96
64.63
49.41
28.24
17.70
11.55
NHBoc
F3C
OTIPS
OH
24
132 130 128 126 124 122 120 118 ppm
74 73 ppm
210 200 190 180 170 160 150 140 130 120 110 100 90 80 70 60 50 40 30 20 10 0 -10 ppm

^{1}H NMR

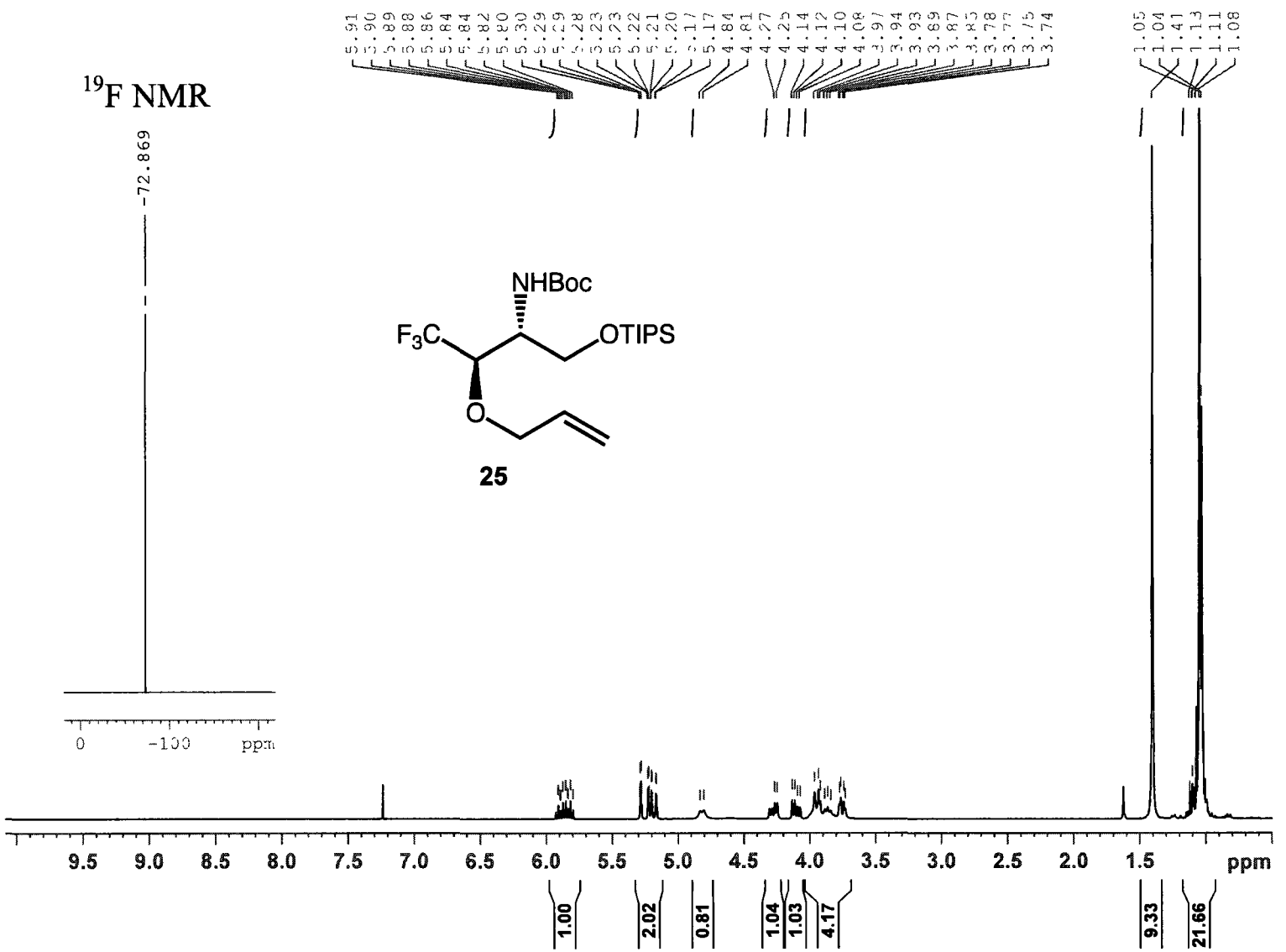

^{19}F NMR

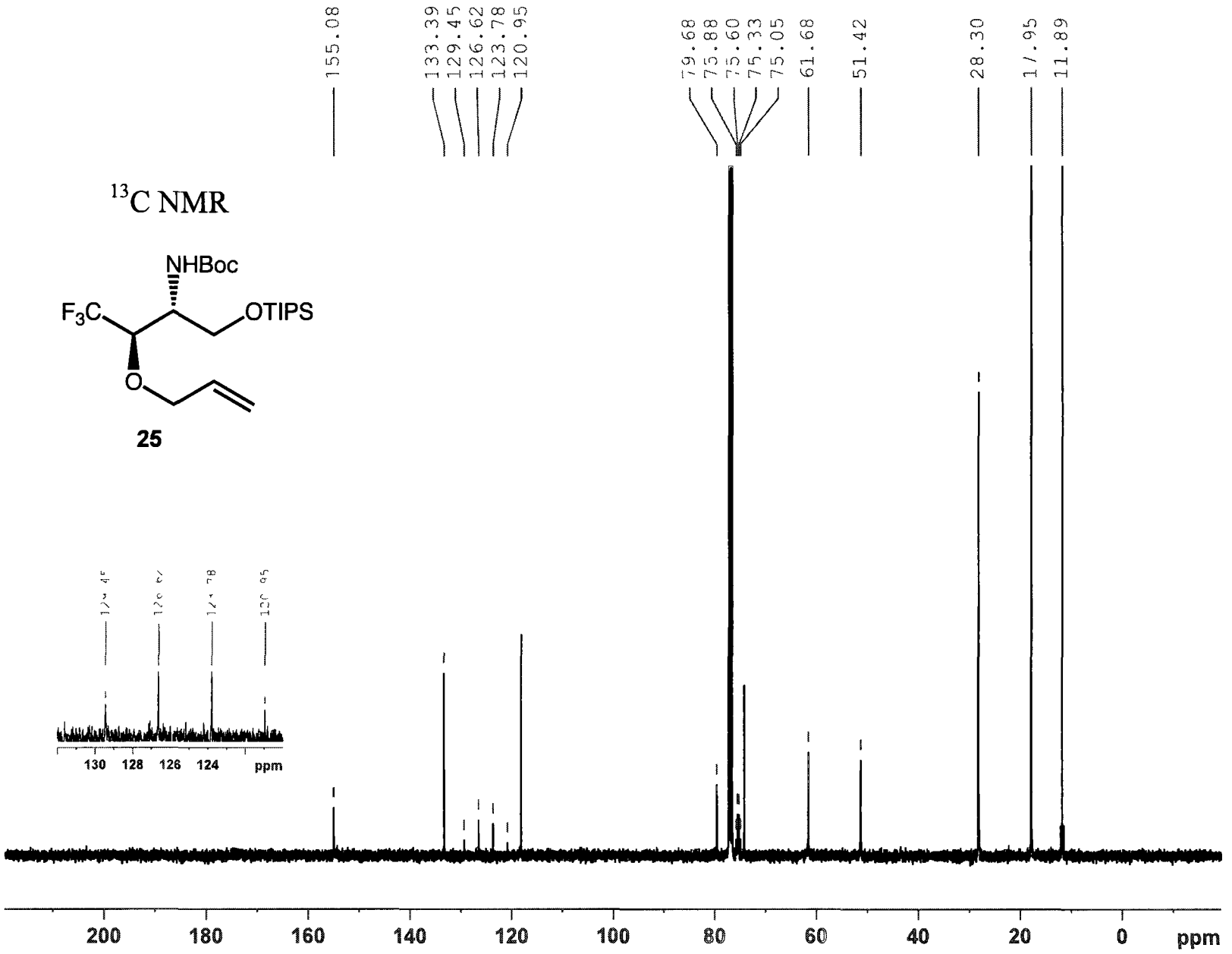
155.08
133.39
129.45
126.62
123.78
120.95
79.68
75.88
75.60
75.33
75.05
61.68
51.42
28.30
17.95
11.89
13C NMR
NHBoc
F3C
OTIPS
O
25
130 128 126 124 ppm
200 180 160 140 120 100 80 60 40 20 0 ppm

^{1}H NMR

^{19}F NMR

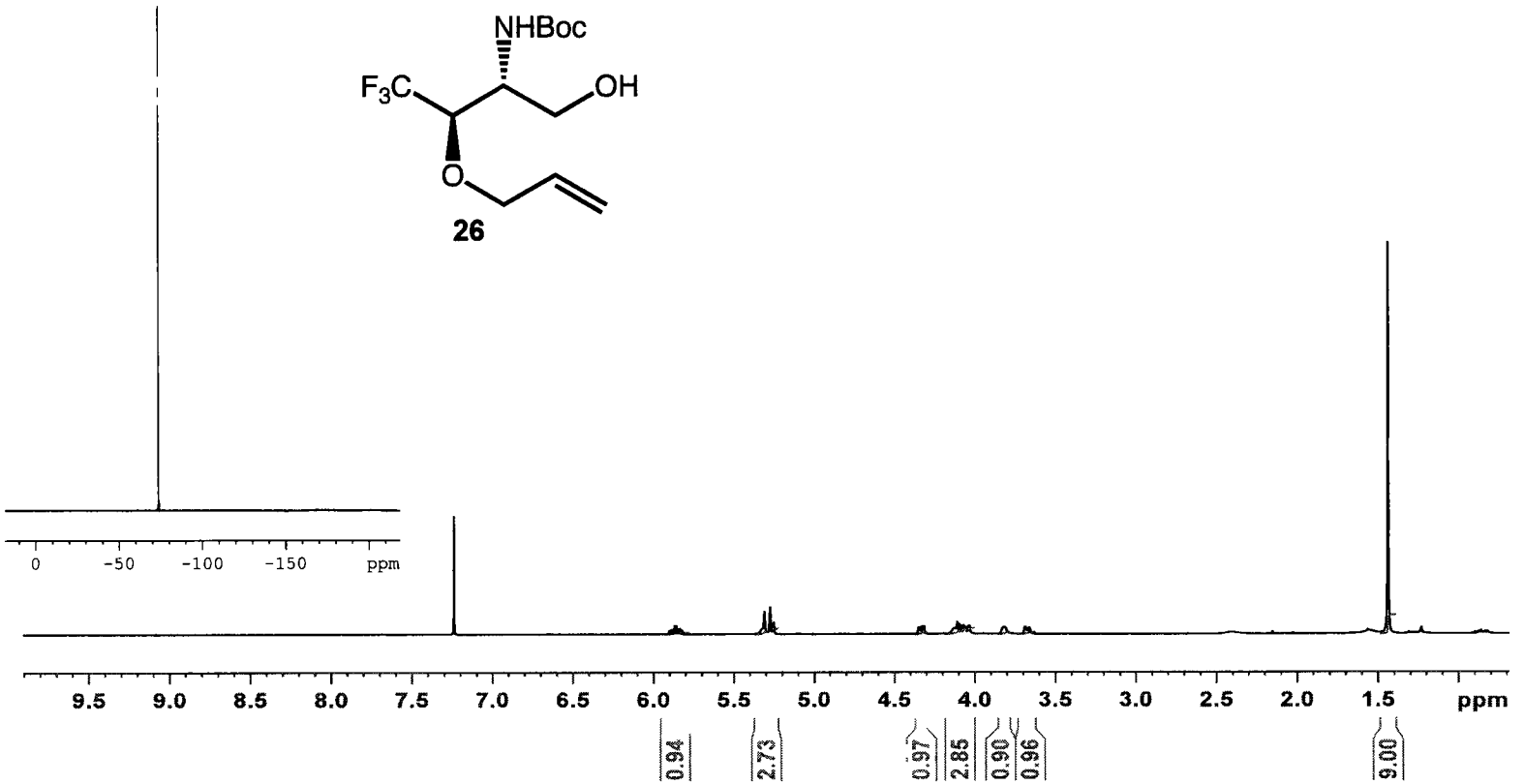

^{13}C NMR

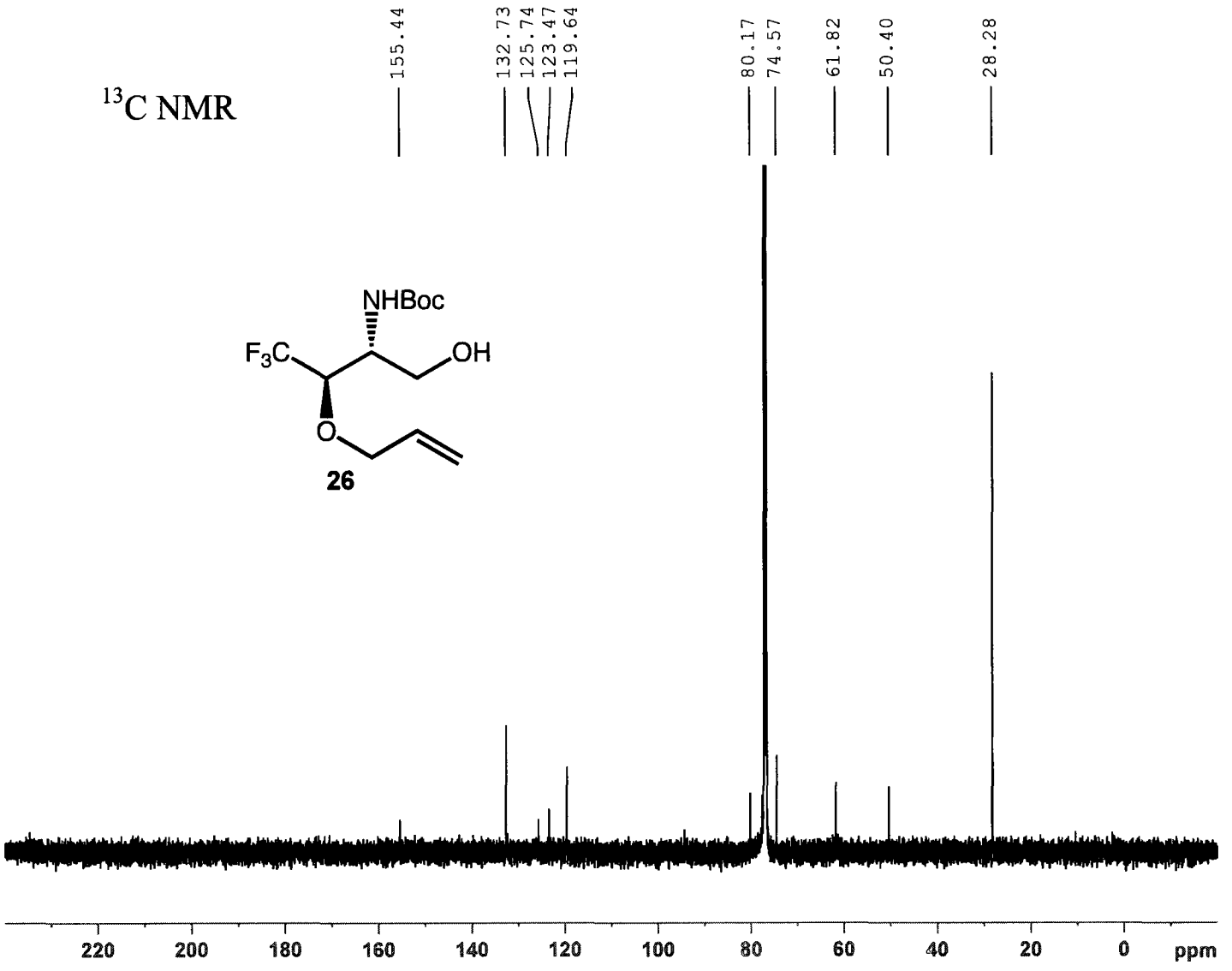
155.44
132.73
125.74
123.47
119.64
80.17
74.57
61.82
50.40
28.28
NHBoc
F3C
OH
O
26
220
200
180
160
140
120
100
80
60
40
20
0
ppm

^{1}H NMR

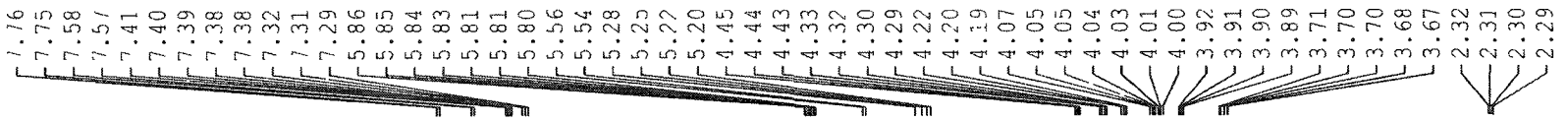

^{19}F NMR

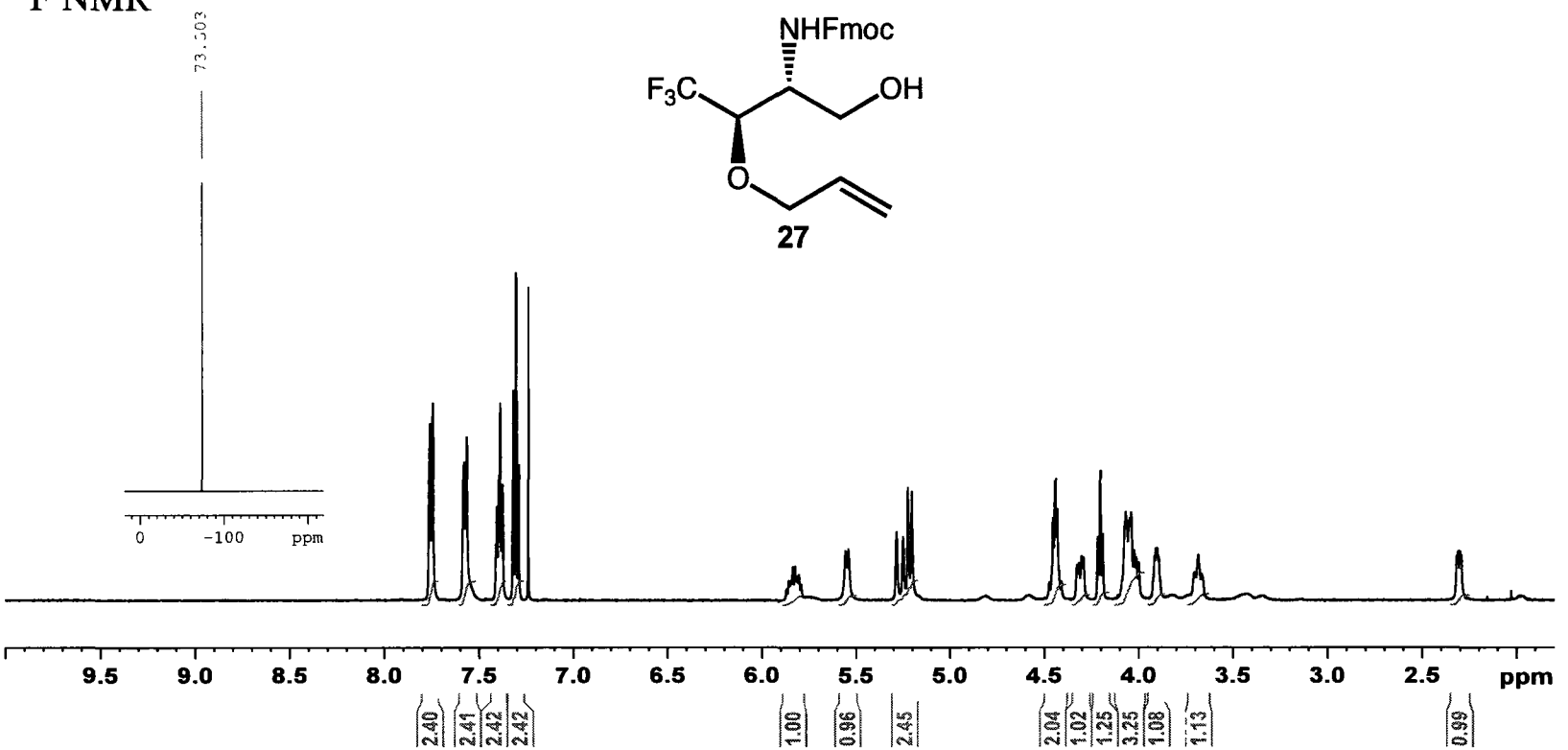

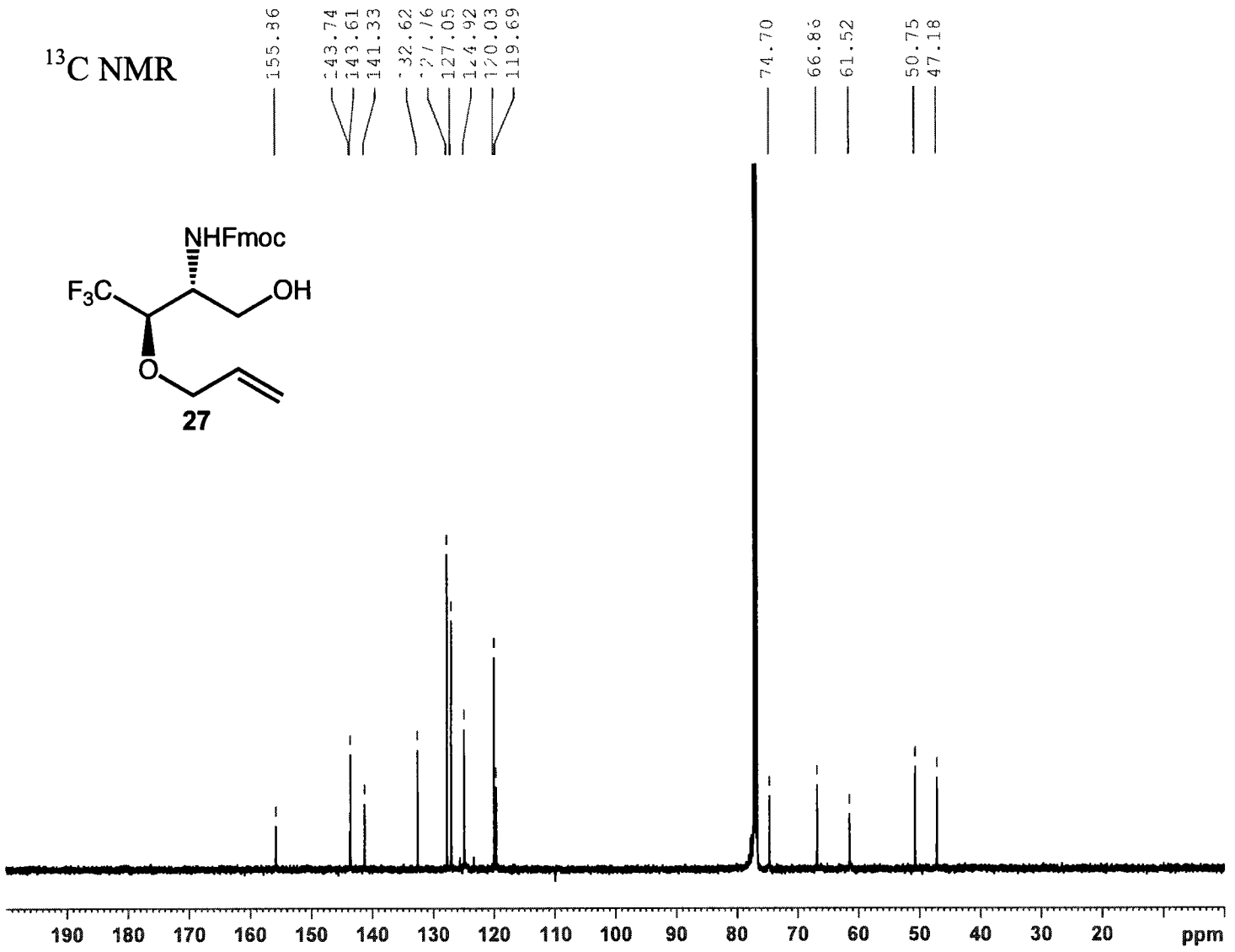
13C NMR
155.36
143.74
143.61
141.33
132.62
127.76
127.05
124.92
120.03
119.69
74.70
66.86
61.52
50.75
47.18
NHFmoc
F3C
OH
O
27
190
180
170
160
150
140
130
120
110
100
90
80
70
60
50
40
30
20
ppm

^{1}H NMR

^{19}F NMR

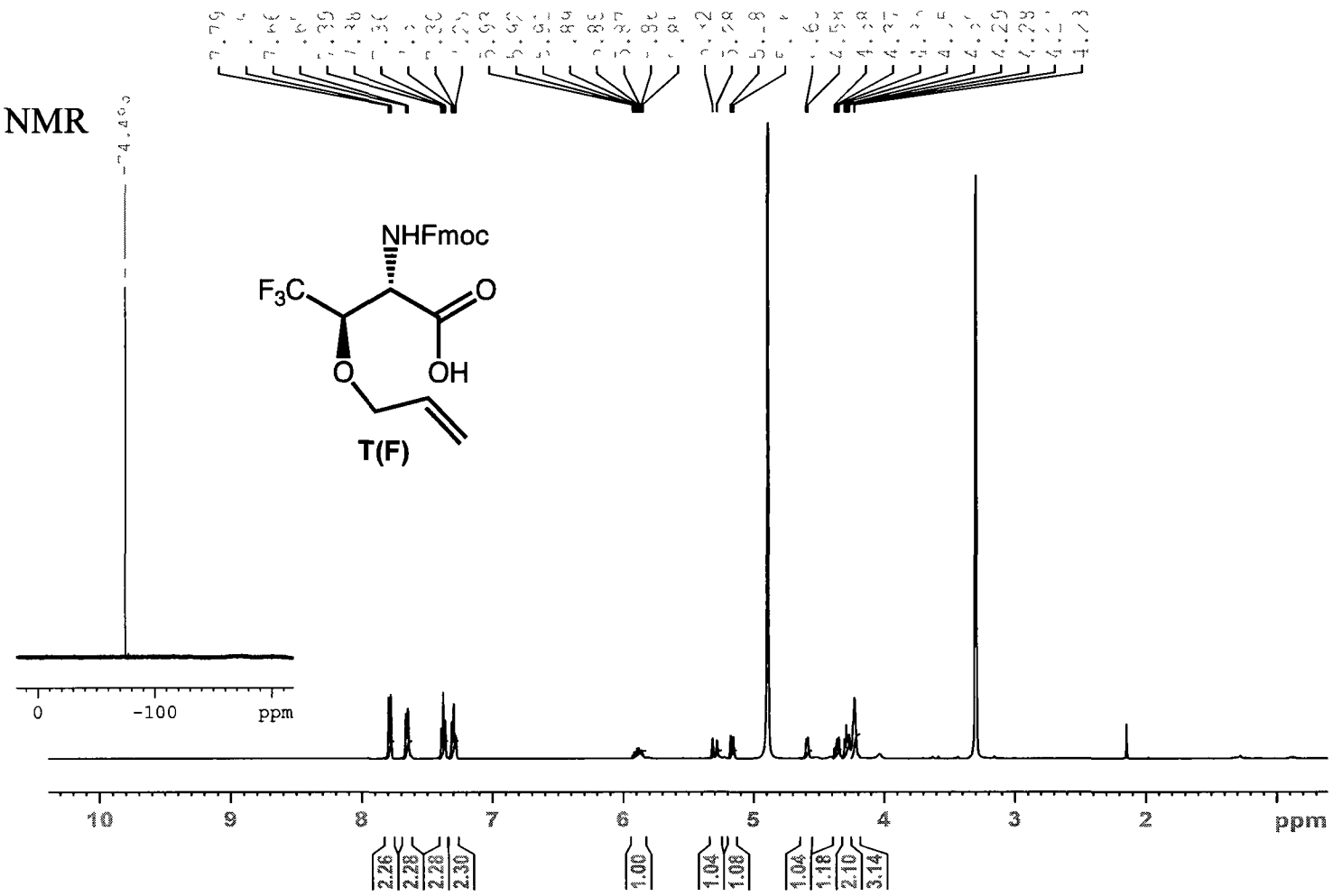

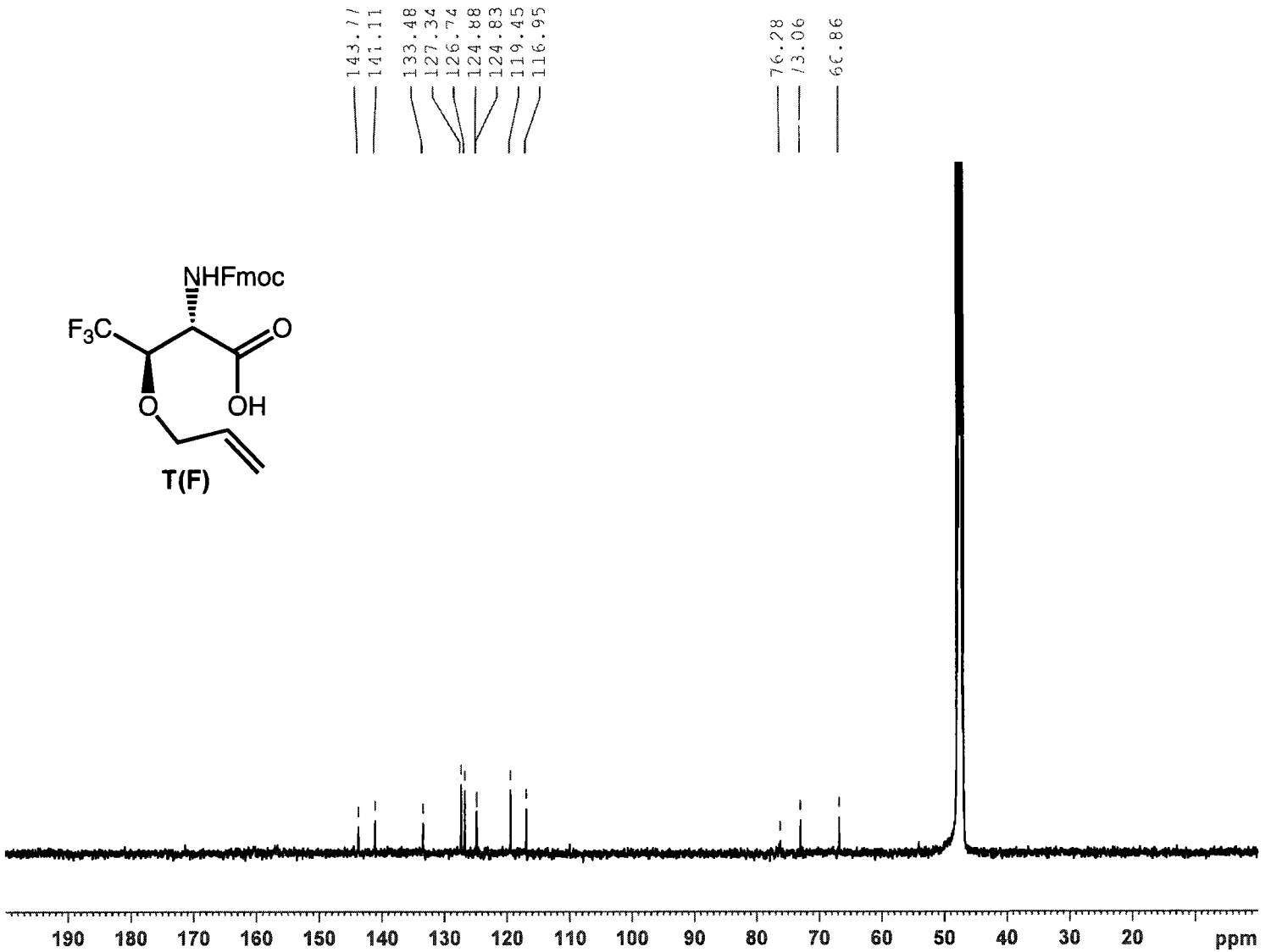
143.11
141.11
133.48
127.34
126.74
124.88
124.83
119.45
116.95
76.28
73.06
66.86
NHFmoc
F3C
O
O
OH
T(F)
190
180
170
160
150
140
130
120
110
100
90
80
70
60
50
40
30
20
ppm

^{1}H NMR

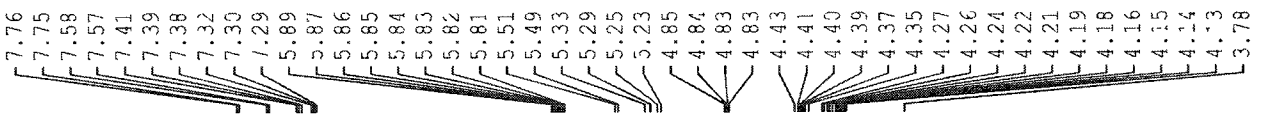

^{19}F NMR

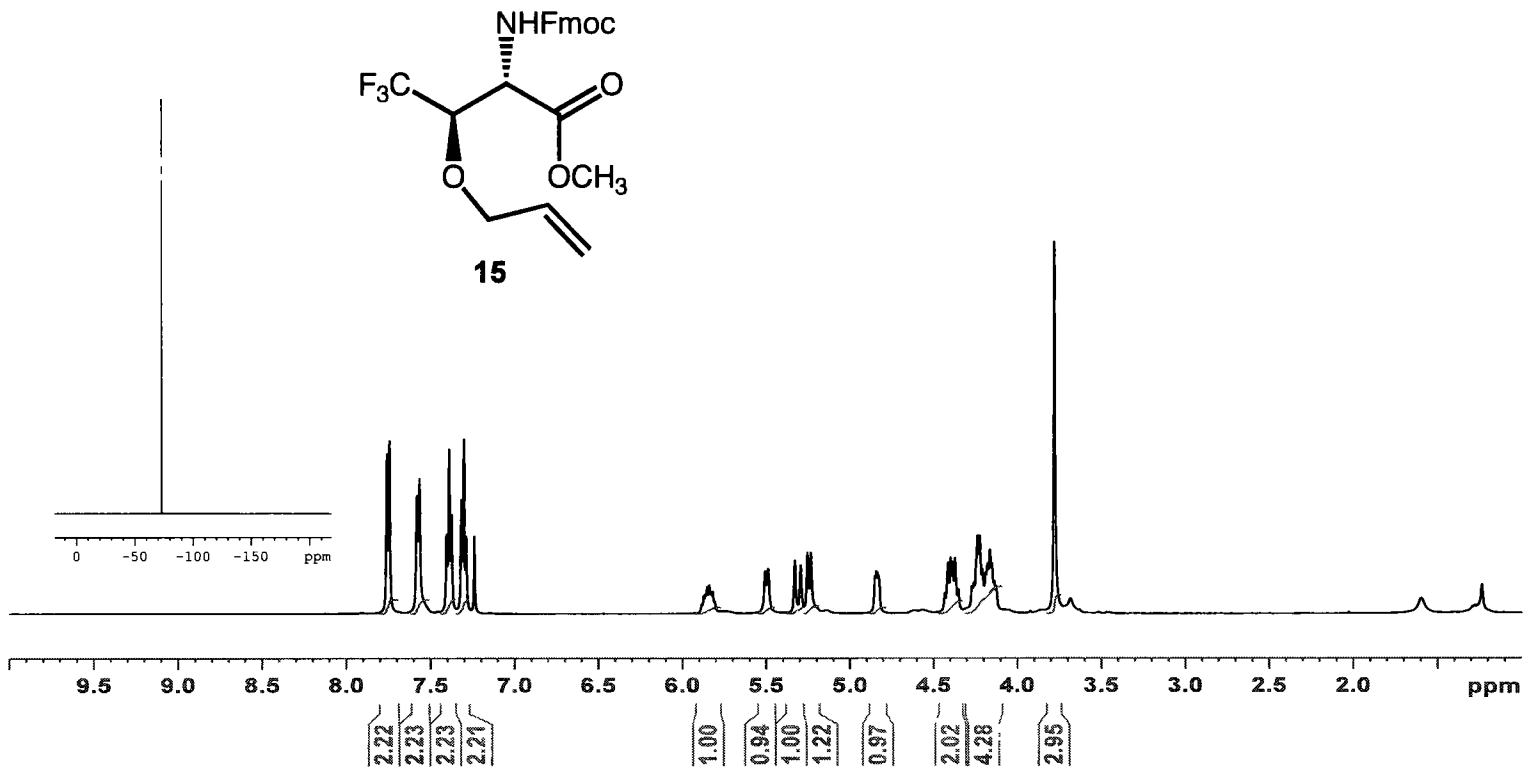

^{13}C NMR

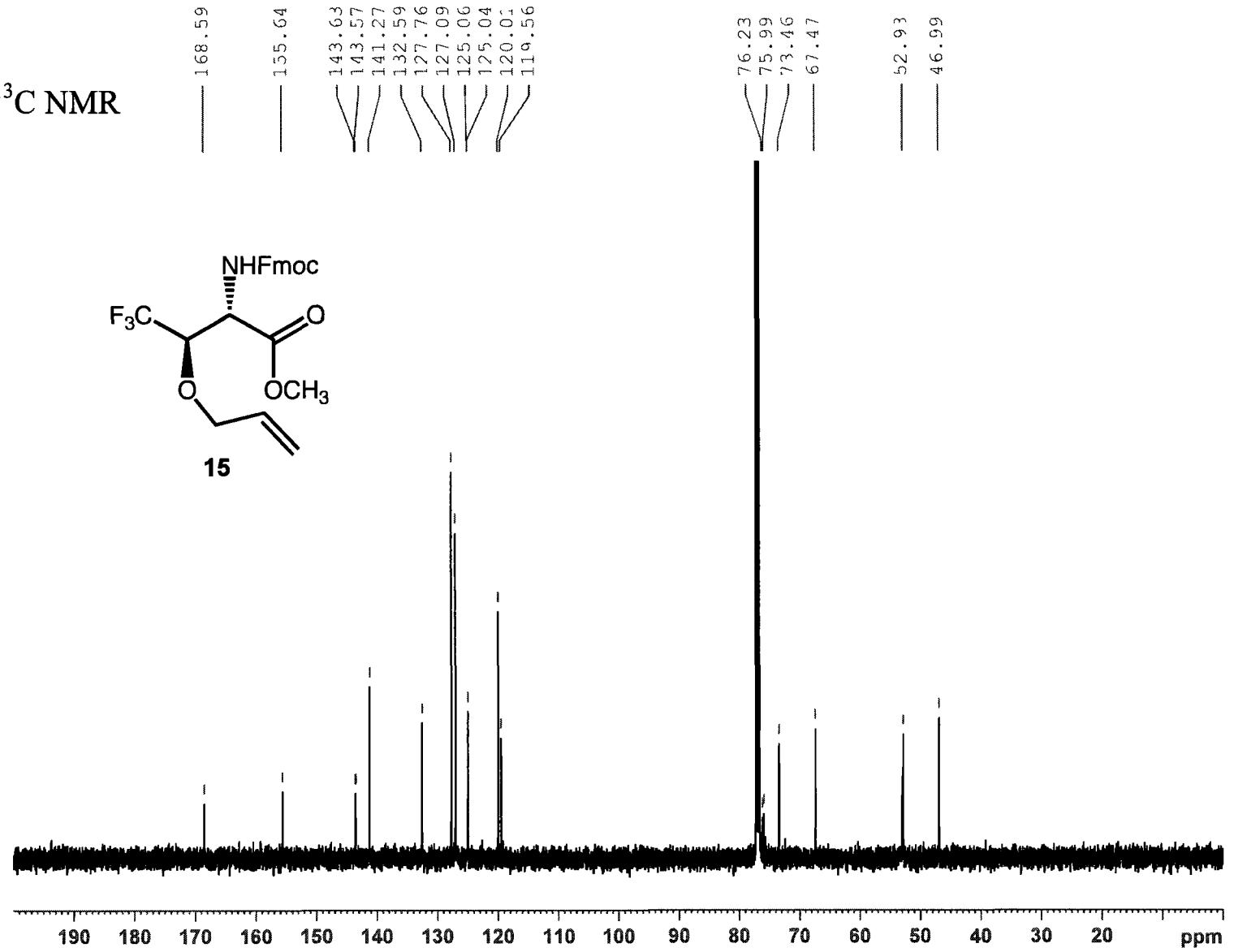
168.59
155.64
143.63
143.57
141.27
132.59
127.76
127.09
125.06
125.04
120.01
119.56
76.23
75.99
73.46
67.47
52.93
46.99
NHFmoc
F3C
O
O
OCH3
190
180
170
160
150
140
130
120
110
100
90
80
70
60
50
40
30
20
ppm

15

^{1}H NMR

^{19}F NMR

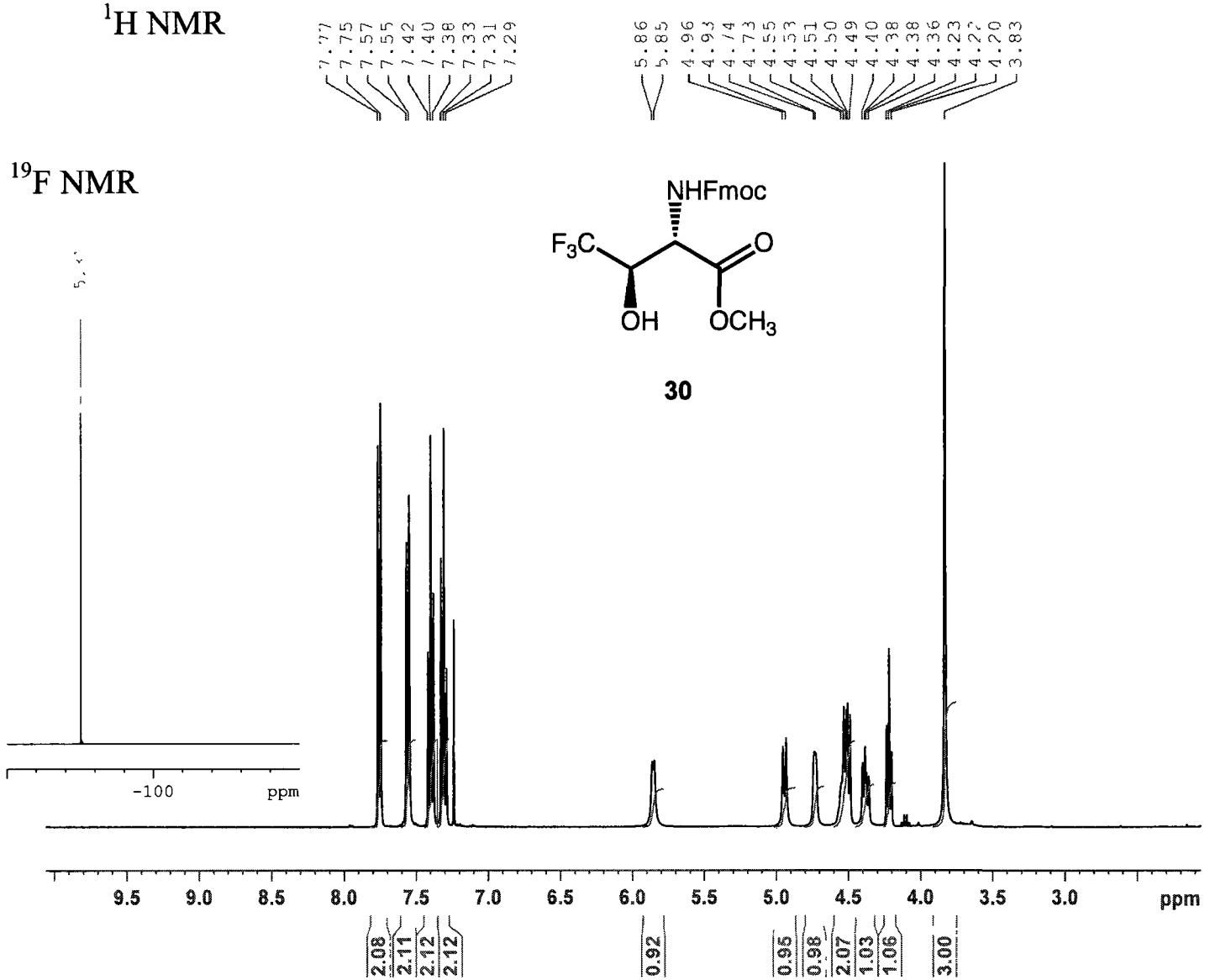

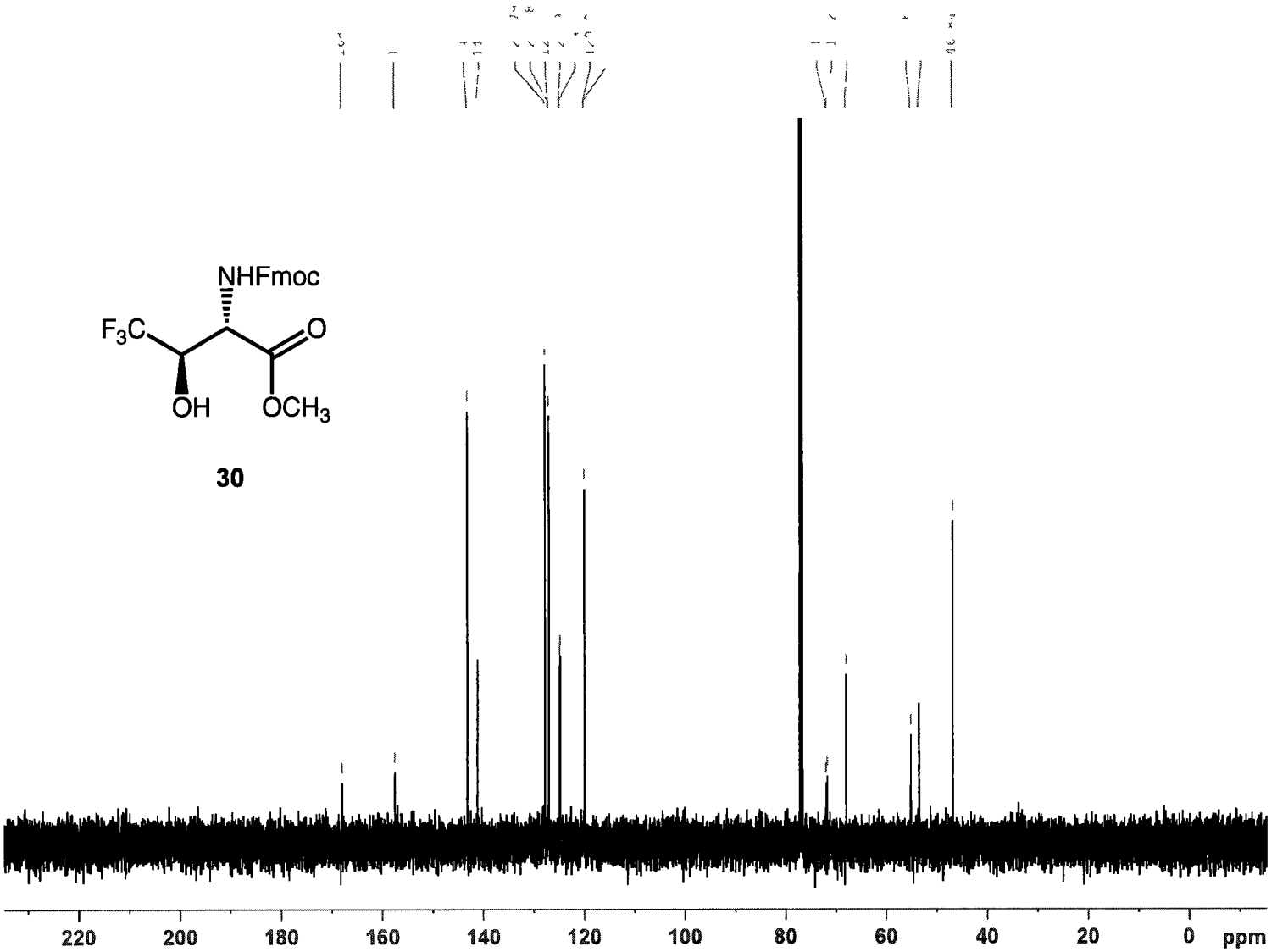
NHFmoc
F3C
O
OH
OCH3
30
220
200
180
160
140
120
100
80
60
40
20
0
ppm

^{1}H NMR [TAA]$_4$

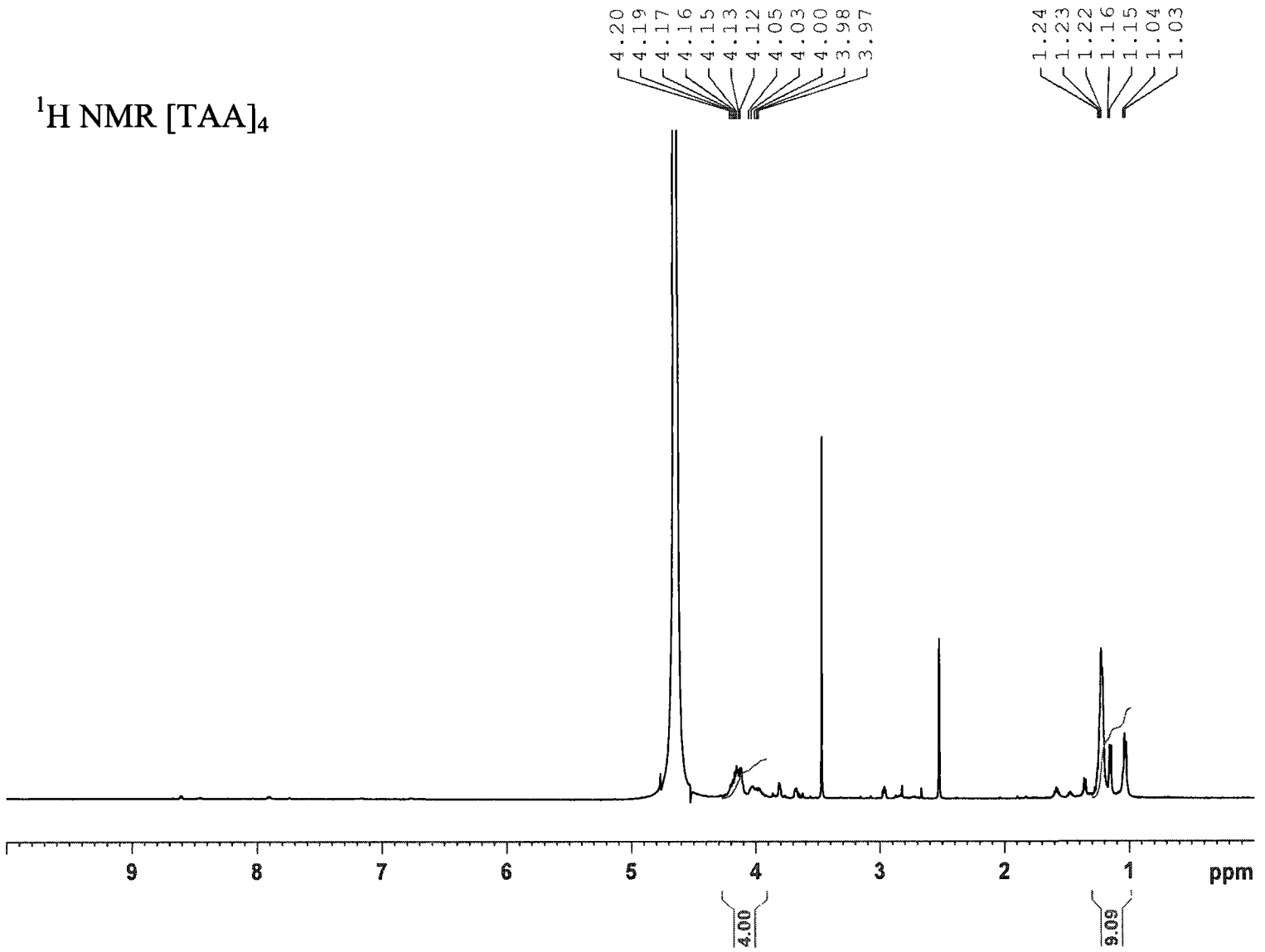
4.20
4.19
4.17
4.16
4.15
4.13
4.12
4.05
4.03
4.00
3.98
3.97
1.24
1.23
1.22
1.16
1.15
1.04
1.03
9
8
7
6
5
4
3
2
1
ppm
4.00
9.09

^{1}H NMR [TGG]$_4$

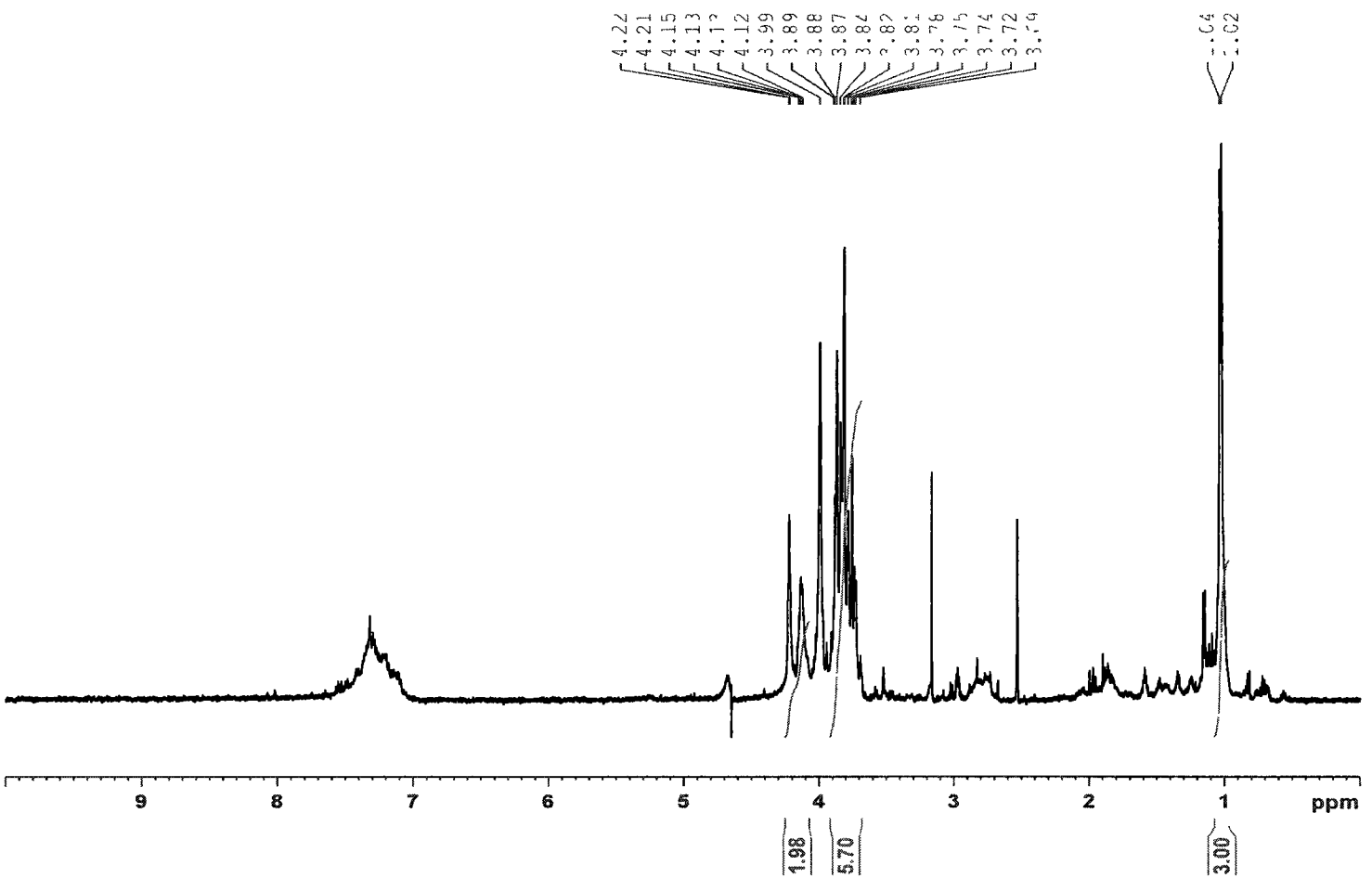
4.22
4.21
4.15
4.13
4.12
3.99
3.89
3.88
3.87
3.84
3.78
3.74
3.72
1.04
1.02
9
8
7
6
5
4
3
2
1
ppm
1.98
5.70
3.00

$[T(F)AA]_4$

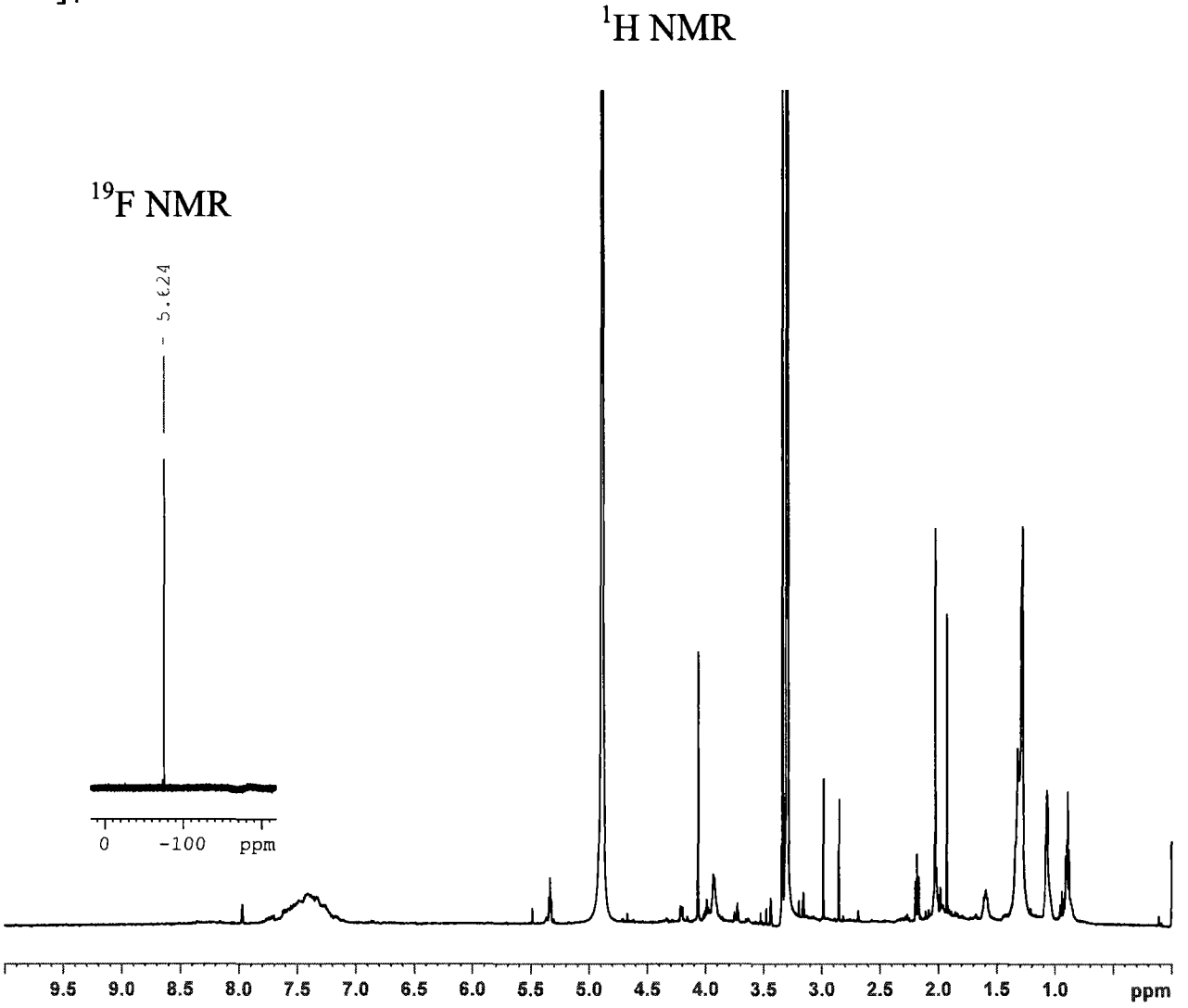
^{1}H NMR
^{19}F NMR
- 5.624
0
-100
ppm
9.5
9.0
8.5
8.0
7.5
7.0
6.5
6.0
5.5
5.0
4.5
4.0
3.5
3.0
2.5
2.0
1.5
1.0
ppm

$[T(F)GG]_4$

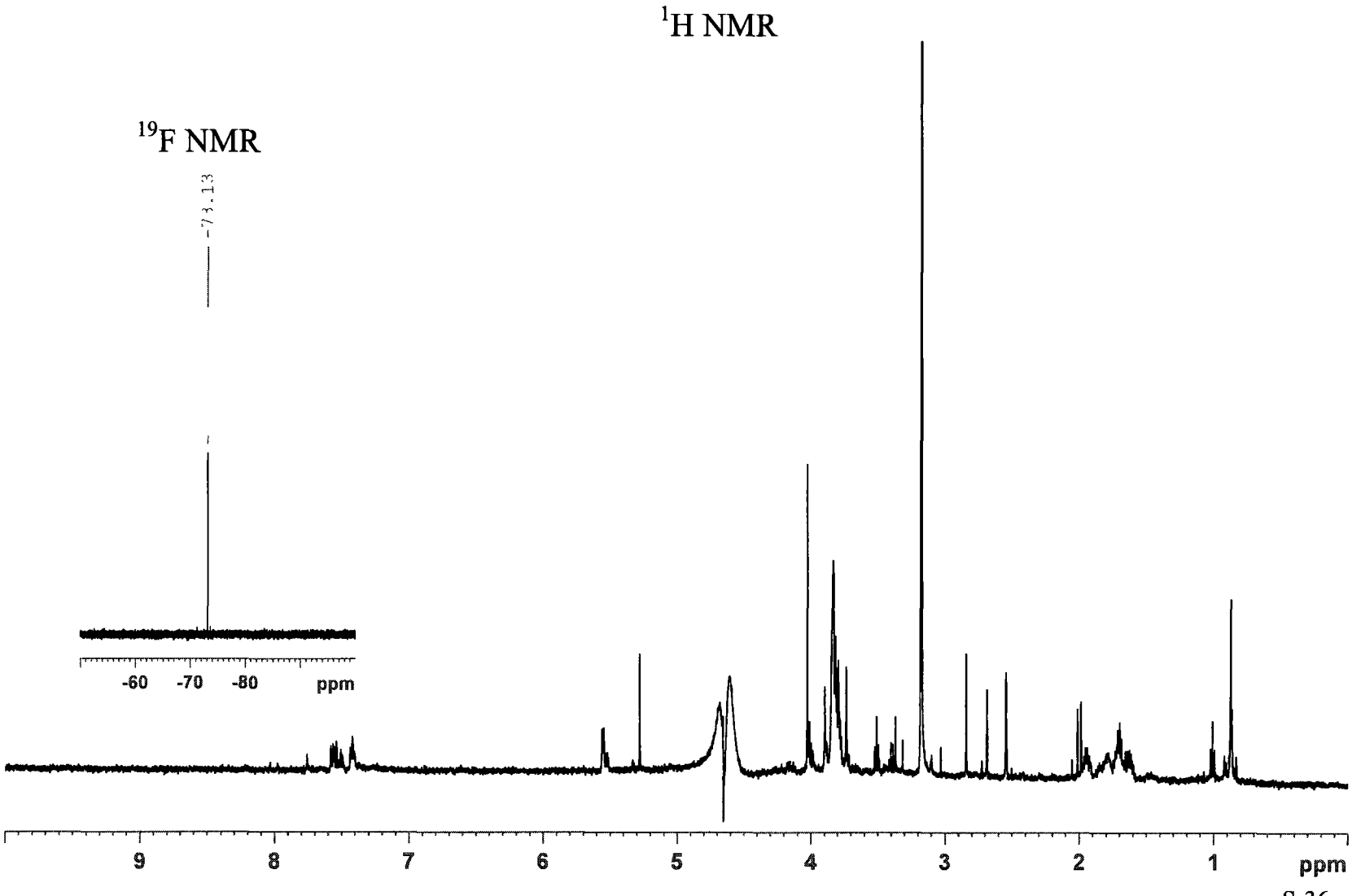

MALDI-TOF

$[T(F)AA]_3$ [M+H]: 1277.422;; [M+Na]: 1300.411. Found 1301.3

MALDI-TOF
$[T(F)GG]_4$ [M+H] : 1151.281

(g) References

1. Tam, R. Y.; Ferreira, S.S.; Czechura, P.; Chaytor, J.L.; Ben, R.N. *J. Am. Chem. Soc.* **2008,** *130*, 17494-17501.

2. Xiao, N.; Jiang, Z-X.; Yu, B. *Biopol. Pept. Sci.* **2007,** *88*, 781-796.

3. Jiang, Z.-X.; Qin, Y-Y.; Qing, F-L *J. Org. Chem.* **2003,** *68*, 7544-7547.

4. Knight, C. A.; Hallett, J.; DeVries, A.L. *Cryobiology* **1988,** *25*, 55-60.

5. Chakrabarrty, A.; Hew, C.L. *Eur. J. Biochem.* **1991,** *202*, 1057-1063.